Tribuser Lukas, BSc

Synthesis of New Fluorescent Indicator Dyes and Receptors for Optical Ion Sensors

MASTER THESIS

to achieve the university degree of

Master of Science (MSc)

Master's degree programme: Technical Chemistry

submitted to

Graz University of Technology

Supervisor:

Ass. Prof. kand. Sergey Borisov

Institute of Analytical Chemistry and Food Chemistry

Graz, January, 2017

Abstract

In this thesis the synthesis and characterisation of new optical ion sensor materials are investigated. The synthesis of various receptors for Ca^{2+}-ions and the modification of borondipyrromethene (BODIPY) was performed. The indicators are characterized in respect to their photophysical properties and their suitability as sensor materials by embedding them into polymer matrices. The new fluoroionophores were tested against other analytes such as Na^{+} or Mg^{2+} to investigate their cross sensitivity.

Calibrations of the ionophores in solution and in polymer matrices were performed. Aggregation effects could be observed when the indicator is embedded in hydrogel matrices which was investigated further in this thesis.
Furthermore, a new way of BODIPY-synthesis was developed for a asymmetric synthesis of BODIPY dyes. With this synthesis strategy three different dyes can be obtained by using a single one-pot reaction. They are likely to be useful for preparation of new Ca^{2+} fluoroionophores.

Additionally to the synthesis of the Ca^{2+}-chelator several other reactions were performed for the development of new indicators for calcium sensing.
The developed system represents a new platform for future high performance sensing materials, hence in this thesis also future improvements for the development of new fluoroionophores are presented.

Kurzfassung

In Rahmen dieser Arbeit wurde die Synthese neuer ionensensitver Farbstoffe und die Charakterisierung neuer Materialien für optische Ionensensoren durchgeführt. Der synthetische Schwerpunkt lag in der Herstellung neuer Ca^{2+}-Ionenrezeptoren, sowie in der Modifikation von Borondipyrromethenen (BODIPY). Durch die gezielte Einbettung der Indikatoren in unterschiedliche Trägerpolymere konnte die Charakterisierung der photophysikalischen Eigenschaften und die Eignung als Sensormaterial untersucht werden. Des Weiteren wurde die Quersensitivität der Fluoroionophore gegenüber anderer Analyten, wie Na^+ oder Mg^{2+} überprüft.

Kalibrationen der Ionophore wurden sowohl in Lösung, wie auch in verschiedenen Polymermatrizen durchgeführt, wobei Aggregationseffekte in Hydrogelmatrizen beobachtet werden konnten. Die Entwicklung einer neuen Synthesestrategie für asymmetrisch aufgebaute BODIPY Farbstoffe ermöglicht die Synthese von drei unterschiedlichen Indikatoren in nur einer „one-pot" Reaktion, was von ausgesprochenem Nutzen für die Herstellung weiterer Ca^{2+}- Ionophore sein wird.

Zusätzlich zur Synthese des Ca^{2+}-Chelators konnten einige weitere Reaktionen, zur Entwicklung neuer Farbstoffe für Calciumsensoren, durchgeführt werden. Das in dieser Arbeit vorgestellte Sensorsystem, sowie Fortschritte in der Synthese neuer Fluoroionophore bilden die Grundlagen einer neuen Plattform für zukünftige High Performance Sensormaterialen.

AFFIDAVIT

I declare that I have authored this thesis independently, that I have not used other than the declared sources/resources, and that I have explicitly indicated all material which has been quoted either literally or by content from the sources used. The text document uploaded to TUGRAZonline is identical to the present master's thesis.

EIDESSTATTLICHE ERKLÄRUNG

Ich erkläre an Eides statt, dass ich die vorliegende Arbeit selbstständig verfasst, andere als die angegebenen Quellen/Hilfsmittel nicht benutzt, und die den benutzten Quellen wörtlich und inhaltlich entnommenen Stellen als solche kenntlich gemacht habe. Das in TUGRAZonline hochgeladene Textdokument ist mit der vorliegenden Masterarbeit identisch.

_____   _____
Datum/Date   Unterschrift/Signature

Danksagung

An erster Stelle möchte ich mich bei Prof. Ingo Klimant bedanken. Deine lehrreichen Diskussionen, Ideen und Besprechungen haben mir während meiner Arbeit sehr geholfen. Ohne Deinen Input wäre all dies nicht möglich gewesen.

Sergey, ich möchte mich bei dir bedanken das du mich erstklassig betreut und mich zu jedem Zeitpunkt unterstützt hast. Dein wissenschaftlicher Input erstaunt mich jeden Tag auf ein Neues, ich habe dank Dir in dieser kurzen Zeit noch nie soviel gelernt und werde diese Erfahrung sicherlich nie vergessen.

Berni, danke das du mich während meiner Masterarbeit immer auf höchsten Niveau betreut hast. Als ich angefangen habe, war mir gar nicht bewusst was ich alles von dir lernen werde! Ohne dich wäre ich nie so weit gekommen und vieles wäre nie möglich geworden. Du warst und bist ein Weltklasse Betreuer sondern auch ein sehr guter Freund, mit dem ich hoffentlich noch einige gute Biere in gemütlicher Atmosphäre genießen darf.

Fips, danke ich dein Freund sein darf, ohne dir wäre mein Studium nie so gut verlaufen. Mit dir konnte ich eine tolle Zeit genießen und du bist mir jederzeit zur Seite gestanden und warst für mich auch da wenn es mir einmal nicht so gegangen ist. Ohne unseren gemeinsamen Stunden im Tintenfass hätte ich mein Studium nie so genießen können, danke.

Andi, du hast mich während der Masterarbeit immer unterstützt und immer weitergeholfen, danke. Wofür ich mich noch mehr bedanken möchte waren die lustigen Konversationen im Eisbärbüro sowie die Kochabende auf der Uni. I hoff das wir in nächster Zeit wieder in einem Büro sitzen werden und weiter gemeinsam ein Büro-Team sein können.

Liebe Dumpfbacken, ich bin froh das ich mit euch studieren konnte und ich werde diese Zeit sicher nie vergessen. Sei es unser gemeinsames fortgehen, das zusammen lernen oder einfach die unzähligen sinnlosen Diskussionen die wir gemeinsam hatten, all dies wird mir ewig in Erinnerung bleiben.

Natürlich möchte ich mich am ganzen ACFC-Institut bedanken. Es herrscht auf unserem Institut eine unglaublich gute Atmosphäre, was einen in so manchen nervenaufreibenden Stunden im Labor aufmuntert und anspornt sich reinzuknien und nie aufzugeben. Es ist keine Selbstverständlichkeit in so einen gemütlichen und freundlichen Umfeld zu arbeiten und sich Freitag schon wieder auf Montag zu freuen. Danke.

Max, eigentlich hat ja alles mit dir angefangen! Hättest du mir in meinen noch jungen

Jahren nicht Graz gezeigt, wäre ich wohl nie hierher gekommen um zu studieren und hätte all dies nicht erleben können. Auch meinen anderen Brüdern (Mich, Basti) gebührt großes Lob. Seien es unsere alljährlichen Projekte daheim, oder auch die gemütlichen Stunden bei Speis und Trank, ich hoffe das wir das beibehalten und weiter so gut verstehen. Danke Nici das du mich immer unterstützt hast und mir immer zur Seite gestanden bist.

Abschließend möchte ich mich bei meinen Eltern bedanken. Danke das ihr mir dieses Studium ermöglicht habt. Ohne euch wäre das alles nicht möglich gewesen und ich wäre jetzt nicht hier, hättet ihr mich nicht immer unterstützt und immer an mich geglaubt. Ich weiß mit mir war und ist es nicht immer leicht ;-) aber ich glaube ich bin auf einen guten Weg, donksche.

Tribuser Lukas, BSc   Graz, January, 2017

Contents

1 Introduction

The ocean chemistry has an extensive direct and indirect effect on organisms and their inhabitants. One of the most important factors of acidification of the oceans relates to the production of calcium carbonate ($CaCO_3$) shells and plates.[1, 2] This acidification of the ocean is creating an imbalance in the $CaCO_3$-formation making the dissolution of formed $CaCO_3$ more likely. Hence, the measurement of free Ca^{2+} in the sea is of great interest.[3]

In recent years optical sensors received increasing attention in both academia and industry. They offer distinct advantages compared to commonly used analytical methods (e.g. electrochemical sensors) by their insensitivity to electromagnetic influences and cost effective preparation. They offer various sensing formats ranging from foils to nanoparticles. Especially pO_2 sensors are already well established and commercially available.
Optical sensors for ionic species are of great interest for marine, clinical and biological application. However, there is a lack of high performance ion sensing materials due to challenges in selectivity and stability in polymer matrices.

The aim of this work was the development of new Ca^{2+} ion sensing materials. The synthesis as well as the characterization of a new fluorescent Ca^{2+}-indicator dye was performed. A possible application of the new indicator dye would be the measurement of Ca^{2+}-ions in sea water. A receptor for calcium[4, 5] was directly linked to different BODIPY dyes, enabling the determination of free calcium ions in solutions. Photophysical properties of the probes were characterized and further embedded in different polymer matrices to obtain a suitable sensor material.

2 Theoretical Background

2.1 Fundamentals of Luminescence

Luminescences describes the emission of photons/light from an organic/anorganic compound during relaxation of an electronically excited state. A molecule taking part of this phenomena is called "luminophore" or "dye". The excitation of an electronic ground state to an electronically excited state can occur via an enormous variety of ways, whereas absorption of electromagnetic radiation is one of the most notable ones. The sensitivity to many environmental parameters is used in sensors for their monitoring. [6]

2.1.1 Absorption

If a photon is absorbed by a dye an electron is promoted to an energetically higher state. During this absorption process, the electron can pass through many transitions before the dye relaxes back to the ground state. Photon absorption is a very fast process and takes place in a time period of about 10^{-15} seconds. [6]

In case of transitions in absorption, the $\pi \to \pi^*$ and $n \to \pi^*$ transition are the majority. All other transitions (e.g. $\sigma \to \sigma^*$, $n \to \sigma^*$) occur at higher energies and therefore at lower wavelengths. The energy needed for a $\pi \to \pi^*$ transition is decreasing with higher conjugated π-systems, and therefore several conjugated bonds are required to achieve an absorption in the UV-VIS region. Notably, the dye maintains its spin multiplicity during excitations to an energetically higher state. For this reason direct transitions from a ground state to the excited triplet state is spin forbidden. [6]

The molar absorption coefficient ϵ displays the ability of the dye to absorb light. The Beer-Lambert law, describes the absorption efficiency at a certain wavelength, whereby the absorbance A, is defined as the decadic logarithm of the ratio of the light intensity I_0 (before) and I (after) the sample. Furthermore it contains the optical path length through the sample as well as the dye concentration itself.

$$A = \log \frac{I_0}{I} = \epsilon * c * d \tag{2.1}$$

I_0 ... Intensity of light before the sample
I ... Intensity of light after the sample

ϵ ... Molar absorption coefficient

c ... concentration of the dye

d ... optical path length of the sample

2.1.2 Frank-Condon principle

The movements of electrons compared to the heavy nuclei are much faster. This concept is demonstrated by the Born-Oppenheimer approximation. In this theory the atoms can be considered as stationary, because the excitation process is multiple times faster. (10^{-15} seconds compared to 10^{-10} - 10^{-12} seconds)

Using this approximation the nuclei of a molecule is not changing its position during electron transitions. Which concludes that atoms in the ground state as well as in the excited state can be seen as equidistant.
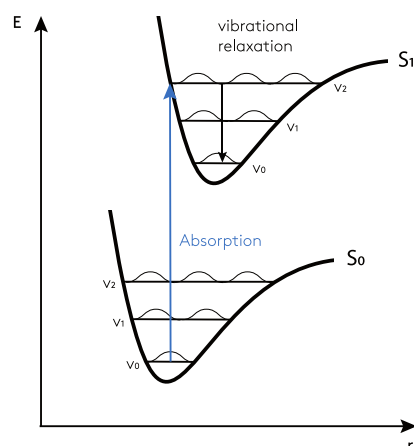

Figure 2.1: Frank-Condon diagram of a two atom model, the excited state S_1 and the ground state S_0.

In a simplified two atom model, the excited state has weaker bonds, because the morse potential minimum has greater nuclei distances compared to the ground state. Wherefore the electrons in the excited state are in a energetically higher vibrational level.

Subsequently after the excitation, a relaxation to the lowest vibrational level of the excited state is followed. The relaxation energy is either transformed to heat or rotation of the molecule. Informations about the vibrational state of the ground state are gathers using emission spectra as well as information about the excited state using the absorption spectra.

2.1.3 Transitions between Electronic States

Usually the energy states of an electron is visualized by a Jablonski diagram, whereby the spin multiplicity is displayed horizontally and the energy, vertically. The Jablonski diagram illustrates the major photo-physical processes which are connected to luminescence.
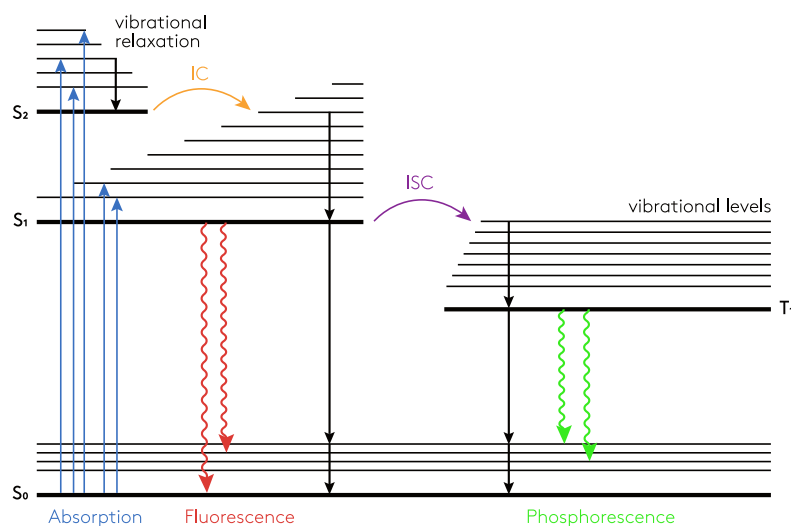

Figure 2.2: Jablonski diagram of the main photo-physical processes belonging to luminescence.

In figure 2.2 the singlet ground state S_0, the excited singlet states, S_1 and S_2 as well as the excited triplet state, T_1 are illustrated. The triplet state is according to the rule of Hund energetically lower then the singlet state. The absorption of light induces the increasing of an electron to one of the vibrational levels to an excited state.

Electronic transition is only allowed if the multiplicity of the entire transition state does not change, which concludes that only singlet-singlet and triplet-triplet transitions are allowed. Whereby the singlet-triplet transition is according to the quantum mechanics forbidden as the spin is changing. However, under certain conditions, de-excitation can cause transitions to different electronic states.

2.1.4 Internal Conversion

Internal Conversion is one of the possible non-radiative de-excitation pathways. It illustrates an isoenergetic transition from a higher to a lower electronic state with the same spin multiplicity (e.g. $S_1 \rightarrow S_0$ and $S_2 \rightarrow S_1$). This de-excitation is followed by vibrational relaxation of the electron to the corresponding ground state.
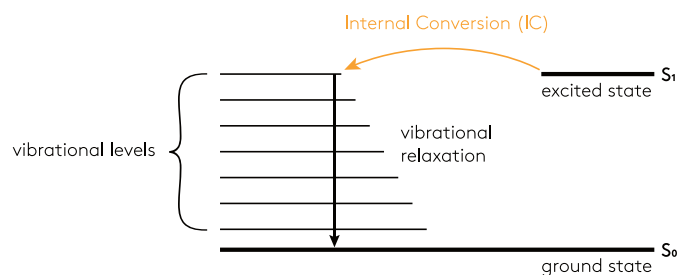
Figure 2.3: Internal Conversion and the corresponding isoenergetic transition via vibrational relaxation

The time scale of such conversions are between $10\,\mathrm{ps}$ and $1\,\mathrm{ns}$, whereby the vibrational relaxation is ten times faster. As expected, this process is increasing with decreasing energy gaps between the electronic states, wherefore the conversion from S_2 is predominant. The transition from $S_1 \to S_0$ is beside the higher energy gap competing with fluorescence and inter system crossing (ISC).

2.1.5 Fluorescence

Fluorescence is in conjunction with the transition of the two singulet states $S_1 \to S_0$ and the corresponding emmission of photons. Due to vibrational relaxation, emission is always occuring from the lowest vibrational level (S_1) which can be seen in figure 2.4. As a result, the excitation wavelength and the emission wavelength are independent of each other.

It has to be considered that this vibrational relaxation is just possible of internal conversions beforehand, which are connected with energy losses. For that reason the emitted light has a lower energy and vice versa a longer wavelength than the absorbed light. This phenomena is called Stokes shift.
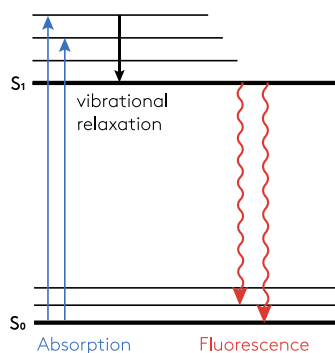

Figure 2.4: Jablonski diagram showing fluorescence de excitation.

According to the Frank-Condon-principle, mainly excited vibrational levels (of the ground state) are occupied. The emission can be seen as a mirror of the absorption spectra shifted to

longer wavelengths, due to energy differences between the singulet states.

2.1.6 Intersystem Crossing

Another isoenergetic non-radiative transition during the lifetime of the excited singlet state S_1 is the intersystem crossing, ISC. It describes the transition from the singlet state to the triplet state, which includes the spin reversal at an equal vibrational level and its relaxation to the lowest vibrational level, T_1.
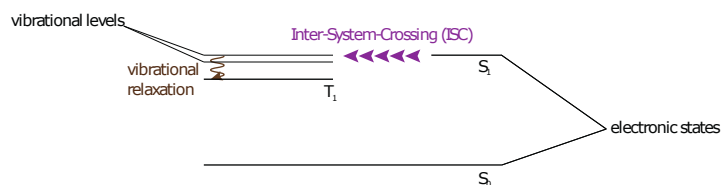

Figure 2.5: Illustration of Intersystem Crossing (ISC), the transition from the S_1 to T_1.

The change of the spin is forbidden, however spin-orbit coupling enables the possibility for ISC. The spin orbit coupling is increased with heavy atoms like Br or Pb, which enhances the ISC. Time rates of about $10^{-7} \rightarrow 10^{-9}$ seconds are fast enough to be completable with other deactivation processes. After vibrational relaxation to the lowest vibrational level, the electron can remain up to $10^{-6} \rightarrow 1$ seconds.

2.1.7 Phosphorescence

Compared to the the singlet state, the triplet state T_1 has very long lifetimes, since radiative de-excitation processes are spin forbidden. Typically no radiative de-excitation is observed because of the fast relaxation caused by collisions with solvent molecules. Reduction of the temperature as well as increasing rigidity of the system decreases the deactivation processes, which increases the chance of radiative relaxation.

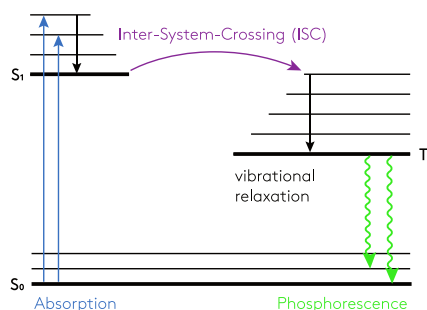In the last decades many emitters with efficient RT phosphorescence have been prepared.

Figure 2.6: Scheme of phosphorescence.

The triplet state T_1 is usually positioned at lower energies than the singlet state S_1, resulting in higher wavelengths of the phosphorescence emission compared to the fluorescence emission. The emission of the photons is as fast as the emission in fluorescence (10^{-15} seconds), whereas the lifetime of the triplet state itself can reach up to seconds or even minutes.

2.1.8 Delayed Fluorescence

The delayed fluorescence is a result of the intersystem crossing to the triplet state and the conversion back to the S_1 state, called reverse intersystem crossing, (RISC). As a result the same emission spectrum as in fluorescence is obtained, whereas the luminescent lifetime is increasing. The energy difference between the T_1 level and the S_1 level has to be small enough, and the lifetime of T_1 has to be long enough in order to make RISC possible.
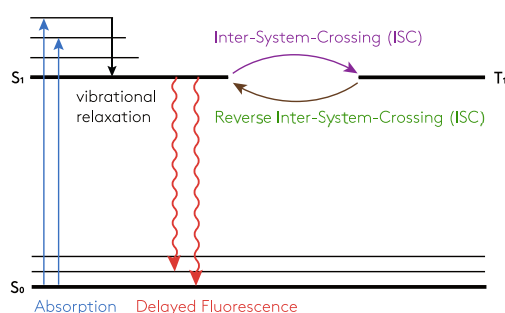

Figure 2.7: Delayed Fluorescence, caused by reverse intersystem crossing (RISC).

It has to be considered that the delayed fluorescence is thermally activated, meaning that with increasing temperature the efficiency of the delayed fluorescence is increased. The first time this phenomena was observed was with using eosin, that the reason why it is also called, delayed fluorescence of E-type.
In addition, collisions of two molecules (T_1) in concentrated solutions can provide enough energy to convert one molecule back in the S_1 state and consequently resulting in the delayed fluorescence. This is called delayed fluorescence of P-type. (first discovered in pyrene)

2.1.9 Lifetimes

The time dependence of all described processes are all of different time-scales, concluding in a certain period of time for the excited state S_1. Consequently, the kinetics of the various de-excitations to the ground state S_0 can be described by first order kinetics. (equation 2.2)

$$-\frac{d[A^*]}{dt} = k * [A^*]$$

(2.2)

$[A^*]$ represents the amount/concentration of species A in the excited state, wheras k the sum

of all de-activation rates.

$$k = k_{radiative} + k_{non-radiative} \tag{2.3}$$

If the equation 2.2 by integration from $t_0 \to t$ and $[A^*]_0 \to [A^*]$ yields:

$$[A^*] = [A_0^*] * e^{-kt} \tag{2.4}$$

The unit for first-order reactions is s^{-1}, the inverse of the first-order rate constant is the unit of time, characteristic for the reaction. In the case of luminescence τ is described as the lifetime of the excited state.

$$\tau = \frac{1}{k} \tag{2.5}$$

resulting to:

$$[A^*]_t = [A^*]_0 * e^{\frac{-t}{\tau}} \tag{2.6}$$

In words, after excitation the intensity of the fluorescence decreases exponentially. The decay time τ describes the time window for dynamic phenomena. Lifetimes for the different excited states S_1, T_1 range from $10^{-11} \to 10^{-7}$ and $10^{-6} \to 1$ seconds.

2.1.10 Quantum Yields

The quantum yield is the ratio between emitted and absorbed photons. Not all absorbed photons are emitted via fluorescence or phosphorescence since non-radiative de-excitation is competing. The quantum yield is an important parameter for sensors because it illustrates the brightness of the dye.

$$\phi_F = \frac{emitted\,photons}{absorbed\,photons} = \frac{\tau_S}{\tau_r} = k_r * \tau_S \tag{2.7}$$

θ_S ... lifetime of the excited state
θ_r ... radiative lifetime
k_r ... radiative rate constant

2.1.11 Quenching

All presented de-excitation processes are intrinsic phenomena. Quenching describes the interactions of a quencher (Q) with a excited or non-excited molecule (M). The result of this phenomena is a de-excitation of the molecule (M). The outcome results in a bimolecular reaction,

whereas K_q is its rate constant.

Several intermolecular processes are known which can cause de-excitation, e.g. electron transfer, collisions of M with heavy atoms, proton transfer or energy transfer and the formation of excimer/exciplexes. Notably, it has to be considered that these processes at excited molecules are not causing a chemical alteration but just a de-excitation of the system.
Fluorescence characteristics, such as QY or decay time can be affected, due to this interactions, resulting in a competition between intermolecular and intrinsic de-excitation.

A more general way for describing the quenching processes is by dividing these phenomena into dynamic and static quenching. Whereas, if the formation of excited molecules is possible, static quenching is dominant. However, if collisions with molecules are involved which cause an de-excitation of the excited molecule, we talk about dynamic quenching.
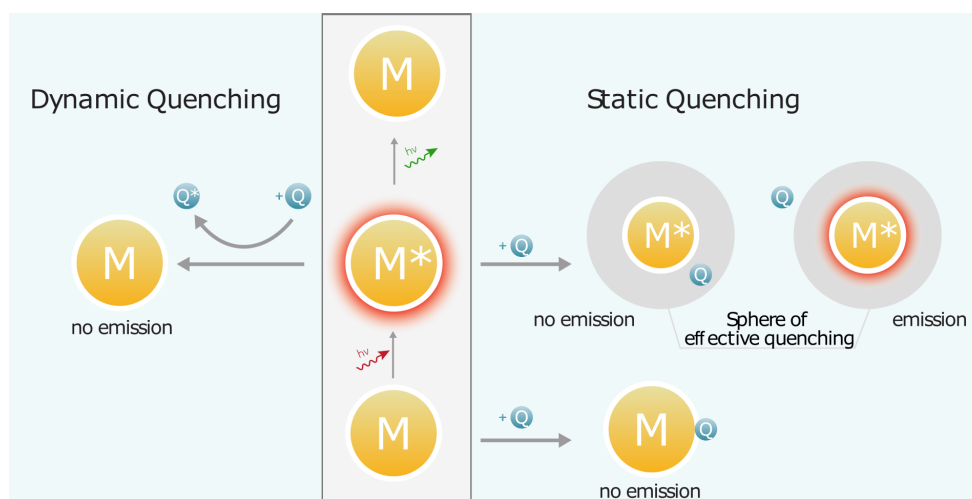

Figure 2.8: Quenching caused either by dynamic quenching or static quenching.

Dynamic quenching

Dynamic quenching describes the interaction of a quencher (Q) with a molecule (M) in its excited state (M^*). Collisions of Q with M^* results in the transfer of energy via a non-radiative process. Consequently the probability of such collisions is increased with increased lifetime of the excited state.
Dynamic quenching is a diffusion controlled process, hence the corresponding rate constant is time dependent. The lifetime of a luminophore is reduced in the presence of Q. Self quenching is possible if the quencher and the luminophore are in the high concentration, which has its own characteristic fluorescence spectrum as well as lifetime. Such compounds are called excimer, or more specific, excited dimer. The ratio of the fluorescent intensity I_0/I is proportional to the luminescence τ_0/τ.

Static quenching

Static quenching is a result of the formation of a MQ complex, which is non-fluorescent. Such complexes are formed by M (molecule) and Q (quencher) in the ground state or at the excited state of M, where effective quenching is possible. This so called sphere of effective quenching requires a small distance.

The effect of both phenomena results in a reduction of the amount of effective luminophore and consequently in a decrease in the fluorescence intensity. It has to be considered that the concentration of the luminophore is decreased, but its characteristic lifetime is not affected at all.

2.2 Chemical Sensors

2.3 Ion Selective Electrodes

In the past decades the history of ion selective electrodes (ISE) has experienced an enormous expansion and became very popular. Since the rapid growth of new electrodes for a large number of different ions, new formats and materials were developed. The functioning of these electrodes has caused the application of ISE's as instrumental components in diverse fields, especially in clinical and environmental chemistry. [8]

2.3.1 Basics

Potentiometric ion selective sensors are mostly electrochemical devices, in which changes of the electromotive force (emf) are monitored. [9]
Therefore an ISE and the reference electrode is immersed in an aqueous solution containing the desired ions. The voltmeter connects both electrodes using low-noise cables and connectors. A potential difference is induced across the ISE membrane when the desired ions diffuse through the the high concentration side to the lower concentration side. (see figure 2.9)
So Ion selective electrodes work on the basic principle of the galvanic cell. The measured electric potential is generated by the selected ions across the membrane compared to the reference electrode. The strength of this charge is directly proportional to the concentration of the desired selected ion.
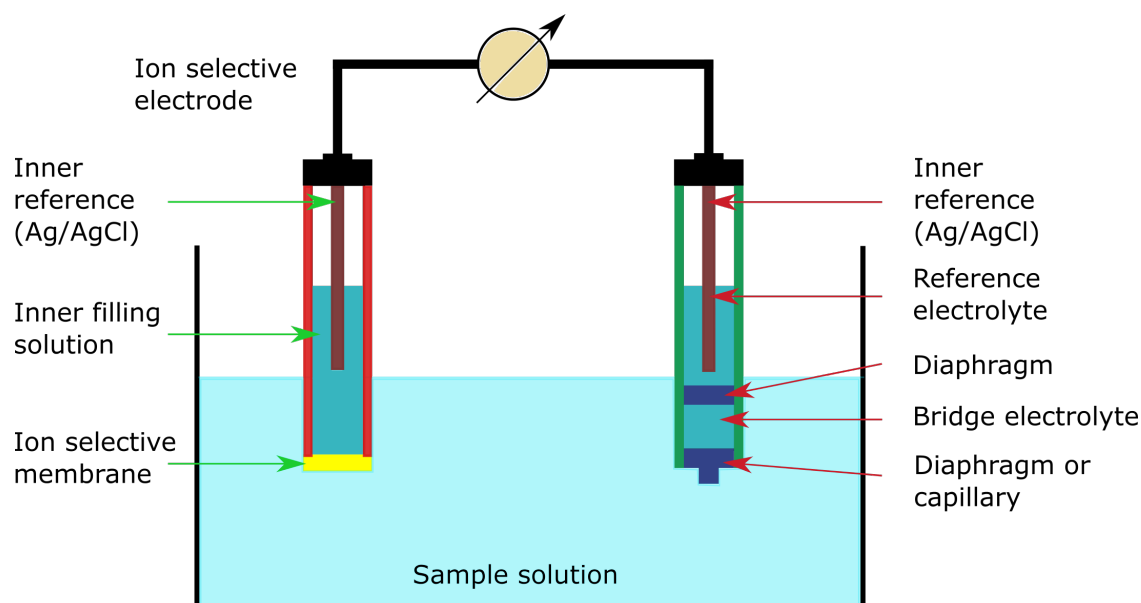

Figure 2.9: Schematic of a potentiometric cell with an indicator (ion selective electrode) and a reference electrode.

Different types of ISE's are excisting, the glass membrane electrode (H^+, Na^+), the solid

state electrode (selective primarily to anions), liquid membrane electrode (several polyvalent cations), gas sensing electrodes (ammonia, carbon dioxide and nitrogen oxide). Compared to other analytical techniques, ISE are relatively inexpensive and simple to use. The have an extremely wide concentration range and measurements in extremely dilute solutions are possible without problems with interfering ions.

2.3.2 Ion selective electrodes for Ca^{2+}

Ca^{2+} ISE's were one of the first commercially available ion selective electrodes. Various applications made calcium to one of the analytes of top interest in ion-selective potentiometry. [9, 10] In Ca^{2+} potentiometry a liquid membrane is used where an ion-exchanger or ionophore is dissolved in a viscous organic liquid membrane (PVC and plasticizer), whereas the exchanger or ionophore is mainly responsible for an effective separation to other interfering ions.

Phosphoric acid esters

The use of phosphoric acid esters as ionophores dates back to the beginning of the ISE membrane technology. The excellent stability of complexes of Ca^{2+} and phosphate or polyphosphate led to didecyl phosphate **1** to the first carriers of this class. The choice of dialkyl esters provides the formation of Ca^{2+}/H^+ in the ISE membrane. An improved selectivity versus sodium and proton interference could be achieved using phenyl substituted phosphates, like bis[4-(1,1,3,3-tetramethylbutyl)phenyl)] phosphate **2**. [11]
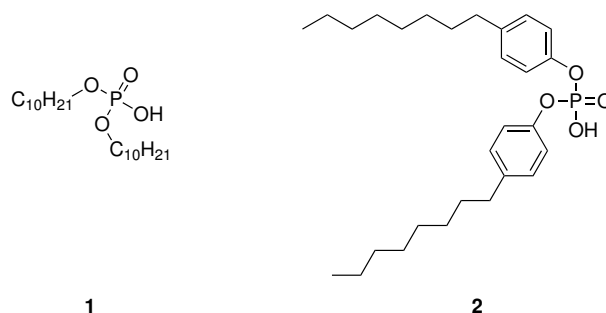

Figure 2.10: Phosphoric acid esters: didecyl phosphate **1** and bis[4-(1,1,3,3-tetramethylbutyl)phenyl)] phosphate **2**.

Amide Ionophores

In contrast to phosphoric acid esters also amide ionophores were developed. First attempts were based on neutral macrocyclic ionophores inspired by cryptands, which are known as famous chelating reagents with a similar structure to EDTA. The first developed cyclic ionophores were not very selective and led finally to noncyclic diamides **3** as Ca^{2+} carriers. The idea was the development of ligands without a functional group that could be easily protonated (see figure 2.11). [11]
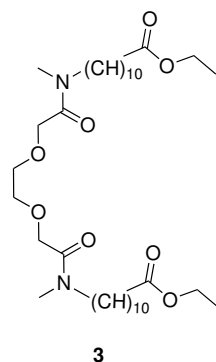
3

Figure 2.11: Example of an amide ionophore: 3,6-dioxaoctanedioic diamide **3**.

2.3.3 Basic Concepts in Chemical Optical Sensors

Since chemical sensors became of more and more importance, there is a high demand in analytical chemistry, medicine, clinical biochemistry, the enviroment, etc. There are already numerous chemical and biochemical analytes which can be detected by using fluorescence techniques: cations ($H^+, Na^+, Li^+, Ca^{2+}, Mg^{2+}, Zn^{2+}, Pb^{2+}, Al^{3+}, etc \cdot$), anions (halide ions, phosphates, ATP, etc.), neutral molecules (sugars, e.g. glucose, etc.) and gases (O_2, CO_2, NO, etc.).

The basic function of an optical sensor is the production of an analyte signal without changing of decomposing the analyte itself. If this condition is fulfilled, such compounds or systems are suitable for long term measurements, real-time monitoring and also in-vivo analysis.
Optical sensors offer a major advantage to various other analytical instruments, because they can monitor chemical reactions. They enable the measurement of physical properties like absorbance, temperature, refractive index, conductivity, etc..

In principle a chemical sensor consits of a recognition element (receptor), transduction element (transducer) and a signal processor. Such systems deliver a continuous and reversible signal, whereas the function of the receptor is the transformation of a chemical information in an energy form the transducer is capable to convert and measure. The recognition unit is usually immobilized on a platform, which acts as a linkage between the receptor and the transducer. If so, the task of the transducer is the transformation of the energy (which is related to the chemical information about the sample) into an exploitable analytical signal.
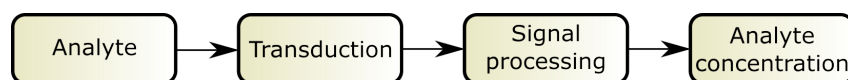

Figure 2.12: Basic principle of a chemical sensor consisting of the transduction unit, the signal processing unit and the corresponding signal.

It has to be considered that the transducer does not show a selectivity for the corresponding analyte, therefore the receptor is even more important and can be based on different principles. A sensor can be enhanced by modifying either the recognition unit or the transducer to either eliminate disturbing signals and enhance the binding of specific compounds to the receptor as well as receiving better immobilization on a platform.

In order to prepare a proper optical sensor certain crucial parameters need to be fulfilled. Reversibility, high accuracy and an ease of use are of great importance. Detection limit and the corresponding dynamic range in the concentration of interest, fast response time, a long operating time as well as specificity and selectivity are desired. For a future mass production, the produced sensor should be minituarizable and cost-effective.

2.3.4 Sensing Mechanisms of Luminescent Optical Sensors

Luminescence molecular sensors can be divided into three major classes concerning their operating modes. The first class (visible in figure 2.13) are fluorophores which undergo quenching upon collision with the analyte of interest (e.g. O_2, Cl^-). The second class are sensors which can reversibly bind analytes. If in that case the analyte is an proton the term fluorescent pH-indicator is used. If it is an ion, we are talking about fluorescent chelating agents. Furthermore, the signal can be gathered either via CEQ (Chelation Enhancement of Quenching) or CEF (Chelation Enhancement of Fluorescence), whereas in the latter case the compound is said to be fluorogenic. In the third class, the fluorophore is linked to a receptor, either directly linked or separated via a spacer.
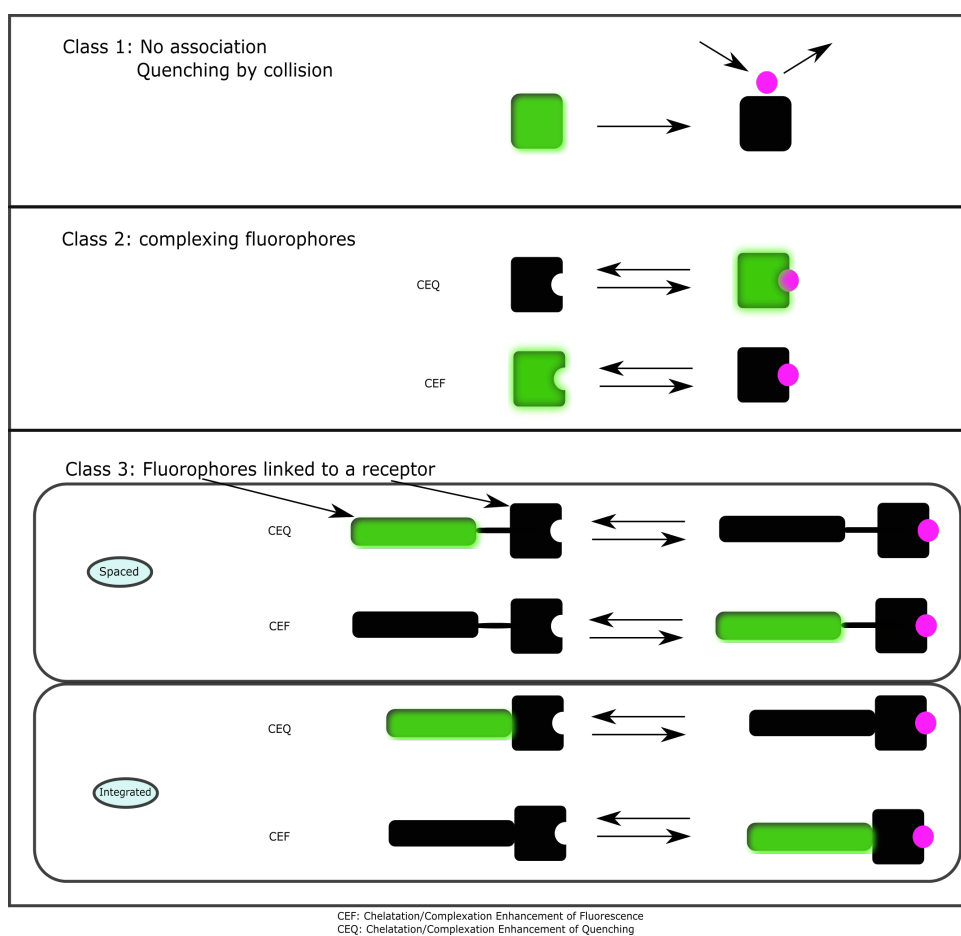

Figure 2.13: Different types and classes of chemical fluorophores. [6]

In cases where the analyte is bound to a receptor (class 2 and 3) the dissociation constant of the fluorescent sensor should fit to the expected range of the analyte concentration, which varies greatly to the field of application.

2.3.5 Fluorescent Ion Sensing

Much attention should be paid to the ionophore moiety as well as the expected changes of the fluorescence characteristics of the linked fluorophore moiety during the cation binding.

The stability and the reversibility of a fluorionophore in presence of ions and its complexation depends on many factors, such as temperature, pH and the nature of the solvent and the cation (e.g. other cations present).

In this respect, the characteristics of the ionophore, for example the topology and the number of complexing atoms or groups should fit to the desired characteristics of the cation on the basis of the fundamental principles of the supramolecular chemistry (ionic diameter, charge density, hardness of the metal, coordination number).

The ionophore (figure 2.14) can be an openchain sturcture, a chelator, a macrocycle, a macrobicycle, etc.. For example the large stability of cryptands is a result from the three-dimensional encapsulation. Additionally they show a higher selectivity then other ionophores due to their incapability to deformation. If using coronands and cryptands, the diameter of the corresponding ionic diameter should fit to the ligand cavity.
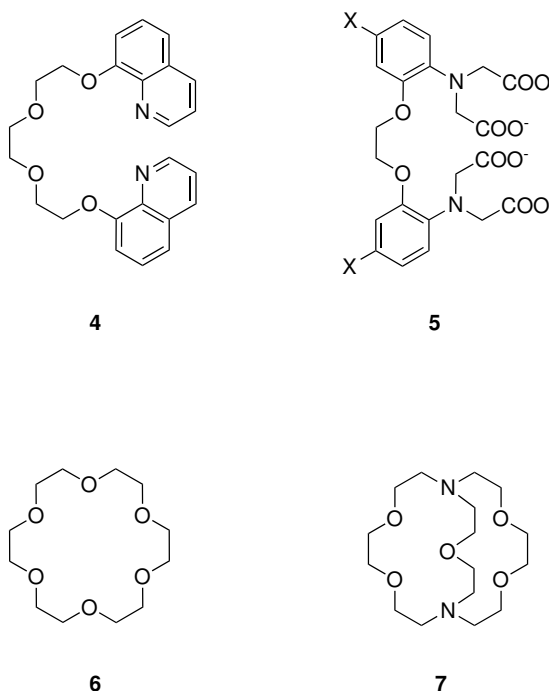

Figure 2.14: Example of a podand **4**, a chelator **5**, a coronand **6** and cryptand **7** which can be used for cation sensing.
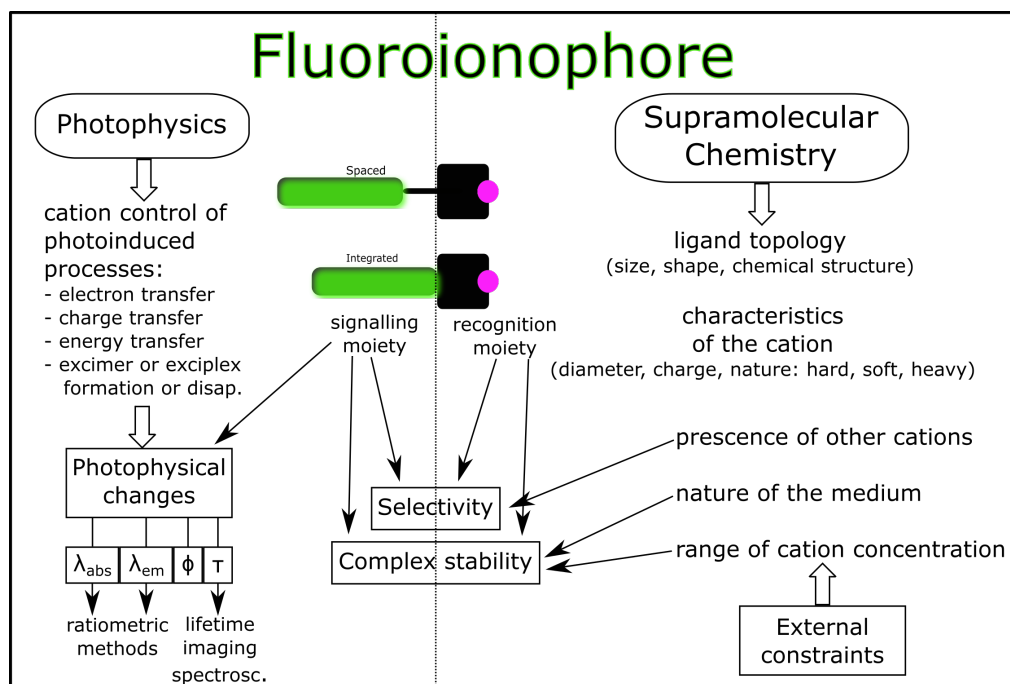
Figure 2.15: A fluoroionophore divided in its two major parts, the fluorophore and the recognition unit, as well as the main characteristics which have to be considered. [6]

Stabilities as well as the selectivities of the complexation of a cation are influenced by the medium (see figure 2.15). It has to be considered that there is a difference between ligand coordination energy and the solvation energy. For instance, there can be a difference in the solvating power of the ligand. There is also a difference in the interaction of the ligand shell and the outer dielectric medium of the first solvation shell. Furthermore in aqueous solutions, the ionic strength and pH plays an important role in complexation and their corresponding stabilities and selectivities.

Finding the highest change of photophysical properties caused by the cation is crucial. However if the fluorophore is either linked or spaced to the receptor, atoms or other groups (e.g. other ions) are participating in the complexation associated to the complexation.
Selectivity of the desired molecule/ion can be seen as a result of the entire fluoroionophore, both signaling and recognition moieties.

It should be considered that there is a variety in binding stoichiometry with the possibility of the existence that several complexes have a different stoichiometry. Recording of the fluorescence excitation spectra under consideration of contributing factors as close as possible to the desired medium of the cation has to be detected (e.g. solvents, medium composition, pH, ionic strenght). If the excitation and emission wavelengths (several emission and excitation wavelenghts) are analyzed as a function of the corresponding cation concentration, information

about the stoichiometry and its stability (stability constant of the complex) is gathered.

It has to be considered if talking about fluoroionophores that in general they are poorly soluble in water and often measurements are done in organic solvents or mixtures with water. However, this is not a drawback but an advantage for optode design, because if the fluoroionophore is immobilized in a polymer matrix or a sol-gel film, leaching problems are of minor relevance. Hence, such optical sensors are useful devices for biomedical applications as well as monitoring species in the environment.

2.3.6 Fluorescent Ion-Sensitive PET Sensors

PET Effect

Photoinduced electron transfer PET, occurs between an electron donor and an electron acceptor by which an excited electron is transferred. This results in either an exciplex in a non-polar solvent or a radical ion pair in dipolar solvent. The charge transfer returns the electron to the ground state without emission of light. At last, the electron on the acceptor is returned back to the electron donor. The basic principle for the electron transfer is the excitation of the donor and the acceptor. Electronically excited molecules possess a higher energy content than at their ground state and they are better reductants and oxidants.

Compared to RET (resonance-energy-transfer), the excited fluorophore can either be the electron donor or acceptor, whereas the direction of the electron transfer is set by the oxidation/reduction potential in the excited and ground state.

PET Quenching

The main requirement for the PET effect is that the HOMO of the donor (receptor) is energetically higher then the HOMO of the acceptor (fluorophore) or vice versa that the LUMO of the fluorophore is energetically higher as the one of the receptor, if the fluorophore is acting as the donor.
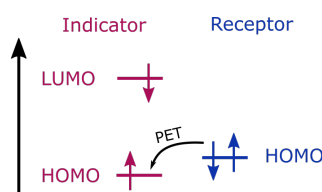

Figure 2.16: PET-fluorescence-quenching, molecular orbital energy diagram which shows the relative energetic disposition of the LUMO and HOMO orbitals of the fluorophore (acceptor) and the receptor (donor) in the analyte-free situation.

If the receptor binds a cation, the HOMO of the receptor is energetically reduced. The result of the reduction of the HOMO concludes that the electron transfer to the HOMO of the acceptor is not possible.
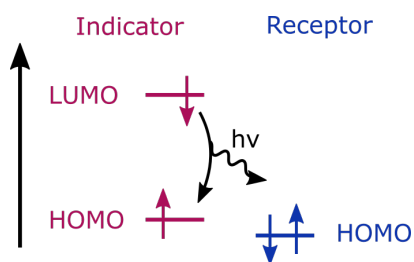
Figure 2.17: No PET-fluorescence-quenching, molecule orbital energy diagram in the analyte bound situation.

PET Sensors

More common, PET quenching is induced when the excited state of a fluorophore is acting as an electron acceptor. For instance, dimethylaniline (DMA) and its derivatives are electron-rich species, which are donating electrons to a broad range of aromatic systems which act as an acceptor. Moreover, quenching can occur by the transfer of electrons from an excited fluorophore to the quencher, for instance, the electron transfer from the excited state to an electron-deficient quencher.

In figure 2.18 the PET-concept in case of the presents of potassium and the corresponding fluoroionophore is illustrated. [7] In this case, when there is no analyte, the sensor is in the "off-state". If the molecule is excited, an electron transfer from the receptor to the fluorophore is allowed. This means that the excited state energy of the fluorophore provides enough energy for the reduction potential of the fluorophore and the oxidation potential of the receptor.
In the other scenario, when potassium occupies a place in the receptor it is in its "on-state". Thereby the analytes bound receptor HOMO is reduced to a lower energy below the energy level of the excited HOMO of the fluorophore, hence no PET-effect is observed. PET occurs if the oxidation potential of the receptor is in a smaller magnitude than the fluorophore.
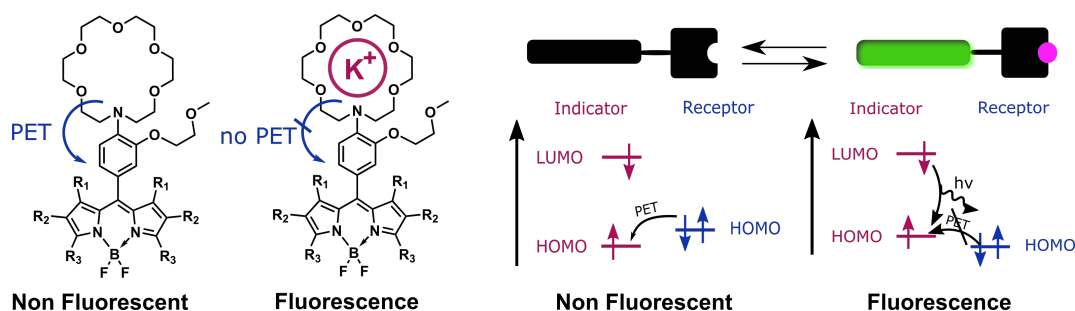

Figure 2.18: PET effect and its operating principle of a fluorescent K^+ probe. The enhancement of the fluorescence is caused by the complexation of K^+ and the corresponding reduction of the photoinduced electron transfer (PET).

2.4 Calcium Sensors

Fluorescent ion sensors are a powerful tool for sensing metal ions because of the high sensitivity, good selectivity, simplicity and their widespread applications in clinical diagnostics as well as environmental monitoring. [12, 13]

By mass, calcium is the fifth most abundant element in the earth crust. It plays a crucial role in biological and environmental processes. [14] The acidification of the ocean plays a enormous role in the food chain an the biodiversity in the ecosystem, hence the shells and skeletons are getting thinner or even stopped growing. Due to that of, measurement of calcium in the seawater is of great importance in the enviroment. [15]

Tsien [16] was the first one who published a calcium indicator with a high selectivity against magnesium and pH. They synthesised a derivative version of EGTA (Ethylene glycol-bis(2-aminoethylether)-N,N,N,N-tetraacetic acid) **8** which is well known for selective binding for calcium ions. BAPTA (1,2-bis(o-aminophenoxy)ethane-N,N,N,N-tetraacetic acid) **9** and the methoxyquinoline derivative **10** showed quite good sensitivity and selectivity in aqueous solution in the μM-range. Since then the development of new ionophores and indicator dyes steadily increased. [17, 18, 4, 19, 20, 21]
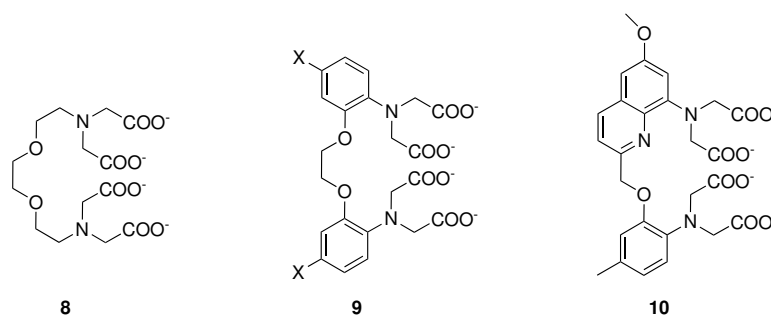

Figure 2.19: EGTA **8**, BAPTA **9** and the methoxyquinoline version **10** of BAPTA used as Ca^{2+} receptor.

One of the first groups using N-phenyliminodiethoxyacetic acid **11** (2.20) as a receptor for calcium were He [4] and Liu et al. [5]

Due to the sensitive range of BAPTA (μM) it is not suitable for the determination of extracellular ionized calcium. The N-phenyliminodiethoxyacetic acid **11** shows a dynamic sensitivity in the mM range, which makes it applicable for measurements in seawater.

Furthermore the receptor has to fulfil some other criteria. It must contain a tertiary nitrogen which acts as an electron donor during interaction with a bound calcium cation. (see PET-effect) Preferably the ionophore's binding properties should be insensitive to pH changes in the clinically or seawater important range to minimize undesired pH interferences. The dissociation

constant (K_d) in aqueous medium should be in the measuring range of 0.3-2.0 mM, as well as in the presence of blood concentrations of other cations. At least, a chemostability during wet storage is desired.
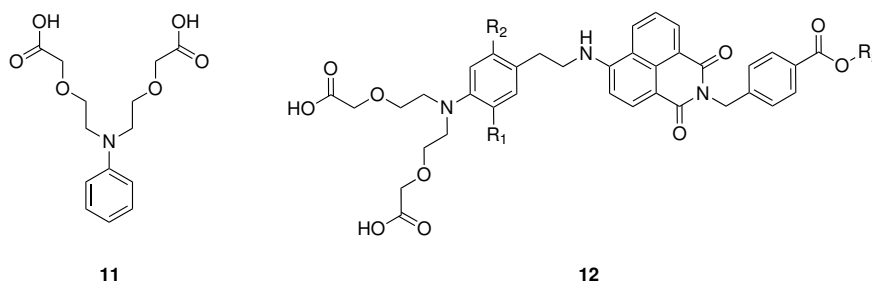

Figure 2.20: N-phenyliminodiethoxyacetic acid **11** as a receptor for calcium and the corresponding fluoroionophore **12** synthesised by He. [4]

2.5 BODIPY Dyes

In the year 1968, Treibs and Kreuzer discovered that the acylation of 2,4-dimethylpyrrole with acetic anhydride and boron trifluoride (Lewis acid catalyst) results in the formation of a highly fluorescent compound. Such compounds arose via an acid catalysed condensation of the appropriate pyrrole to a dipyrrin intermediate. Following complexation with boron difluoride leads to a highly fluorescent borondipyrromethene (BODIPY) dye **13**. [22]
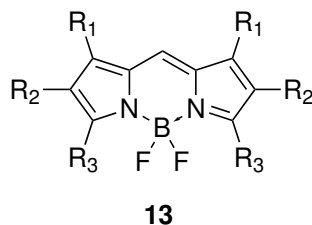
Figure 2.21: BODIPY.

BODIPY's are, in general, dyes that absorb light in visible range and show a high quantuum yield of fluorescence. [23] A further advantage of such compounds is their relatively sharp absorbance and emission. However,the dyes have a small Stokes shift. Such dyes are uncharged, and further, their characteristics are in most of the cases nearly independent of solvent polarities. Such complexes, posses a high stability in physilogical pH-range and decompose only in strong acidic and basic conditions. Those features make them excellent probes for biological systems and novel materials in the industry. [24, 25]

2.5.1 Synthetic Routes

In principle, there are two different synthetic routes to the borondipyrromethene intermediate, both are well known from the porphyrin research field. [26]

The condensation of aldehydes **14** with different pyrroles **15** affords dipyrromethanes **16** in an acidic medium (see figure 2.22). Due to the fact that dipyrromethanes **16** are unstable compounds because they are sensitive to light, acid and air, the best procedure is to use them directly after preparation. After formation of the dipyrromethane, oxidation with DDQ or p-chloranil yields dipyrromethene **17**, also called dipyrrin.

Treatment with base and boron trifluoride etherate yields the desired borondifluoride complex **18** in quite good yields if considered that this reaction is normally carried out in a one pot reaction.
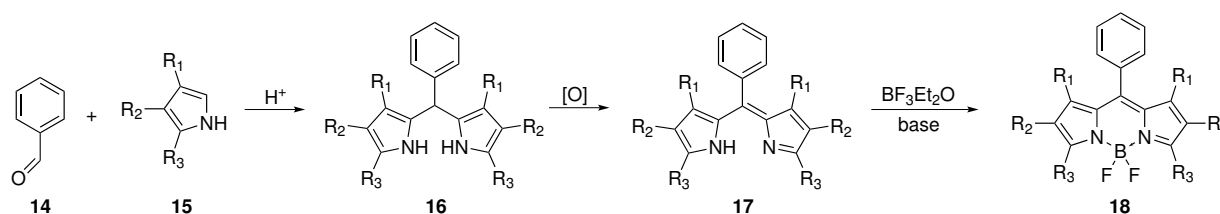
Figure 2.22: Typical BODIPY synthesis.

A slightly different approach uses a condensation reaction of a pyrrole **19** with a acylium equivalent **20** visualized in figure 2.23. The achieved acylpyrrole **21** is in general not isolated, as it is reacting with pyrrole to form a dipyrrin **22**. The corresponding acylium equivalent can either be an acid chloride, orthoester or an anhydride. This synthetic route offers the possibility for the synthesis of asymmetric dipyrrins, if the formed acylpyrrole is treated with a second pyrrole moiety. As before, the treatment with excess of base and boron trifluoride etherate yields in the desired BODIPY dye **23**.[27, 28, 29, 30]
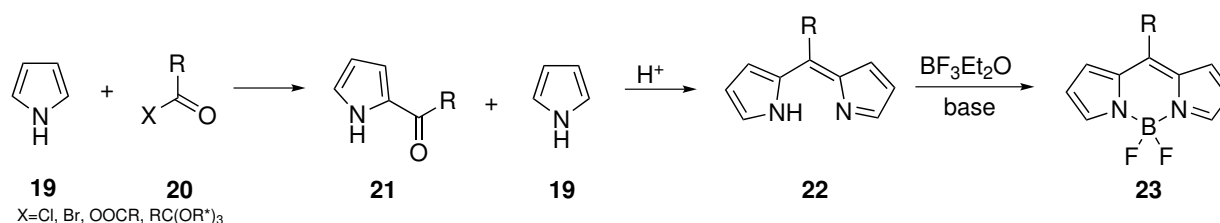

Figure 2.23: BODIPY synthesis via an acylpyrrole intermediate **21**.

2.5.2 Influence of Structural Factors on Spectral Properties

Using the standard synthetic approaches and combining them with different reactive systems (pyrroles) has lead to an enourmous amount of different structures. [31, 23]

Different substitution patterns result in a huge variety of spectral properties and characteristics. Even if the analysis of such compound is not always obvious and straightforward, there are some general trends which can be observed.

Worth mentioning, with increasing substitution of the dye, the stability improves, both the dye itself as well as its precursors (pyrroles). As it can be seen in figure 2.24 the introduction of alkyl groups **25** does not have a strong effect on the spectral properties of the dye and both dyes are highly fluorescent in polar media.

Meso-arylated dyes **26** normally show low quantum yields because fast rotation of the substituted aryl group acts as a non radiative pathway of decay. Blocking this rotation for example with methyl groups **27** dramatically improves the QY of the dye.
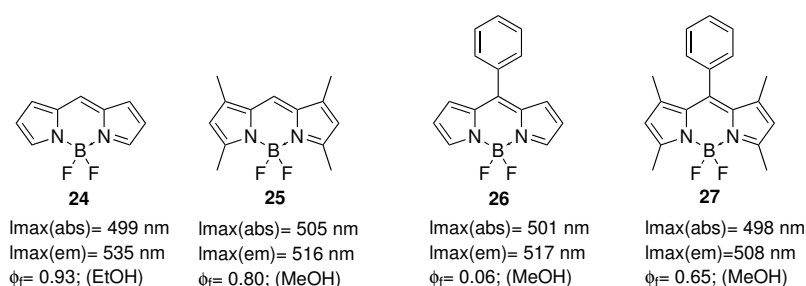

24
lmax(abs)= 499 nm
lmax(em)= 535 nm
ϕ_f= 0.93; (EtOH)

25
lmax(abs)= 505 nm
lmax(em)= 516 nm
ϕ_f= 0.80; (MeOH)

26
lmax(abs)= 501 nm
lmax(em)= 517 nm
ϕ_f= 0.06; (MeOH)

27
lmax(abs)= 498 nm
lmax(em)=508 nm
ϕ_f= 0.65; (MeOH)

Figure 2.24: Influence of alkyl and meso-aryl substituents on the spectroscopic properties.

Red shifts in the absorption and emission spectra can be achieved by increasing the conjugation of the dye. Introduction of a aryl group **28** in position 3,5 also called the α-position causes a shift to 555 nm (2.25) However, the aryl group is still free to rotate, thats why the red shift is not very strong. Locking this rotation **29** does not only cause higher quantum yield but also a larger bathochromic shift.
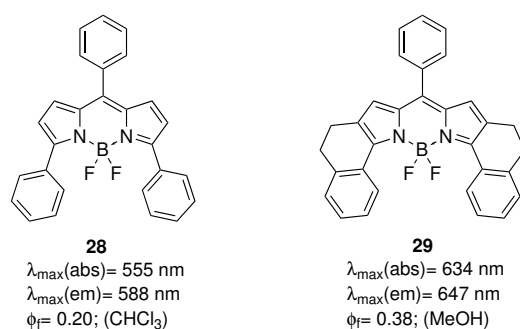

28
λ_{max}(abs)= 555 nm
λ_{max}(em)= 588 nm
ϕ_f= 0.20; (CHCl$_3$)

29
λ_{max}(abs)= 634 nm
λ_{max}(em)= 647 nm
ϕ_f= 0.38; (MeOH)

Figure 2.25: Extended conjugation, with **28** and without **29** restriction of the rotation.

Furthermore, the introduction of heteroatoms on the BODIPY dye have similar effects. In figure 2.26 the thiomethylated dye **30** has a red shifted emission and absorption maxima. This is also evident for the 3-sulfur-5-chloro substituted dye **31**, whereas it has lower quantuum yields because of the aryl substitution in the meso position.
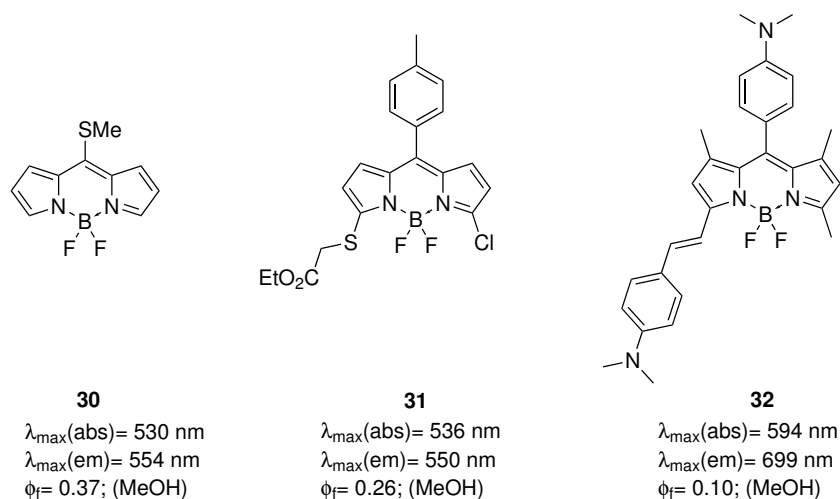

30	**31**	**32**
λ_{max}(abs)= 530 nm	λ_{max}(abs)= 536 nm	λ_{max}(abs)= 594 nm
λ_{max}(em)= 554 nm	λ_{max}(em)= 550 nm	λ_{max}(em)= 699 nm
ϕ_f= 0.37; (MeOH)	ϕ_f= 0.26; (MeOH)	ϕ_f= 0.10; (MeOH)

Figure 2.26: Directly substituted electron donating groups **30**, **31** and conjugated BODIPY dye **32**.

Knowing all these features by modifying BODIPY dyes helps for the identification of the target dye for a specific application. So with this knowledge, dyes with a high red shift and high quantum yields can be synthesized.

BODIPY Dyes in Optical Sensing

BODIPY dyes offer tunable optical properties with sharp peaks, show a high brightness with good quantum yields and large molar absorption coefficients.

Furthermore those dyes show a high thermal, chemical, pH and photo stability. If used in integrated systems they offer a good bio-compatibility, as well as fast response times and reversible applications when used as a fluoroionophore.

For example, measurement of pH using fluorescence-based techniques is established for imaging and sensing applications. (see figure 2.27)Using BODIPY dyes offers major advantages over other techniques due to the generally non-destructive character, high sensitivity and specificity and their huge range of indicator dyes available. [32, 31, 33, 34]
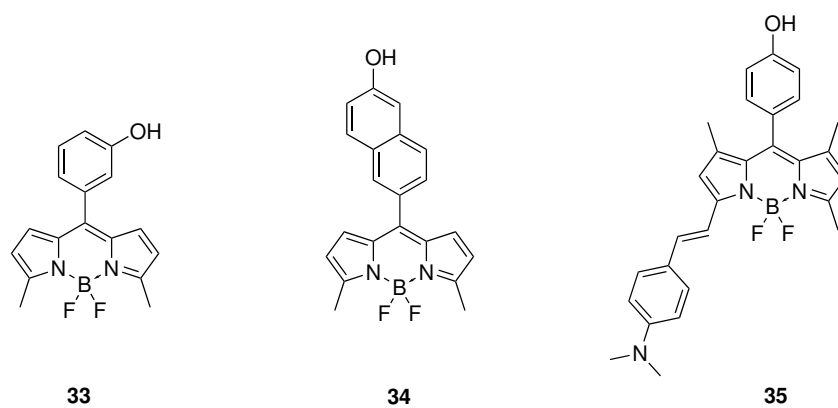
Figure 2.27: pH optodes based on OH-phenyl substituted BODIPY dyes with deprotonation/protonation dependent fluorescent on/off switching.

3 Materials and Methods

3.1 Structural and Chemical Measurements

3.1.1 NMR

The NMR spectra were recorded on a 300 MHz Bruker instrument (www.bruker.com). The analysis of the data was conducted with MNova NMR software (www.mestrelab.com).

3.1.2 Mass Spectrometry

Mass Spectrometry was performed on a Micromass TofSpec 2E Time-of-flight Spectrometer by Ing. Karin Bartl at the Institute for Chemistry and Technology of Materials, Graz University of Technology. The mass spectra were analysed with FlexAnalysis software (Bruker Daltonics).

3.2 Chromatography

3.2.1 Thin Layer Chromatography

TLC-plates from Merck (silica gel 60; F254) were used, and detected with UV as well as the corresponding staining agent. (KMnO$_4$, CAM, Bromcresol green, vanilin sulfuric acid)

3.2.2 Flash Column Chromatography

Silica gel from Acros Organics (0.035-0.070 mm, 60 Å) was used for preparative flash column chromatography. Depending on the separation problem different amounts of silica were used, whereas in general 80-100 fold of the amount of crude product was used. Normally the filling level was between 20 to 35 cm using the right column diameter.

3.3 Photophysical Measurements

3.3.1 Absorption

Absorption measurements were recorded between 800 nm and 350 nm using a Varian Cary 50 conc, UV-VIS spectrometer by Varian. (Palo Alto, United States, www.varianinc.com) The corresponding measurements were done using a fast scan rate with a baseline correction of the corresponding solvent. As cuvettes 10 mm Hellma Analytics 100-OS precision cuvettes were

used.

The listed molar absorption coefficients were measured by preparing solutions with the dye, using THF as solvent and calculating the coefficients with the Lambert-Beer law.

3.3.2 Emission and Excitation Spectra

The emission and excitation spectra were measured on a Hitachi-F-7000 spectrofluorometer in Hellma Analytics 100-OS (10 mm) precision cuvettes an *Fluorescence^{TM}* software.

3.3.3 Quantum Yields

A Fluorolog 3 Spectrofluorometer with a Quanta-ϕ integrating sphere from Horiba Scientific was used to measure Quantum yields. All QY's were measured in THF.

4 Results and Discussion

4.1 Synthetic Considerations
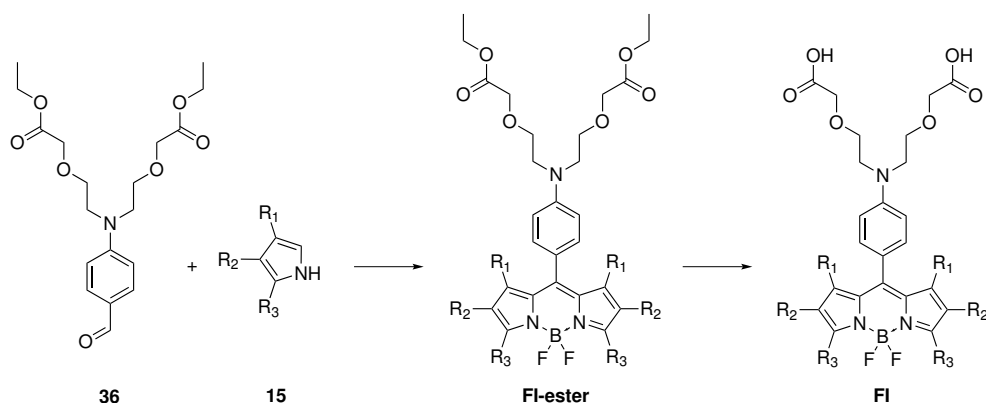
Figure 4.1: Synthesis-plan: The synthesis of a ion-sensitive Ca^{2+} chelator and further conversion to a fluoroionophore **FI** which can be used for optical ion sensing in solutions.

The aim of this work was the synthesis of a fluoroionophore **FI** which can be used for Ca^{2+}-ion sensing. Therefore the first goal was the synthesis of N-(4-Formyl)-phenylimino-diethoxyethylacetate **36** which acts as the receptor for ions. The aldehyde group of the chelator can be used for further synthesis to connect the receptor with a fluorescent dye. After deprotection of the ester, the photophysical properties were investigated either performing measurements in aqueous solutions or embedding the fluoroionophore in polymers and measure in different concentrations of Ca^{2+}.

4.2 Synthesis of Ca^{2+} chelating agents

4.2.1 N-(4-formyl)phenylimino-diethoxyethylacetate

The first approach was to synthesize the receptor as well as the corresponding aldehyde, which is suitable for the BODIPY synthesis. Therefore the 2-chloroethoxyethanol **37** was oxidized with HNO$_3$ as well as further protected with EtOH to form the corresponding ester **39**. This procedure is well known by the literature.[4]

The alkylation of aniline **40** was performed mixing 2-chloroethoxyacetate **39**, NMP, DIPEA and KI in a Schlenk tube and heating the solution in an oil bath for 3 days at 100°C.[5]

The formation of the aldehyde was performed via the typical Vilsmeier Haack reaction[35, 36]. As expected, the N-(4-formyl)phenylimino-diethoxyethylacetate **36** could be isolated in a quite good yield. (77%)
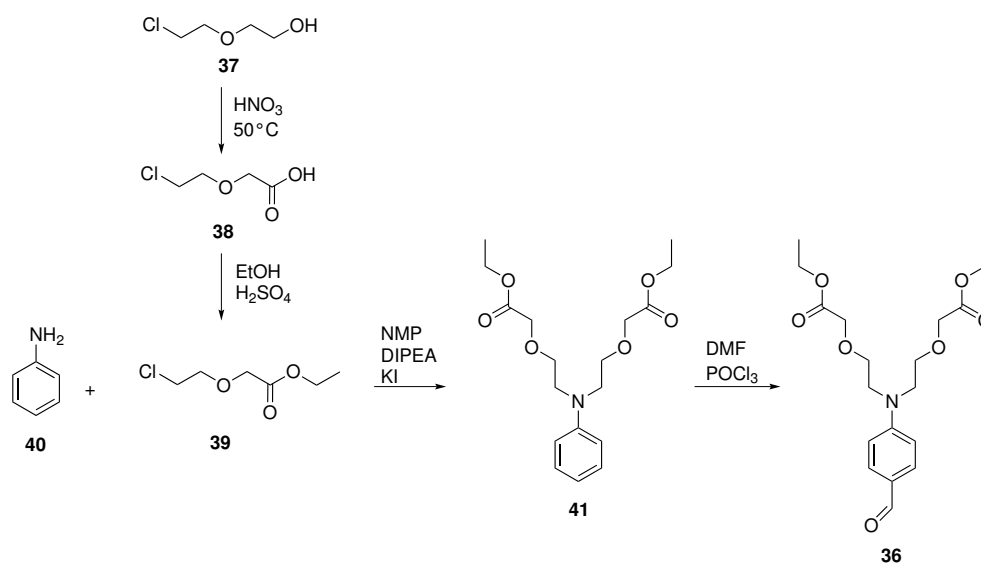
Figure 4.2: Synthetic strategy for the formation of the Ca^{2+}-receptor, which can be directly used for the BODIPY formation.

The synthesis of the Ca^{2+}-chelator seems easy and straight-forward. Nevertheless, several months of synthetic research were necessary for the development of the receptor building block. In figure 4.3 the synthetic strategies for the formation of the chelator are illustrated as an overview. The major problem of the mentioned synthetic strategies was the alkylation of the amine. Several different conditions, educts and solvents were tried. None of these reactions yielded to the desired product and described more in detail in the following pages.
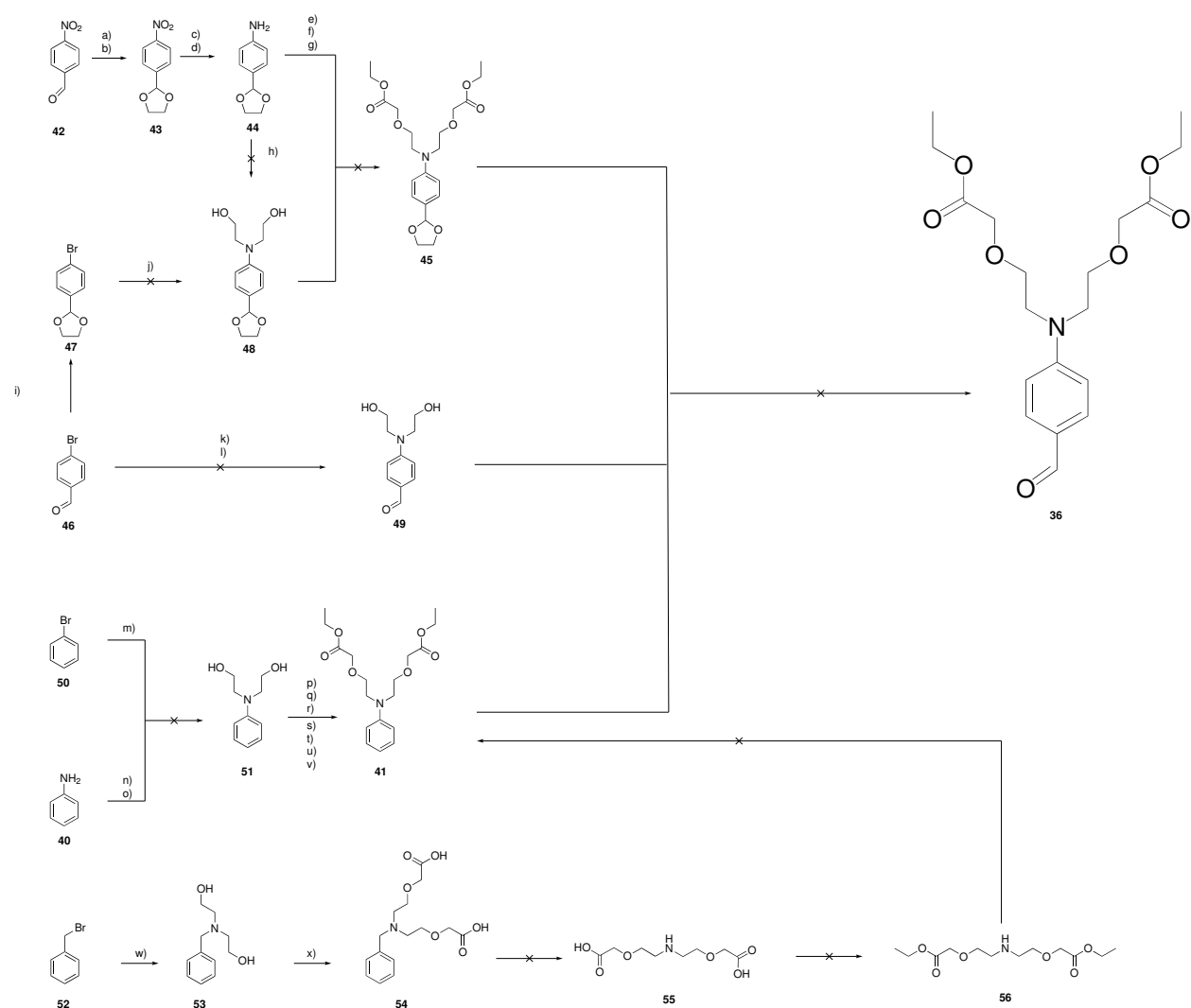
Figure 4.3: Overview of the performed synthesis-strategies for the Ca^{2+}-ion chelator **36**.

Originally planned synthesis

Originally it was planned to synthesize the receptor by using 4-nitrobenzaldehyde **42** and protect the aldehyde by using ethylene glycol in acidic conditions (reaction a and b). The protection worked out well and the following hydration with H$_2$ in different solvents (MeOH; DMF) was successful too. Further alkylation of the amine **44** using ethyl-2-chloroacetate **39** as reactive agent failed. A possible explanation could be that the protected aldehyde is electron withdrawing which hinders the alkylation of amines due to reduced electron density on the nitrogen atom. In contrast, the reaction worked out by using aniline instead of the protected version.
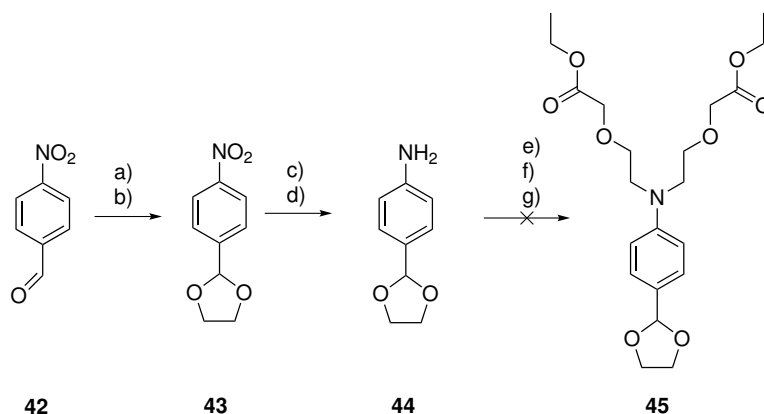
Figure 4.4: Original Ca^{2+} receptor synthesis plan.

Table 4.1: Reaction conditions for the originally planned synthesis.

#	educt	solvent	T [°C]	reagents	time [h]	yield [%]
a	ethylene glycol	CH	R.T.	H$_2$SO$_4$	62	70
b	ethylene glycol	Toluene	145	*p*TsOH	5	85
c	H$_2$	MeOH	R.T.	Pd/C	24	72
d	H$_2$	DMF	R.T.	Pd/C	24	96
e	ethyl-2-chloroacetate	NMP	100	DIPEA / KI	10	0
f	ethyl-2-chloroacetate	DMF	80	K$_2$CO$_3$ / KI	28	0
g	ethyl-2-chloroacetate	DMF	100	K$_2$CO$_3$ / KI	72	0

Synthesis of 2-[(4-[1,3]dioxolan-2-yl-phenyl)-(2-hydroxy-ethyl)-amino]-ethanol 48

In figure 4.5 the idea was the production of 2-[(4-[1,3]dioxolan-2-yl-phenyl)-(2-hydroxy-ethyl)-amino]-ethanol **48** which can be further used for the synthesis of the desired Ca^{2+}-receptor. Therefore 4-bromobenzaldehyde **46** was protected with ethylene glycol which worked out in good yields. The following alkylation of diethanolamine using the standard palladium-based

alkylation agent (Peppsi) in toluene did not worked out. Only educts where seen in TLC an no products were formed at all. The alkylation of 4-(1,3-dioxolan-2-yl)aniline **44** (reaction h) with 2-chloroethanol was unsuccessful too.
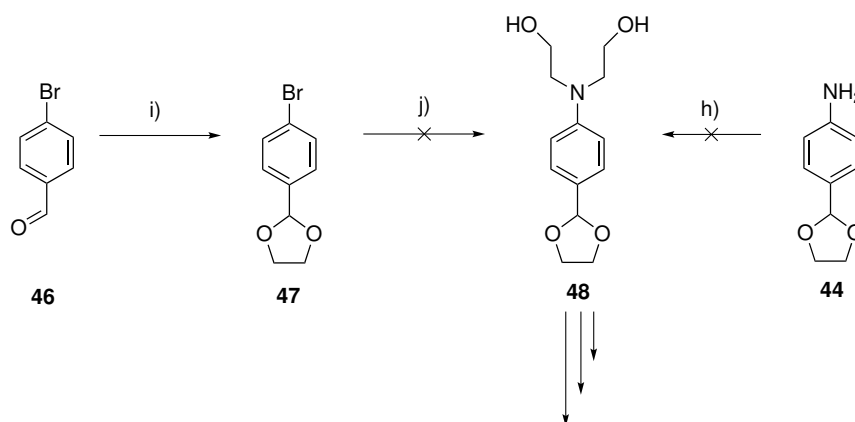

Figure 4.5: Different alkylation ways performed for the synthesis of 2-[(4-[1,3]dioxolan-2-yl-phenyl)-(2-hydroxy-ethyl)-amino]-ethanol **48**.

Table 4.2: Reaction conditions for the synthesis of 2-[(4-[1,3]dioxolan-2-yl-phenyl)-(2-hydroxy-ethyl)-amino]-ethanol **48**.

#	educt	solvent	T [°C]	reagents	time [h]	yield [%]
h	2-chloroethanol	H_2O	85	K_2CO_3	72	0
i	ethylene glycol	Toluene	140	pTsOH	6	89
j	diethanolamine	Toluene	90	Peppsi cat./KOtBu	30	0

Reactions with diethanolamine and 2-chloroethanol

Different alkylation reactions were performed to get the corresponding receptor-intermediate **49**, **51** (see figure 4.6). As it can bee seen in the associated table none of these reactions worked out. There was no product formation at all of the performed reactions according to TLC. Because of that, a reference experiment using diethylamine and bromobenzene **50** was made in toluene/Peppsi-cat./KOtBu and yielded with 52% of the desired product. Concluding that the polarity of the diethanolamine and the 2-chloroethanol has to play a role in alkylation reactions.

The attempt of using *N*-aryl diethanolamine, *t*-BuOH and chloroacetic acid according to Bartsch[37] failed. Furthermore the standard procedure of alkylation, using K_2CO_3/KI/DMF shown by He[4] failed too.
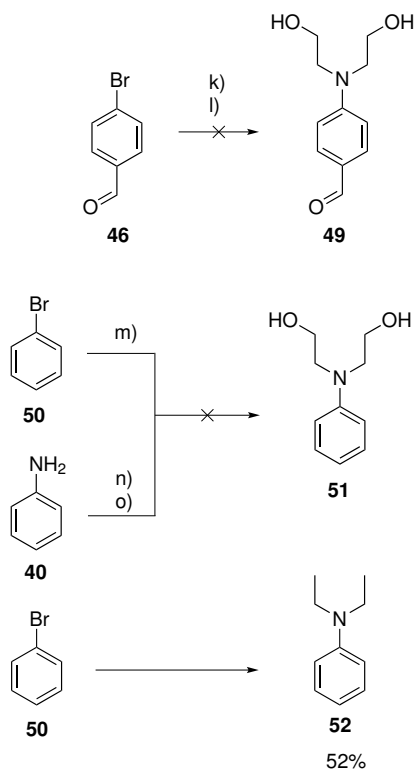
Figure 4.6: Unsuccessful alkylation reactions using different routes by choosing divers educts.

Table 4.3: Reaction conditions of the performed alkylations.

#	educt	solvent	T [°C]	reagents	time [h]	yield [%]
k	diethanolamine	acetone	65	Na$_2$CO$_3$	72	0
l	diethanolamine	Toluene	65	Peppsi cat. / KOtBu	72	0
m	diethanolamine	Toluene	90	Peppsi cat. / KOtBu	72	0
n	2-chloroethanol	H$_2$O	85	K$_2$CO$_3$	108	0
o	2-chloroethanol	H$_2$O	100	K$_2$CO$_3$ / KI	42	0

Reactions on *N*-phenyldiethanolamine 51

In figure 4.7 different reactions on *N*-phenyldiethanolamine **51** were made using either ethyl chloroacetate or ethyl bromoacetate. In this reaction the *N*-phenyldiethanolamine **51** was dissolved in different solvents (THF/dioxane/DMF) and the alcohol groups activated with either NaH/LDA/K$_2$CO$_3$ or with pure sodium. After this activation the alkoxide was formed, which could be seen via TLC due to the polarity-change. Afterwards, the second educt was added dropwise to the alkoxide solution. To summarize the performed reaction it is worth mentioning that by using the ethyl chloroacetate no product formation could be observed. The bromo-version was more reactive, or even too reactive because all of the gathered products were

identified as side products using NMR-spectra as the method of choice.
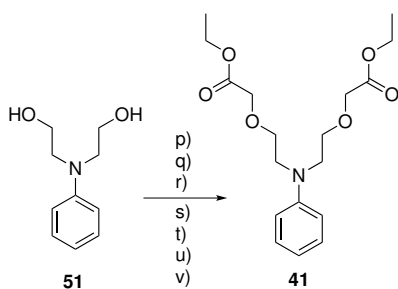
Figure 4.7: Reactions on *N*-phenyldiethanolamine.

Table 4.4: Reaction conditions for the reactions on *N*-Phenyldiethanolamine **51**.

#	educt	solvent	T [°C]	reagents	time [h]	yield [%]
p	ethyl chloroacetate	THF	R.T. –>60	NaH	144	2
q	ethyl chloroacetate	THF	-60 –>R.T.	NaH	4	0
r	ethyl chloroacetate	Dioxane	80°C	LDA	10	0
s	ethyl chloroacetate	THF	-10 –>70	Na	12	0
t	ethyl bromoacetate	THF	80	NaH	10	14
u	ethyl bromoacetate	THF	-70 –>R.T.	NaH	48	8
v	ethyl bromoacetate	DMF	R.T.	K$_2$CO$_3$	24	0

Synthesis of *N*-diethoxyethylacetate 56

The idea of the reaction in figure 4.8 was the synthesis of the receptor and couple it afterwards on the phenyl ring. Furthermore this strategy would offer the possibility to synthesize compounds were the receptor is connected to the fluorophore at different positions. The synthesis looked promising and the first two synthesis steps were successful. Nevertheless this synthetic route was not further investigated due to time reasons as well as in the meantime the desired receptor was successfully synthesized
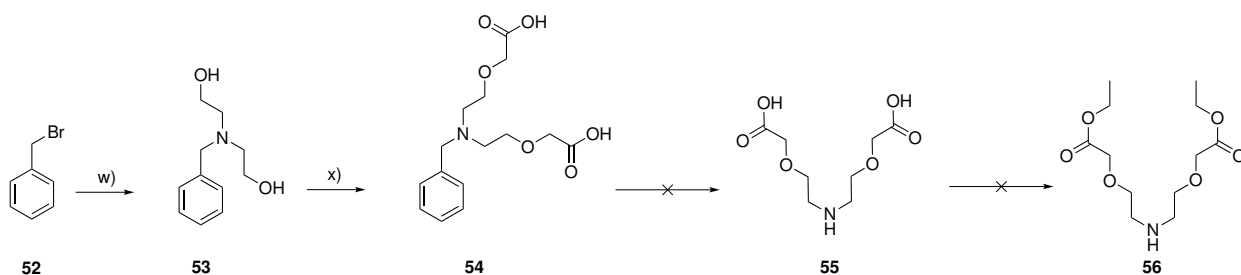
Figure 4.8: Synthetic strategy for *N*-diethoxyethylacetate **56**.

Table 4.5: Synthetic conditions for the synthesis of *N*-diethoxyethylacetate **56**

#	educt	solvent	T [°C]	reagents	time [h]	yield [%]
w	diethanolamine	acetone	63	Na_2CO_3	15	83
x	chloroacetic acid	THF	0 – R.T.	NaH	8	2

4.2.2 Sulfur-substituted Ca²⁺-receptor

A similar receptor was synthesised, where the oxygen is replaced by a sulfur. Therefore N-phenyldiethanolamine **51** was converted to 4-(bis(2-chloroethyl)amino)benzaldehyde **57** via the Vilsmeyer-Haack reaction, which is already known in the literature.[35] The purified compound was further treated with ethyl-2-mercaptoacetate **58** (2.3 eq Na; EtOH; 0°C) according to Fan et al.[39] to achieve the desired product **59**. (see figure 4.9)
After extraction with DCM and evaporation, NMR spectra indicated slight impurities as well as solvent and grease peaks. A purification via column chromatography was avoided, due to the toxicity of the ethyl-2-mercaptoacetate **58**.

Nevertheless, a derivative of the original Ca²⁺ receptor was synthesized The mercury concentrations in the ocean are mostly lower then 10 pM.[40] The concentration of interest concerning calcium is in the mM range. Although measurements were never done with this receptor, it can be assumed that there will be a cross sensitivity to mercury, due to the high affinity of sulfur to mercury. If so, this cross sensitivity can be neglected because of the relatively high concentration of calcium in the seawater.
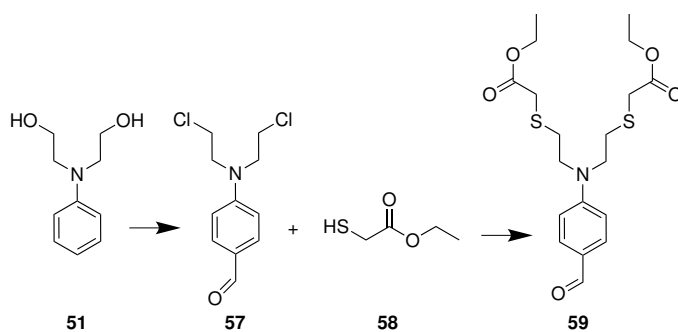
Figure 4.9: Synthesis of the sulfur substituted version of the receptor **59**.

4.2.3 BAPTA/BODIPY

In the second project the idea was the synthesis of a directly linked BAPTA/BODIPY fluoroionophore. 1,2-bis(o-aminophenoxy)ethane-N,N,N,N-tetraacetic acid, BAPTA **63** is used as a high affinity Ca^{2+} chelator. One of the first optical derivatives was synthesised by Tsien[16] in which the methylene links between oxygen and nitrogen are replaced by a benzene ring **60**, which can be seen in figure 4.10. Using BODIPY dyes, two possibilities are available. First the chelator (BAPTA) is linked on the 2,3-position of the dye **61**.[31] Alternatively, the receptor is directly linked to the BODIPY-dye **62**.[38] (see figure 4.10)
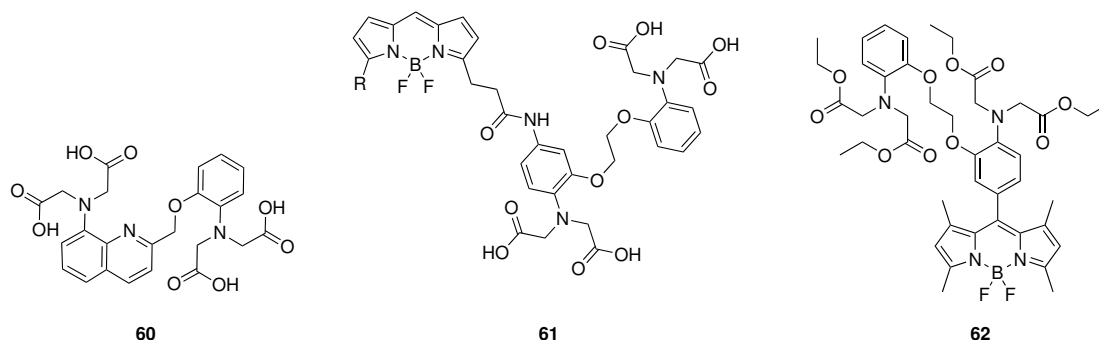
Figure 4.10: Left: one of the first BAPTA derivatives **60** used in optical ion sensing[16]; middle: coupling of the receptor on the side chain of a BODIPY dye **61** [31]; right: direct coupling of the dye **62**.[38]

The aim was to synthesise a BODIPY/BAPTA fluoroionophore which is directly linked together, to enhance the photoinduced electron transfer effect. Furthermore, a rigid pyrrole derivative, 5-chloro-3-phenyl-1,4-dihydroindeno[1,2-b]pyrrole, was used to achieve an emission wavelength higher than 600 nm.

In figure 4.11 the synthetic strategy can be seen. The first step was to protect the four acid groups **63** with an ethyl group. NMR spectra indicated that the conversion to a four times protected BAPTA molecule was incomplete. Separation via column chromatography failed. The BAPTA tetraethyl ester was bought from the company ABCR.
The next step was to introduce the aldehyde **65**, which is necessary for the BODIPY formation. Via the Vilsmeyer-Haack reaction the aldehyde group was introduced. 0.5 eq. of POCl$_3$ were used to achieve a monosubstituted product. According to NMR, 43 % of the product were converted to the corresponding aldehyde.

The formation of the BODIPY fluoroionophore **66** failed after several attempts due to some synthetic difficulties. In the first step of the synthesis, the BODIPY-formation, trifluoroacetic acid is added which forms an unconjugated precursor dye. At this point in the synthesis the molecule should be colourless, whereas the reaction solution became dark blue within seconds

after adding one drop of TFA. Further treatment with DDQ and complexation with TEA and BF$_3$OEt$_2$ indicated according to TLC no formation of the desired product.
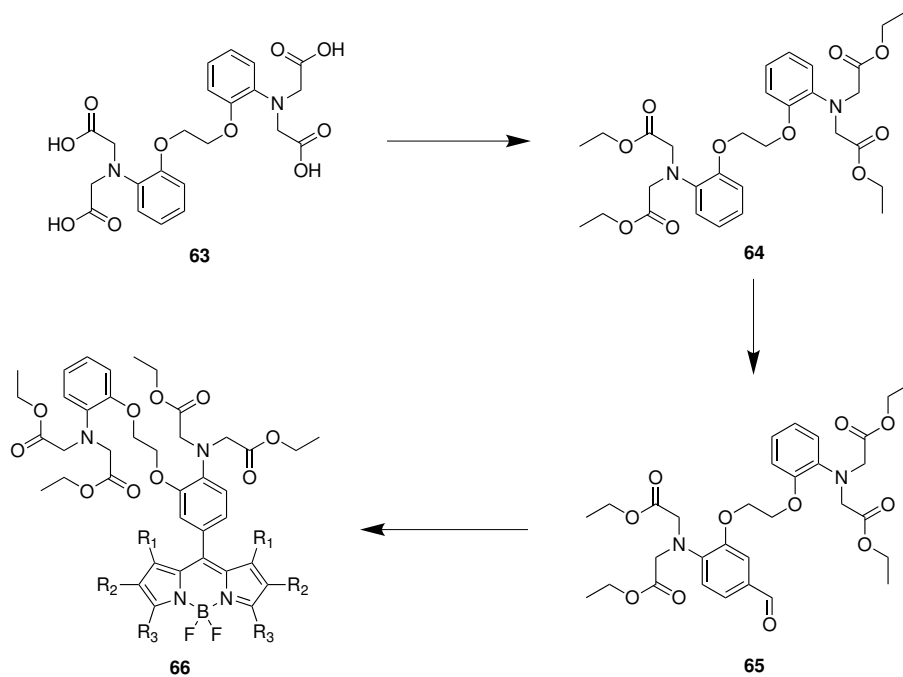
Figure 4.11: Synthetic strategy for the BAPTA fluoroionophore **66**.

4.3 Synthesis of Fluoroionophores

4.3.1 FI1-/FI2-ester

Figure 4.12: Synthesised fluoroionophores **FI1-ester** and **FI-2-ester** in the protected ester-version.

The fluoroionophore **FI1-ester** as well as **FI2-ester** were prepared according to the literature.[7] The purification was done twice via flash column chromatography. As a pretest a small amount of the product was dissolved in DCM and some drops TFA were added to protonate the amino-group. Hence, the HOMO of the receptor is energetically lowered and the electron transfer to the HOMO of the acceptor is not possible anymore, resulting in a fluorescent solution.

This test indicated besides the TLC, NMR-spectra and MS-data, that the synthesis worked out well and the formation of the fluoroionophore was successful.

4.3.2 FI1/FI2

Figure 4.13: Synthesised fluoroionophores **FI1** and **FI2**.

The deprotection of the ethyl group was done by LiOH in a mixture of THF/MeOH 1:1 at room temperature. The reaction was followed via TLC (DCM:MeOH=75:5), whereas the reaction was finished after no more educt as well as one time deprotected educt was visible. The attempt of recording a NMR-spectra, was successful for the compound **FI1**. For the fluoroionophore **FI2** different solvents were tested, but due to solubility problems no spectra of acceptable quality were recorded. A possible explanation for the insolubility is the hydrophobic BODIPY-dye and the hydrophilic receptor chains, which decrease the solubility limit enormously. A slight increase of the solubility was achieved, extracting the fluoroionophores in DCM/acidic H_2O.

4.3.3 Styryl-based fluoroionophore

Hirata et al.[41] presented the coordination of ion-recognizing groups at the styryl moiety at position 3 of the BODIPY chromophore. Therefore the ionophore **36** and the dye **69** is stirred in a solution of toluene, AcOH and piperidine at reflux, according to the known literature.[42, 43, 44] The synthesis of the BODIPY-dye was done by using 2,4-dimetylpyrrole **68** and 4-tert-butylbenzaldehyde **67**. NMR-spectra indicated a high H-grease peak. Further purification via column chromatography failed, but the absorption spectra of the dye (501 nm) corresponds to the known values from literature.[7]
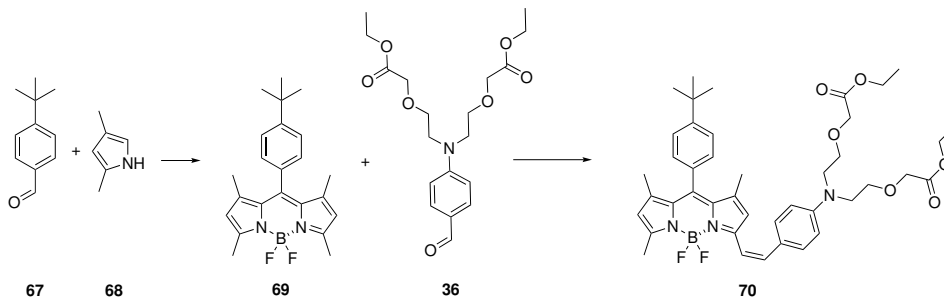
Figure 4.14: Synthetic strategy of a styryl-based BODIPY fluoroionophore **70**.

TLC indicated product, educt and some side products. Separation via column chromatography seemed to work out well. The absorption spectra indicated a bathochromic shift from 102 nm to 603 nm. The extension of the π-conjugation causes an intensity change and wavelength shift of the absorption/emission spectra, which can be explained via the change of the electronic environment/system.[41] This chemical shift can be seen in figure 4.15. Further purification via column chromatography as well as recrystallisation failed, however this experiment has to be considered as an promising approach.
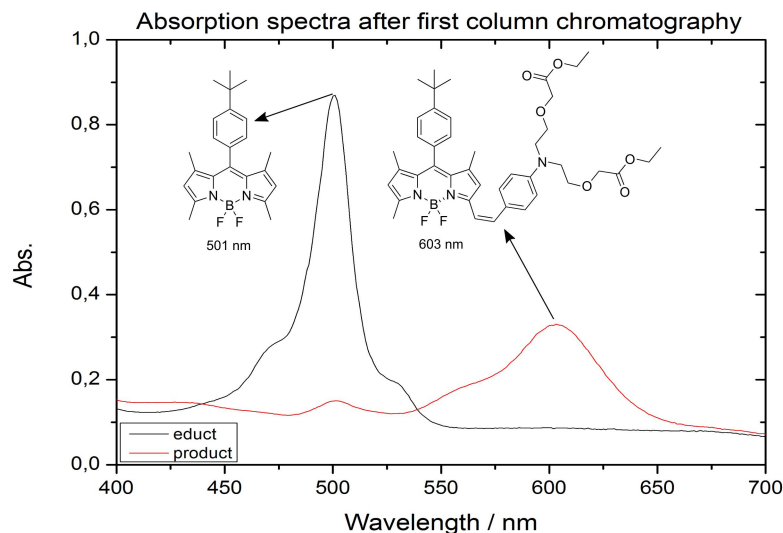
Figure 4.15: Bathochromic shift of a styryl-based BODIPY fluoroionophore, covalently linked to the receptor.

4.3.4 Synthesis of an asymmetric dye

In figure 4.16 the synthesis of an asymmetric BODIPY dye **72** is shown. This reaction with two different pyrroles (2,4-dimetylpyrrole **68** and 5-chloro-3-phenyl-1,4-dihydroindeno[1,2-b]pyrrole **71**) would offer 2 major advantages. First, of all the coupling of the receptor similar to figure 4.15 would lead to a mono-substituted product and allows an usage of an excessive amount of the desired chelator. Second, the reaction gives an information about the reactivity of the pyrrole in the BODIPY formation, which gives information about optimizing procedures in synthesis of fluoroionophores.
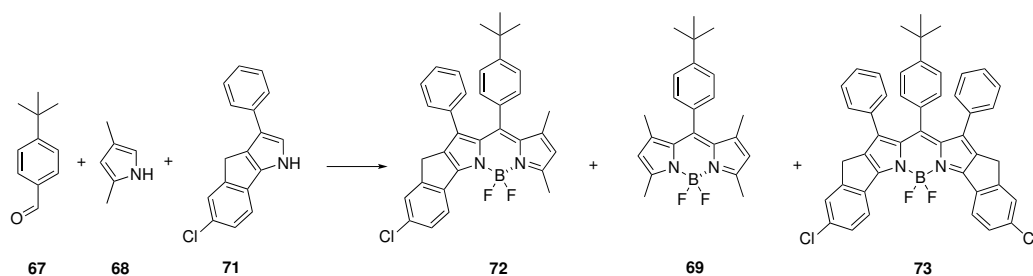
Figure 4.16: Synthesis of an asymmetric BODIPY dye **72** using different pyrroles as educts for the BODIPY synthesis and symmetrical by-products **69** + **73**.

BODIPY synthesis of the desired asymmetric dye **72** worked out good. Three products were obtained from the synthesis, the asymmetric product **72** at 562 nm (49%) as well as the symmetric products **69** and **73**, with an absorptionmaximum at 501 nm and 631 nm. (see

figure 4.17) It shows that the reactivity of the pyrroles are equal, because the asymmetric version is obtained with nearly 50% yield, whereas the other products were obtained in the same amount. This offers the opportunity for further synthesis to use mixtures of two different pyrroles. With this strategy, using a single one pot reaction three different products can be obtained with a single column chromatography, resulting in an enormous time saving synthesis. Furthermore, the asymmetric version is interesting for further modification on a single position of the dye, for example if the molecule in figure 4.17 would be bromo-substituted instead of the chloro-version, Suzuki-Miyaura reaction, Heck-reaction or Negishi coupling would be possible.

Coupling of the receptor to the asymmetric BODIPY version **72** was not done due to time reasons. The asymmetric fluoroionophore (see figure 4.16) would be an interesting alternative to the symmetric one (see figure 4.15) because a bathochromic shift of about 100 nm similar as presented before would be expected. This would cause an expected shift from 562 nm to approximately 664 nm, which would be in the optimum range for exciting with red light and resulting in an emission in the red/NIR part of the spectrum. [7]
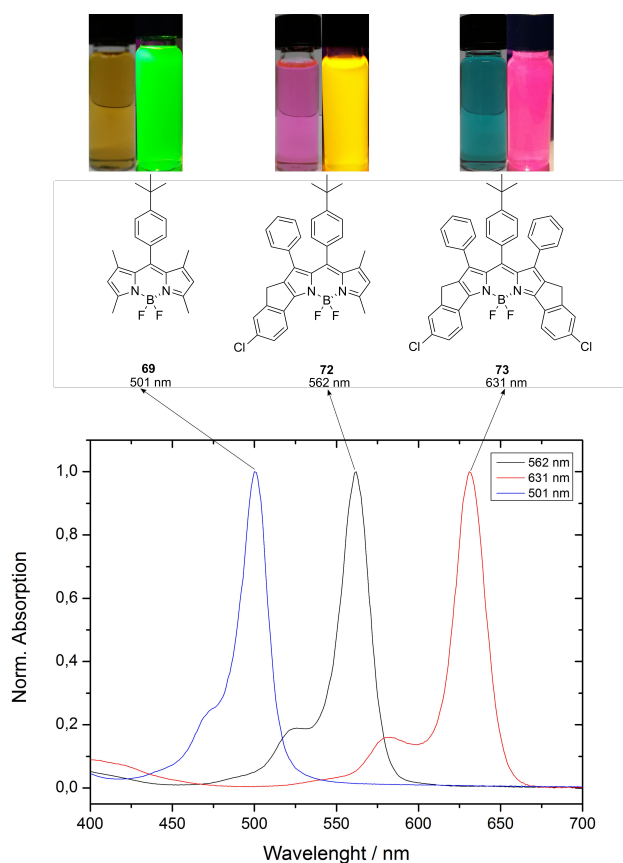
Figure 4.17: BODIPY dyes obtained in the asymmetric synthesis. Above: Photographic images under daylight illumination (left) and under excitation with UV light (right). Below: Corresponding absorption spectra.

4.4 Fluoroionophore Characterization

4.4.1 General

In figure 4.18 the synthesized dyes and fluoroionophores are illustrated. Dye **69** has an absorption maxima at 500 nm, whereas with increasing rigidity and conjugation of the π-system of the dye the absorption as well as the emission spectra are bathochromically shifted.
The replacement of one 2,4-dimethylpyrrole **68** by a 5-chloro-3-phenyl-1,4-dihydroindeno[1,2-b]pyrrole **71** (Dye **72**) causes a red shift of 60 nm to 560 nm and the disubstituted version (Dye **73**) a shift of 130 nm to 630 nm (measured in THF).

As mentioned above, comparing the fluoroionophores **FI1-ester** and **FI2-ester** the same trend is observed. **FI1-ester**, the rigid version shows an absorption at 625 nm. In comparison, the 2-(4-propylphenyl)-4-phenylpyrrole substituted receptor **FI2-ester** is hypsochromically shifted due to the reduced rigidity and conjugation. In case of **70**, the ion-recognizing group is substituted at position 3 of the chromophore which causes a red shift from 500 nm to 605 nm. The extension of the π-conjugation, causes a fluorescence intensity change of the absorption/emission spectra. [41, 45, 46, 42, 47, 48]
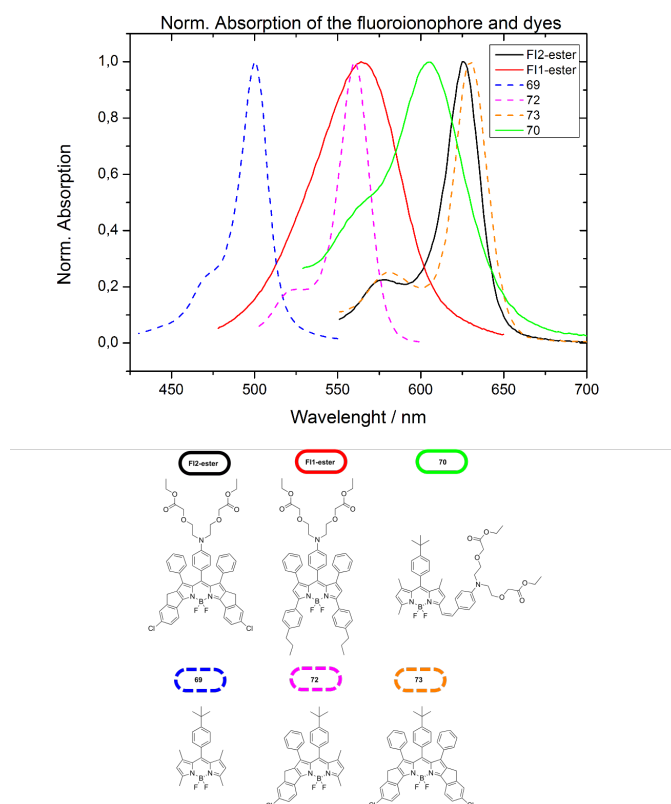
Figure 4.18: Absorption spectra of the synthesized dyes and fluoroionophores.

The measured molar absorption coefficients ϵ, lifetimes and quantum yields are similar as reported in literature. [23] Similar to data reported by Müller et al. [7] the rigid version of the fluorophore has a higher ϵ, longer lifetime and higher quantuum yields, compared to the non-rigid-version, **FI2-ester**.

Beside the bathochromic shift of the illustrated dyes, with increasing rigidity the lifetimes and the molar absorption coefficients are increasing as well, whereas no significant trend was observed in quantuum yields.

Table 4.6: Summary of produced dyes and fluoroionophores

sample	M	λ	ϵ	Lifetime in THF	QY in THF
	[g/mol]	max abs [nm]	[M^{-1} cm^{-1}]	[ns]	0.15 M TFA
FI1-ester	940.66	625	102000	3.9	0.73
FI2-ester	931.91	564	58000	3.8	0.59
70	743.69	605	n.d.	3.2	0.47
69	380.28	500	69000	3.5	0.44
72	550.88	560	85000	4.6	0.63
73	721.47	630	96000	4.8	0.56

4.4.2 Calibrations of FI1 in Aqueous Solution

Calibration of the fluoroionophores **FI1** and **FI2** were made in aqueous solution (H$_2$O:EtOH=1:1) and were measured within one minute after mixing the Ca^{2+}-puffer solution (20 mM TRIS, pH=7.4) with the dye solution (1 mg/ml).

The fluoroionophore **FI1** shows an emission maximum at 611 nm, the similar dye reported by Müller et al. [7] (615 nm). The hypsochromic shift is plausible, because in this case the fluoroionophore has not a methoxyethoxy group in the para position of the phenyl ring of the receptor. This concept is proven by Loudet and Burgess[23] which show that the introduction of electron donating groups to the BODIPY core causes an bathochromic shift (red shift) of the absorption and the emission spectra.

The fluoroionophore **FI1** shows a good sensitivity in the range from 0-150 mM as well as an enhancement of the fluorescent by a factor of 53 compared to the sample with 0 mM Ca^{2+}. A linear behaviour ca be seen in figure 4.19 from 12.5 to 150 mM in aqueous solution.
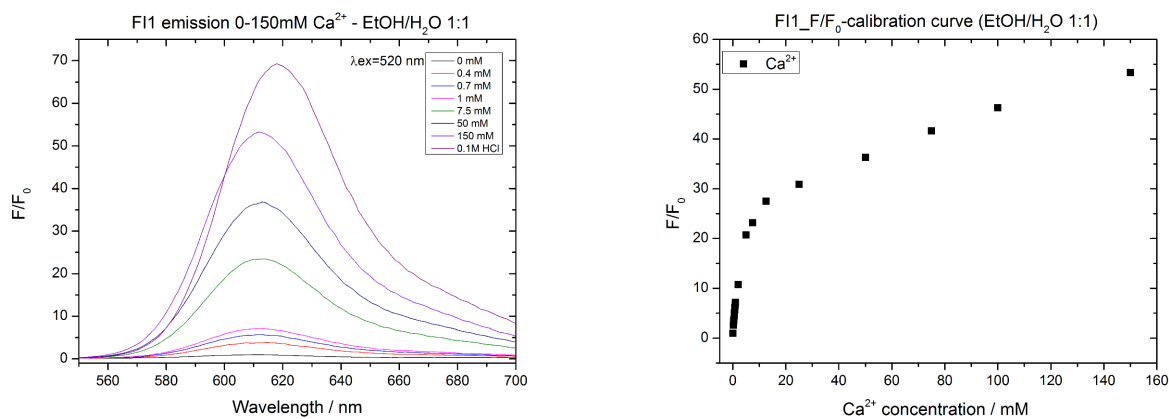
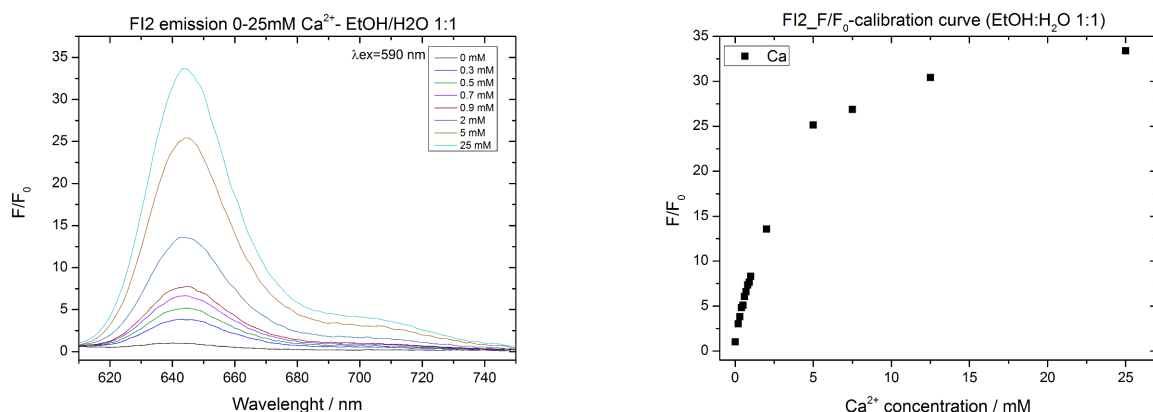**Figure 4.19:** Emission spectra and F/F_0 calibration curve of the fluoroionophore **FI1** for the concentration range 0 to 150 mM, measured in $EtOH/H_2O$ (1:1) using an excitation wavelength at 520 nm.

In figure 4.20 it can be seen that the receptor is already sensitive in the µM-range. Calibrations were made from 0 to 25 µM Ca^{2+}. An enhancement factor of 2.6 in fluorescence at an concentration of 200 µM was observed in aqueous solution and a linear behaviour exists from 0 to 2 mM Ca^{2+}
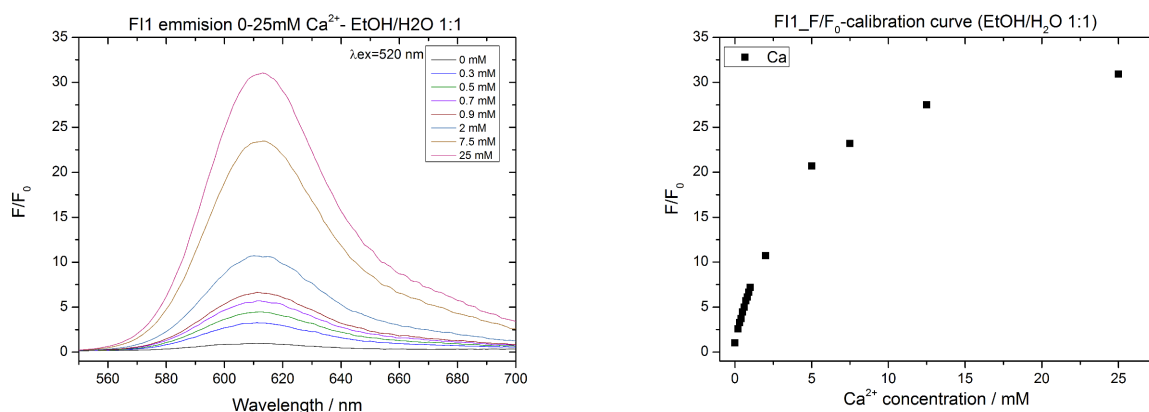
Figure 4.20: Emission spectra and F/F_0 calibration curve of the fluoroionophore **FI1** for the concentration range 0 to 25 mM using an excitation wavelength at 520 nm.

Cross Sensitivity

Cross sensitivity was tested for sodium and magnesium using the **FI1** ionophore. In figure 4.21 it can be seen that the receptor shows nearly no sensitivity to sodium and magnesium, in a solution of H_2O:EtOH=1:1. The highest response was observed at a concentration of $0.2\,mM$ Mg^{2+} (F/F_0=1.33) which can be compared to the value for calcium at the same concentration (F/F_0=2.6) nearly neglected. Astonishingly, even for high ion concentrations the response kept constant around an F/F_0 value of 0.8 to 1.2 over the whole concentration range.

This experiment shows the evidence that this receptor has a good selectivity towards other ions.
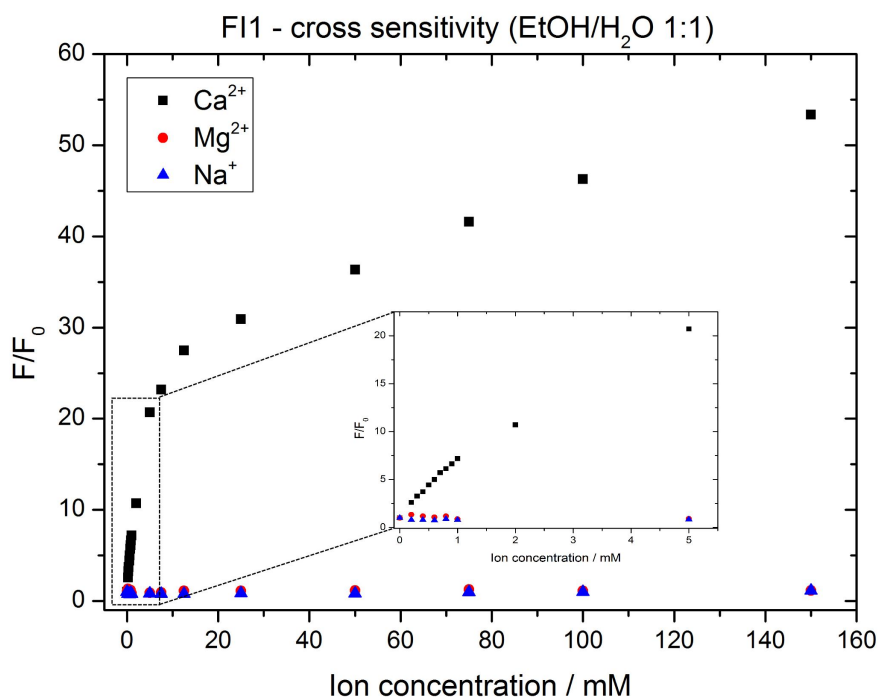
Figure 4.21: Cross sensitivity of sodium and magnesium from 0-$150\,mM$.

4.4.3 Calibrations of FI2 in Aqueous Solution

The sensitivity of **FI2** was measured from 0-$250\,mM$ and shows a great response even at high concentrations. A linear behaviour of the dye was observed in the range of 12.5 to $250\,mM$ Ca^{2+}. An enhancement of the fluorescence by a factor of 84 ($250\,mM$) compared to the sample with $0\,mM$ Ca^{2+} was observed. In aqueous solution in absence of Ca^{2+} the fluorescence of the dye is completely switched off and increases from 0 to $5\,mM$ by a factor of 21.
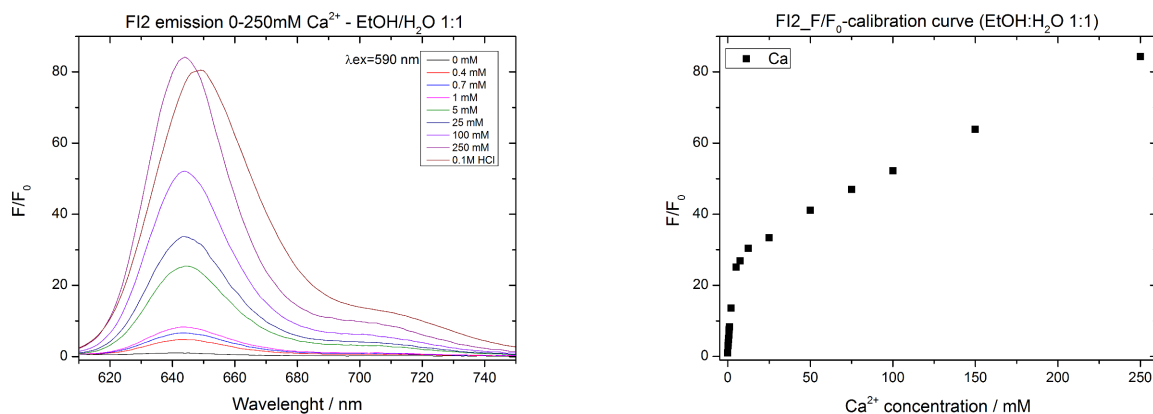
Figure 4.22: Emission spectra and F/F_0 calibration curve of the fluoroionophore **FI2** from 0 to 250 mM using an excitation wavelength at 590 nm.

The fluoroionophore was also characterized at low concentrations from 0 to 25 mM as well as in the µM range. The **FI2** system worked like the **FI1** in the µM range. The difference between the dyes exists in the linearity. While the **FI1** showed a linear tendency up to 2 mM, the rigid version achieves a linear trend up to 5 mM and starts to flatten afterwards until it gets linear again at 12.5 mM. (see figure 4.23) This behaviour can not be explained without further investigation.

Figure 4.23: Emission spectra and F/F_0 calibration curve of the fluoroionophore **FI2** in the concentration range 0 to 250 mM using an excitation wavelength at 590 nm.

Cross Sensitivity

Cross sensitivities were measured up to 150 mM for magnesium and sodium. Highest response was achieved for sodium (F/F_0=1.7) at an concentration of 150 mM. Sensitivities at low concentrations were not observed, which confirms that this receptor dye is applicable for measuring calcium in aqueous solution.
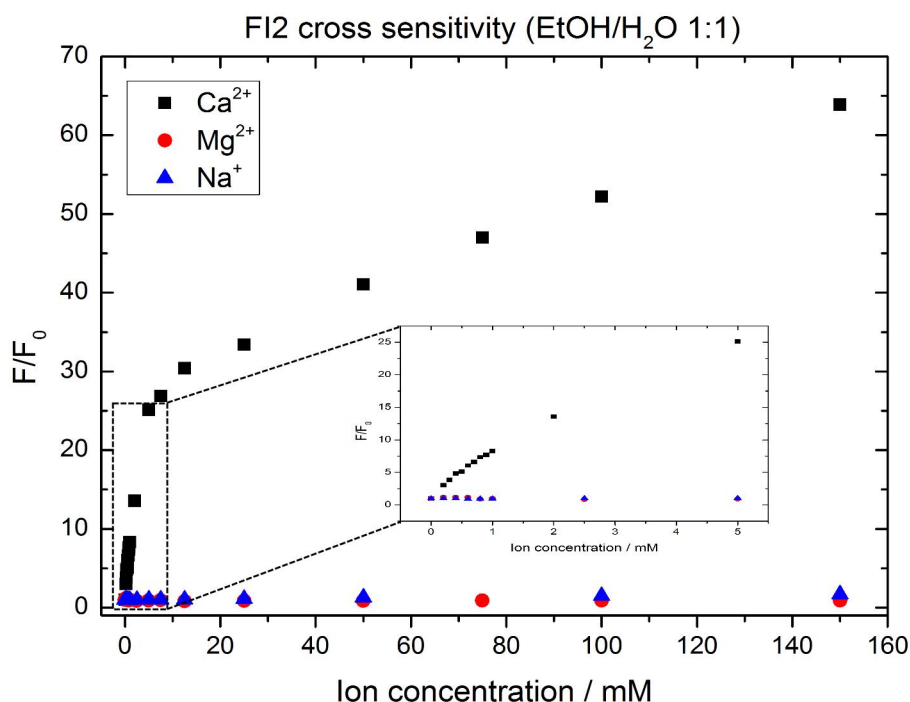
Figure 4.24: Cross sensitivity of sodium and magnesium from 0-150 mM.

4.4.4 Polymer Screening

Hydrogels are suitable for the measurement of ions in aqueous solution because they absorb water (70,50 and 30% for HydroMed D1,D4 and D7). [49] Furthermore they are suitable for a wide variety of applications, eg. contact lenses, wound dressings, drug delivery, tissue engineering, hygenic products.[50, 51] In addition the fluoroionophores are measured in pHEMA, which is a homogeneous polymer.

The fluoroionophores **FI1** and **FI2** were measured in different polymers, using different hydrogels and the exact same conditions. Therefore a 0.5 w% dye - polymersolution in EtOH:H_2O 1:1 was knife coated with a doctor blade (1 MIL). Afterwards the foils were dried in the oven for 1 hour at 60°C. Measurements were done using a cuvette, were the foil was placed in a 45 degree angle.

The screening was performed in the polymers mentioned above and can be seen in figure 4.25. The polymers were measured from 0 to 150 mM Ca^{2+} concentrations. A peak in the emission spectra at ~720nm indicates formation of aggregates.

Obviously the formation of aggregates is favored in unpolar hydrogels like D7 compared to D1. The fluorescence is increasing for D7 in the range from 660 to 750 nm greater then the one for D1 and D4. Measurements in pHEMA can be seen as not interpretable, because aggregation in the hypsochromic region allready occurs and influences the emission spectra in a way that interpretation of the data meaningless.
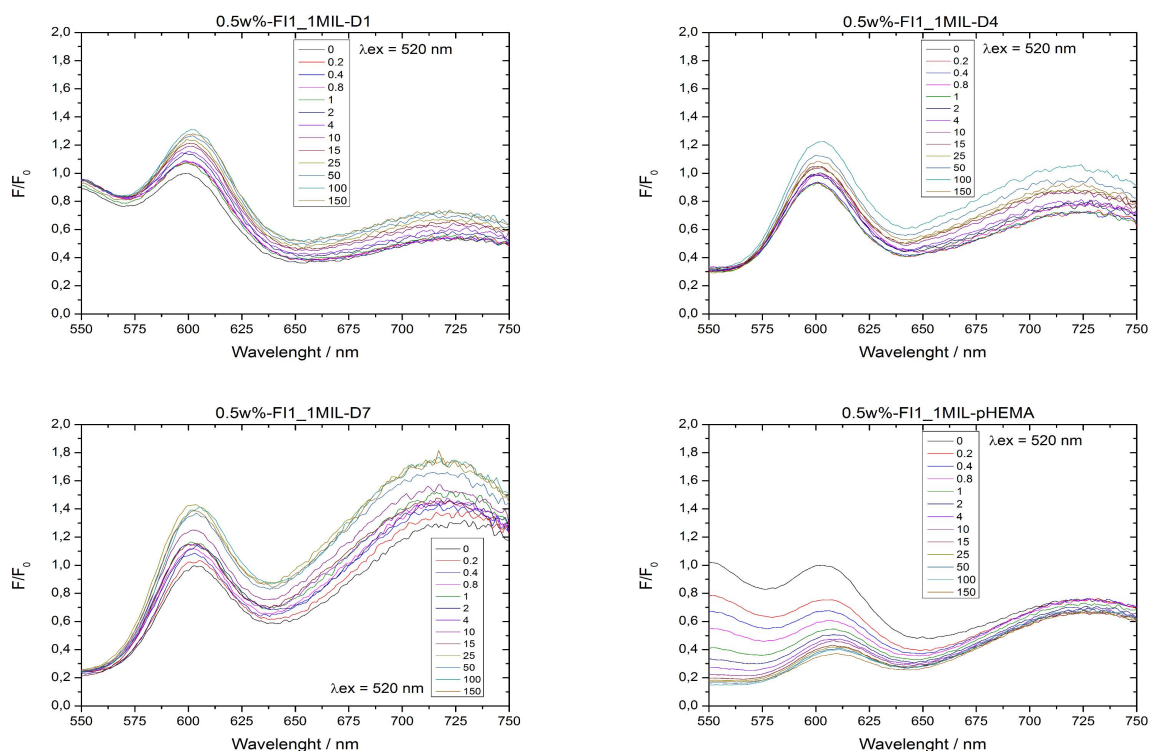
Figure 4.25: Polymer screening of fluoroionophore **FI1**.

Comparing the hydrogels is difficult due to the high aggregation. However, it seems like the fluoroionophore in combination with the hydrogel D7 provides the highest F/F_0 values, whereas the usage of D4 yields in the most favourable curve in the spectrum. Due to the low emission response of the dye in the hydrogels the F/F_0 value at 0 mM is the most important, because it influences the whole outcome, which makes the comparison of different hydrogels challenging. To overcome aggregation, a modification of the dye to a more polar fluoroionophore, would allow better results in hydrogels like D1 and D4.
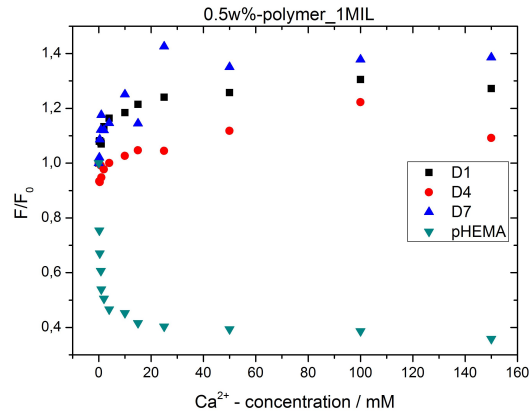
Figure 4.26: F/F_0 calibration curve of the fluoroionophore **FI1** in different hydrogels.

The fluoroionophore **FI2**, seems to work out better in hydrogels than **FI1**. Aggregation problems are not so pronounced even though the same tendency is evident. The most polar hydrogel, D1 shows the lowest aggregation tendency, D7 the highest. Instead, vice versa, the hydrogel D7 shows the highest F/F_0 response. Measurements in pHEMA are not easy interpretable like the one in FI1, but if comparing them, aggregation in the hypsochromic region is not present any more.
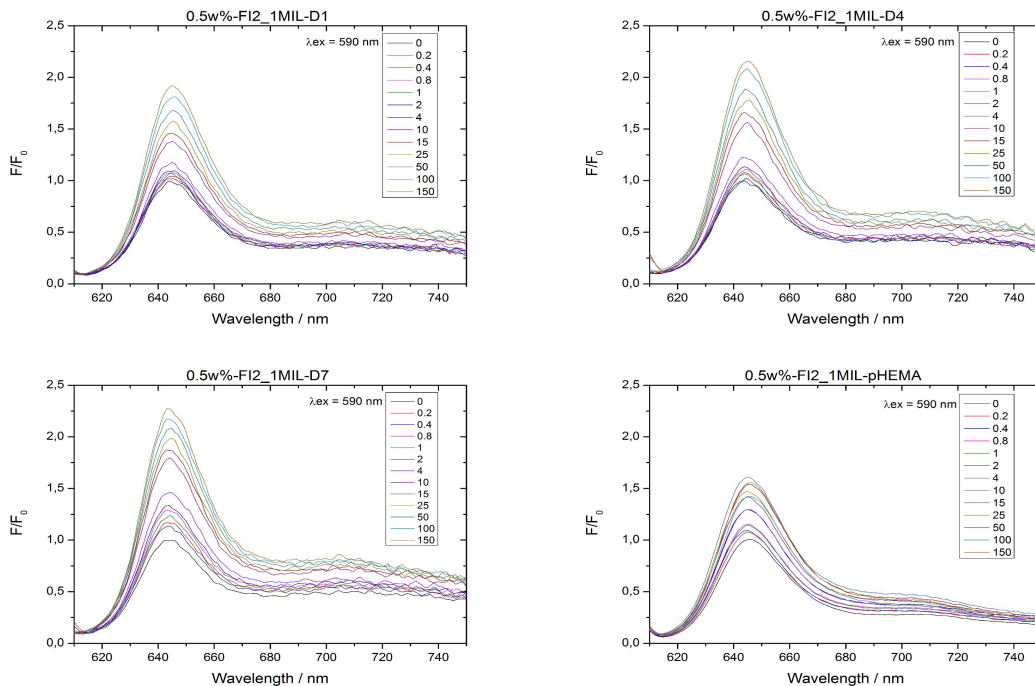
Figure 4.27: Polymer screening of fluoroionophore **FI2**.

Like previously mentioned, the interpretation and the comparison of the different hydrogels is not easy or have to be considered with caution. The F/F_0 values strongly depend on the $0\,mM$ value as well as the aggregation in the different hydrogels makes a comparison difficult. Nevertheless, FI2 in D7 yielded the highest response, whereas D1 resulted in the weakest signals. Further improvement of the matrices as well as the fluoroionophores is unavoidable, for measurements of Ca^{2+} ions in aqueous solutions.
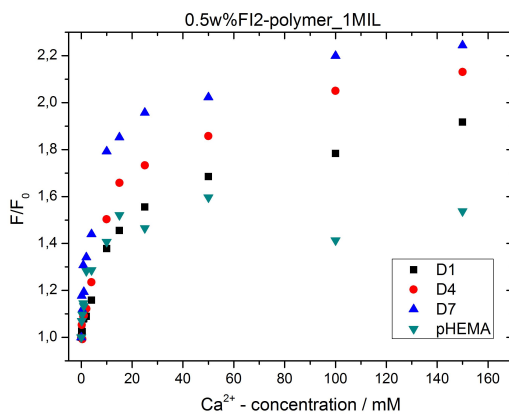
Figure 4.28: F/F_0 calibration curve of the fluoroionophore **FI2** in different hydrogels.

4.5 Outlook

4.5.1 Strategies to prevent aggregation in hydrogels

Due to the fact, that the measurements in the polymers were not that promising, the aggregation problems have to be improved. Therefore the idea arises to modify the BODIPY dye, with the introduction of a butoxy group **78**.(see figure 4.29) This butoxy group would reduce $\pi - \pi$ stacking of the planar pyrrols.
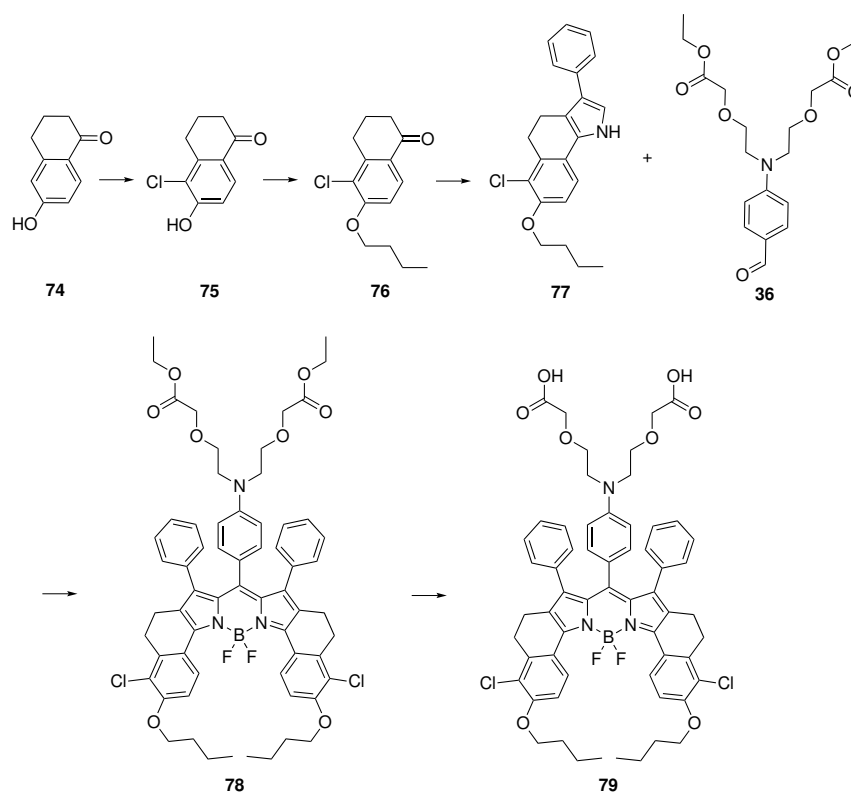
Figure 4.29: Possible synthesis of a new, more soluble and less aggregating fluoroionophore **79**.

Another option to overcome aggregation would be the synthesis of a bromo-substituted version of the fluoroionophore **FI2**. The corresponding pyrrole **82** or fluoroionophore **83** would offer several options of improving the molecule via Suzuki-Miyaura reaction, Heck-reaction or Negishi coupling. This reactions would allow modifications to a more polar fluoroionophore, whereas measurements in hydrogels will become possible and aggregation could be overcome.
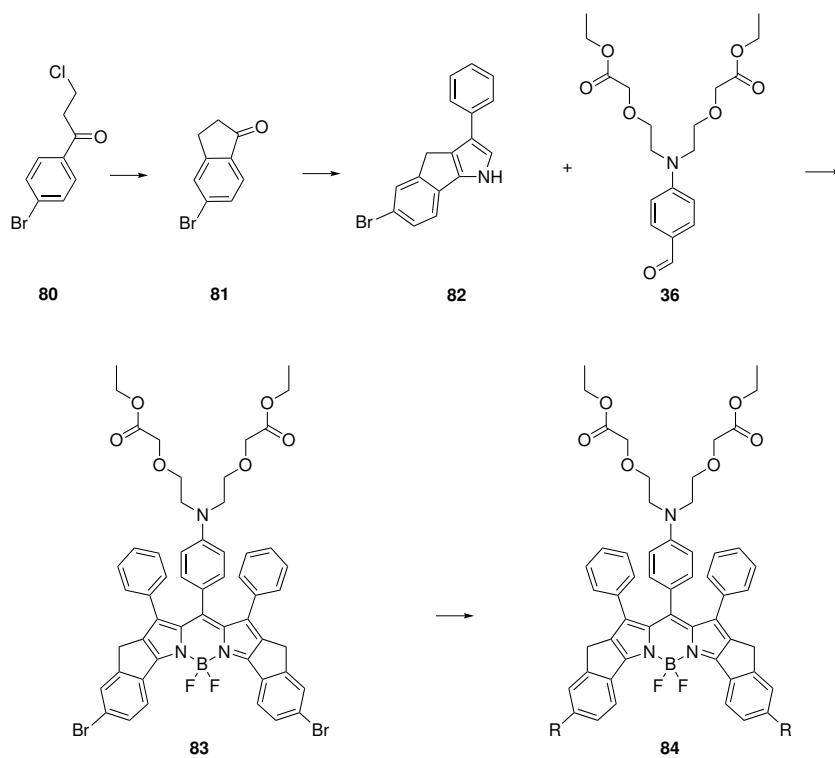
Figure 4.30: A bromo-substituted version of the fluoroionophore **84** offers possibilities for improvements.

5 Experimental

5.1 Synthesis

5.1.1 2-Chloroethoxyacetic acid
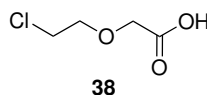
Figure 5.1: 2-Chloroethoxyacetic acid **38**.

4 ml (37.9 mmol) 2-chloroethoxyethanol **37** was added slowly into conc. HNO₃ (65%) at 50°C during 8h. The solution was stirred at RT overnight and then heated up again for 3 hours. The reaction was controlled via TLC (CH:EE 1:5). The solution was poured into ice water (50 ml) and extracted with $(CHCl_3)$(4x50ml). The fractions were combined and dried over Na_2SO_4. The solvent was evaporated to afford 2.2 g (42%) of an yellowish oil. The oil was directly used for the next esterification without further purification.

Yield: 2.2 g, 42%
^{1}H NMR (300 MHz, $CDCl_3$) δ=10.71 (s, 1H), 4.23 (s, 2H), 3.85 (t, J = 5.6 Hz, 2H), 3.68 (t, J = 5.6 Hz, 2H).

5.1.2 Ethyl 2-chloroethoxyacetate

39
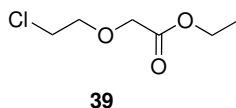
Figure 5.2: Ethyl 2-chloroethoxyacetate **39**.

5.7 g (41.14 mmol) of 2-chloroethoxyacetic acid **38** were dissolved in 50 ml absolute ethanol. The solution was heated to 90°C and 2 drops of conc. H_2SO_4 were added. After 7 hours the reaction was neutralised with 1M NaOH and the solution was evaporated to afford 6.5 g (94%) of an yellow oil.

Yield: 6.5 g, 94%
^{1}H NMR (300 MHz, CDCl$_3$) δ=4.22 (q, J = 7.1 Hz, 2H), 4.15 (s, 2H), 3.83 (t, J = 5.7 Hz, 2H), 3.67 (t, J = 5.7 Hz, 2H), 1.28 (t, J = 7.1 Hz, 3H).

5.1.3 N-phenylimino-diethoxyethylacetate

41
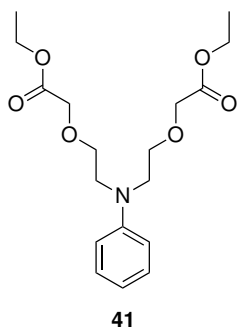
Figure 5.3: N-phenylimino-diethoxyethylacetate **41**.

2.93 g (31.51 mmol,1.0 eq) of aniline **40**, 21.00 g (126 mmol, 4.0 eq) 2-chloroethoxyacetate **39**, 16.29 g (126 mmol, 4.0 eq) DIPEA and 20.92 g (126 mmol, 4.0 eq) KI were dissolved in app. 100 ml NMP and stirred for 3 days at 100°C. The reaction was controlled via TLC(CH:EE 4:1). A flash column chromatography (CH:EE = 4:0 to 4:1) was performed to remove NMP. A second column chromatography was performed the same way to separate mono- and disubstituted product from each other.

Yield: 9,4 g, 80%
^{1}H NMR (300 MHz, CD$_2$Cl$_2$) δ=7.18 (t, J = 8.0 Hz, 3H), 6.72 (d, J = 8.1 Hz, 2H), 6.64 (t, J = 7.2 Hz, 1H), 4.17 (q, J = 7.1 Hz, 4H), 4.06 (s, 4H), 3.69 (t, J = 5.6 Hz, 4H), 3.61 (t, J = 5.6

Hz, 4H), 1.25 (t, J = 7.1 Hz, 6H).

MALDI-TOF: $C_{18}H_{27}NO_6$ calc. 354.1917, found: 354.1603

5.1.4 N-(4-Formyl) phenylimino-diethoxyethylacetate
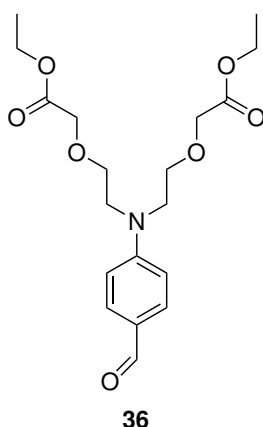
Figure 5.4: N-(4-Formyl) phenylimino-diethoxyethylacetate **36**.

A 100 ml Schlenk-tube was heated out three times under vacuum. 969 mg (2.74 mmol) of N-phenylimino-diethoxyethylacetate **41** were dissolved in 25 ml dry DMF. The solution was cooled to -70°C and stirred for 20 minutes. 2.10 g (13.71 mmol, 5 eq.) POCl₃ were added dropwise over 5 minutes. A color change from yellow to greenish was observed. The solution was stirred for another 30 minutes at -70°C and was then allowed to warm up to room temperature. The reaction was stirred overnight and the next day 20 ml ice water was added to the solution. The solution was extracted in DCM (3x 50 ml), dried with Na_2SO_4 and evaporated. Purification by column chromatography (CH/EE 1:1) afforded 812 mg (77%) of an yellow oil.

Yield: 812 mg, 77%

^{1}H NMR (300 MHz, CD_2Cl_2) δ=9.70 (s, 1H), 7.69 (d, J = 8.9 Hz, 2H), 6.80 (d, J = 8.8 Hz, 2H), 4.16 (q, J = 7.1 Hz, 4H), 4.06 (s, 4H), 3.82 – 3.64 (m, 8H), 1.24 (t, J = 7.1 Hz, 6H).

MALDI-TOF: $C_{19}H_{27}NO_7$ calc. 382.1866, found: 382.1749

5.1.5 FI1-ester
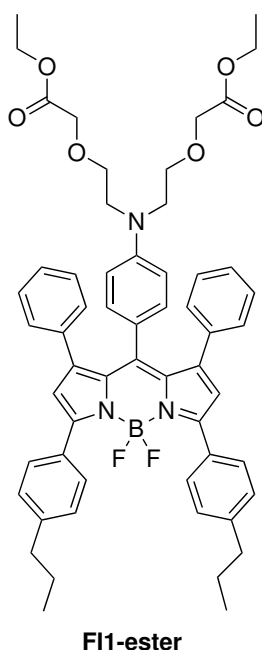
FI1-ester

Figure 5.5: FI1-ester.

N-(4-Formyl) phenylimino-diethoxyethylacetate **36** (100 mg, 0.262 mmol, 1 eq) and 2-(4-propylphenyl)-4-phenylpyrrole (143 mg, 0.550 mmol, 2,1 eq) were dissolved in 5 mL of anhydrous dichloromethane and 1 drop of trifluoroacetic acid was added. The mixture was shielded from light and stirred at RT for 48 hours. DDQ (57 mg, 0.262 mmol, 1 eq) was added. After stirring for another 60 min, N,N-diisopropylethylamine (0.445 ml, 2.62 mmol, 10 eq) and BF_3OEt_2 (0.498 ml, 3.93 mmol, 15 eq) were added and stirred for 60 min. The mixture was extracted with water, dried over Na_2SO_4 and the solvent removed in vacuo. The final product was purified by column chromatography and was obtained as purple crystals.

Yield: 40 mg, 16%

^{1}H NMR (300 MHz, CD_2Cl_2) δ=7.74 (d, J = 8.0 Hz, 4H), 7.27 (d, J = 7.9 Hz, 4H), 7.03 – 6.75 (m, 10H), 6.68 (d, J = 8.6 Hz, 2H), 6.57 (s, 2H), 5.77 (d, J = 8.6 Hz, 2H), 4.23 (q, J = 7.1 Hz, 4H), 4.09 (s, 4H), 3.42 (dd, J = 19.4, 5.3 Hz, 8H), 2.65 (t, 4H), 1.77 – 1.61 (m, J = 15.2, 6.8 Hz, 4H), 1.32 – 1.24 (m, 6H), 0.99 (t, J = 7.3 Hz, 6H).

MALDI-TOF: $C_{57}H_{60}BF_2N_3O_6$ calc. 931.4553, found: 931.4396

5.1.6 FI1
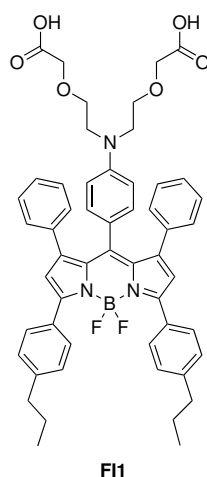
Figure 5.6: FI1.

27 mg (0.029 mmol, 1 eq) **FI1-ester** was dissolved in 8 ml THF/MeOH 1:1 and 10 mg (15 eq) LiOH were added and stirred for 3 days at room temperature. The reaction was controlled via TLC (DCM:MeOH=75:5). After complete consumption of the educt, the solvent was evaporated and extracted in H_2O/DCM. The organic fraction was evaporated to dryness.

Yield: 12 mg (53 %)

^{1}H NMR (300 MHz, CD$_3$OD) δ=7.78 (d, 4H), 7.24 (d, J = 8.0 Hz, 4H), 7.04-6.79 (m, 10H), 6.67 (d, J = 8.5 Hz, 2H), 6.60 (d, J = 6.3 Hz, 2H), 5.88 (d, J = 8.6 Hz, 2H), 3.91 (s, 4H), 3.40 (s, 8H), 2.64 (t, J = 7.5 Hz, 4H), 1.75-1.63 (m, 4H), 0.98 (t, J = 7.3 Hz, 6H).

5.1.7 FI2-ester
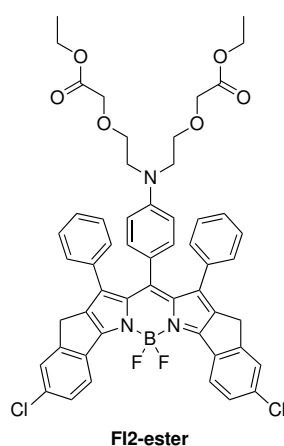
Figure 5.7: FI2-ester.

N-(4-Formyl) phenylimino-diethoxyethylacetate **36** (168 mg, 0.442 mmol, 1 eq) and 5-chloro-3-phenyl-1,4-dihydroindeno[1,2-b]pyrrole **71** (235 mg, 0.884 mmol, 2.0 eq) were dissolved in 5 mL of anhydrous dichloromethane and 1 drop of trifluoroacetic acid was added. The mixture was shielded from light and stirred at RT for 48 hours. DDQ (100 mg, 0.442 mmol, 1 eq) was added. After stirring for another 60 min, N,N-diisopropylethylamine (0.750 ml, 2.62 mmol, 10 eq) and BF$_3$OEt$_2$ (0.815 ml, 3.93 mmol, 15 eq) were added and stirred for 60 min. The mixture was extracted with water, dried over Na$_2$SO$_4$ and the solvent removed in vacuo. The final product was purified by column chromatography and was obtained as purple crystals (48 mg, 12 %).

Yield: 48 mg, 12%

^{1}H NMR (300 MHz, CD$_2$Cl$_2$) δ=8.29 (d, J = 8.6 Hz, 2H), 7.49 (d, 4H), 7.00 – 6.78 (m, 10H), 6.63 (d, J = 8.6 Hz, 2H), 5.75 (d, J = 8.7 Hz, 2H), 4.23 (q, J = 7.1 Hz, 4H), 4.09 (s, 4H), 3.58 (s, 4H), 3.42 (dd, J = 22.4, 5.4 Hz, 8H), 1.30 (t, 6H).

MALDI-TOF: C$_{53}$H$_{47}$BCl$_2$F$_2$N$_3$O$_6$ calc. 940.2912, found: 940.1335

5.1.8 FI2
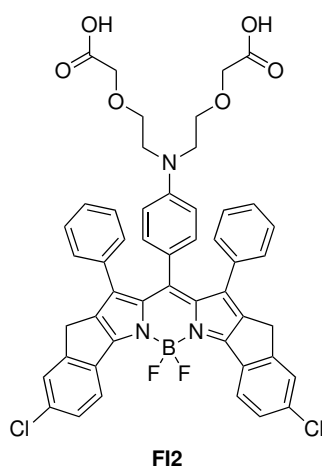
Figure 5.8: FI2.

24 mg (0.025 mmol, 1 eq) **FI2-ester** was dissolved in 8 ml THF/MeOH 1:1 and 9 mg (15 eq) LiOH were added and stirred for 3 days at room temperature. The reaction waas controlled via TLC (DCM:MeOH=75:5). After complete consumption of the educt, the solvent was evaporated and extracted in H$_2$O/DCM. The organic fraction was evaporated to dryness.

5.1.9 2-(4-nitrophenyl)-1,3-dioxolane
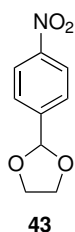
Figure 5.9: 2-(4-nitrophenyl)-1,3-dioxolane **43**.

4-nitrobenzaldehyde **42** (2 g, 13.06 mmol, 1 eq) and p-toluenesulfonic acid monohydrate (200 mg, 0,05 eq) were dissolved in toluene (40 mL). Ethylene glycol (15.8 mL, 15 eq) was added and the solution was refluxed with a Dean-Stark trap to remove water. After 4 hours, the solution was allowed to cool to room temperature and was washed with saturated $NaHCO_3$ solution and a brine solution. The solution was dried over Na_2SO_4, filtered and concentrated under high vacuum to yield an off white solid of crystalline needles.

Yield: 2.2 g (85 %)
^{1}H NMR (300 MHz, $CDCl_3$) δ=8.24 (d, J = 8.7 Hz, 2H), 7.65 (d, J = 8.6 Hz, 2H), 5.89 (s, 1H), 4.17 – 4.02 (m, 4H).

5.1.10 4-(1,3-Dioxolan-2-yl)aniline
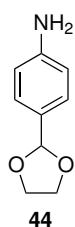
Figure 5.10: 4-(1,3-Dioxolan-2-yl)aniline **44**.

200 mg of 2-(4-nitrophenyl)-1,3-dioxolane **43** (1.01mmol, 1 eq) was dissolved in 15ml MeOH and a catalyst amount Pd/C was added. The solution was stirred overnight under H_2 at roomtemperature. TLC (CH:EE=1:5, $KMnO_4$) indicated complete consumption of educt as well as the formation of the desired product.

Yield: 155 mg (92 %)

5.1.11 2-(4-Bromophenyl)-1,3-dioxolane
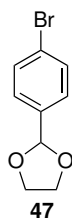
Figure 5.11: 2-(4-Bromophenyl)-1,3-dioxolane **47**.

2.35 g 4-Bromobenzaldehyde **46** (15.35 mmol, 1 eq) and 12.87 ml ethylene glycol (230 mmol, 15 eq) were dissolved in 20 ml toluene and refluxed with a Dean-Stark trap to remove water. After 6h, the solution was allowed to cool at room temperature and was washed with saturated NaHCO$_3$ solution and a brine solution. The solution was dried over Na$_2$SO$_4$, filtered and concentrated under high vacuum to yield a white solid.

Yield: 2.6 g (89%)
^{1}H NMR (300 MHz, CDCl$_3$) δ=7.51 (d, J = 8.4 Hz, 2H), 7.35 (d, J = 8.3 Hz, 2H), 5.77 (s, 1H), 4.19 – 3.97 (m, 4H).

5.1.12 N-Benzyldiethanolamine
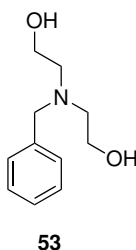
Figure 5.12: N-Benzyldiethanolamine **53**.

636 mg benzyl bromide **52** (3,72 mmol, 1 eq) and 390 mg diethanolamine (3,72 mmol, 1 eq) were dissolved in app. 10 ml acetone and stirred for 10 minutes at room temperature 513 mg Na$_2$CO$_3$ were added and stirred at 64°C for 4 hours. The reaction was stirred at room temperature overnight. TLC (CH:EE=1:5)indicated complete consumption of the educt. The acetone was evaporated and the residue was dissolved in water and extracted with DCM. The organic phase was dried with Na$_2$SO$_4$ and evaporated to dryness under high vacuum.

Yield: 604 mg (83 %)

^{1}H NMR (300 MHz, CDCl$_3$) δ 7.37 – 7.25 (m, J = 15.9 Hz, 5H), 3.70 (s, 2H), 3.62 (t, J = 5.3 Hz, 4H), 2.72 (t, J = 5.3 Hz, 4H), 2.49 (bs, 2H).

5.1.13 N-(benzyl)diethoxyacetic acid
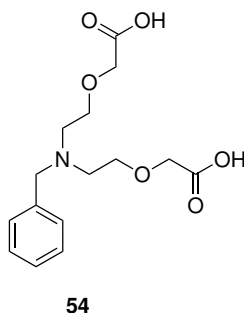
Figure 5.13: N-(benzyl)diethoxyacetic acid **54**.

A Schlenk-tube was heated out 3 times under high vacuum. 10 ml dry THF and 570 mg of N-benzyldiethanolamine **53** (2.92 mmol, 1 eq) were stirred for 5 minutes at 0°C. 0,35 ml of chloroacetic acid (5.84 mmol, 2 eq) was added and stirred for additional 10 minutes. 300 mg of NaH in mineral oil (60%) was slowly added within 10 minutes. After 20 minutes the solution was allowed to heat up to 60°C and stirred over the weekend. The reaction was quenched with app. 2 ml water and stirred for 30 minutes. The water-phase was removed with a pipette and the THF-phase was filtrated through Na$_2$SO$_4$. The organic phase was evaporated to dryness to yield the desired product.

Yield: 50 mg (5.5 %)
^{1}H NMR (300 MHz, D$_2$O) δ=7.46 – 7.35 (m, 5H), 4.04 (s, 4H), 3.76 (s, 2H), 3.70 (t, J = 6.2 Hz, 4H), 2.74 (t, J = 6.2 Hz, 4H).

5.1.14 4-[Bis-(2-chloroethyl)amino]benzaldehyde
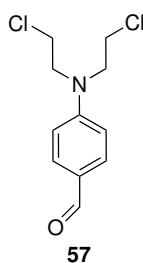
Figure 5.14: 4-Bis-(2-chloroethyl)amino-benzaldehyde **57**.

A Schlenk-tube was heated out 3 times and 1.80 g (10 mmol) N-phenyldiethanolamine **51** were dissolved in 10 ml DMF. The mixture was refluxed and stirred for 10 minutes. 10 ml POCl$_3$ were added dropwise within 30 minutes. The reaction was stirred for 5 hours. Ice-cubes (30 ml)were added and the solution was allowed to cool to room temperature. The solution was extracted with DCM (4x100 ml). The fractions were combined and dried with Na$_2$SO$_4$. The solvent was evaporated to dryness under reduced pressure. The yellow residue was purified via column chromatography (CH:EE=1:5) to afford 1.28 g of an yellow oil.

Yield: 1.28g (52 %)
^{1}H NMR (300 MHz, CDCl$_3$) δ=9.78 (s, 1H), 7.77 (d, J = 8.8 Hz, 2H), 6.74 (d, J = 8.8 Hz, 2H), 3.84 (t, J = 6.8 Hz, 4H), 3.67 (t, J = 6.8 Hz, 4H).

5.1.15 Assymetric BODIPY
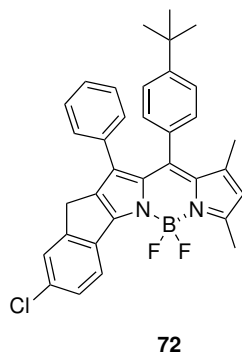
Figure 5.15: Assymetric BODIPY **72**.

A Schlenk tube was heated out 3 times and 300 mg (1.85 mmol) 4-tert.-butylaldehyde **67**, 491 mg (1.85 mmol) 5-chloro-3-phenyl-1,4-dihydroindeno[1,2-b]pyrrole **71** and 176 mg (1.85 mmol) 2,4-dimethylpyrrole **68** were dissolved in 35 ml dry DCM at room temperature. A drop TFA was added and stirred overnight. After 14 hours DDQ (415 mg, 1.85 mmol, 1 eq) was added.
After stirring for another 60 min, N,N-diisopropylethylamine (3.2 ml, 18.5 mmol, 10 eq) and BF$_3$OEt$_2$ (3.4 ml, 18.5 mmol, 15 eq) were added and stirred for 60 min. The mixture was extracted with water, dried over Na$_2$SO$_4$ and the solvent removed in vacuo. The final product was purified by column chromatography and was obtained as shiny crystals.

Yield: 64 mg (6 %)
^{1}H NMR (300 MHz, CDCl$_3$) δ=8.14 (d, 1H), 7.48-7.38 (m, J = 9.7 Hz,2H), 7.06-6.91 (m, 7H), 6.87-6.79 (m, J = 7.7 Hz, 2H), 6.09 (s, 1H), 3.48 (s, 2H), 2.63 (s, 3H), 1.54 (s, 3H).

5.1.16 Synthesis of tert.butyl-dye
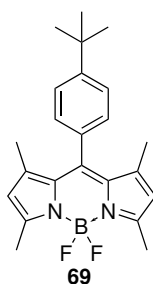
Figure 5.16: Synthesis of dye **69**.

A Schlenk tube was heated out 3 times and 600 mg (3.70 mmol) 4-tert.-butylaldehyde **67** and 704 mg (7.40 mmol, 2 eq.) 2,4-dimethylpyrrole **68** were dissolved in 50 ml dry DCM at room temperature. A drop TFA was added and stirred overnight. After 17 hours DDQ (839 mg, 3.70 mmol, 1 eq) was added.
After stirring for another 60 min, N,N-diisopropylethylamine (3.63 ml, 37.0 mmol, 10 eq) and BF_3OEt_2 (3.4 ml, 18.5 mmol, 15 eq) were added and stirred for 60 min. The mixture was extracted with water, dried over Na_2SO_4 and the solvent removed in vacuo. The final product was purified by column chromatography and was obtained as red crystals with an absorption maximum at 501 nm.

Yield: 124 mg (9 %)
^{1}H NMR (300 MHz, $CDCl_3$) δ=7.49 (d, 2H), 7.18 (d, J= 8.1 Hz, 2H), 5.97 (s, 2H), 2.56 (s, 6H), 2.16 (s, 3H)

5.1.17 Synthesis of styryl-based fluoroionophore
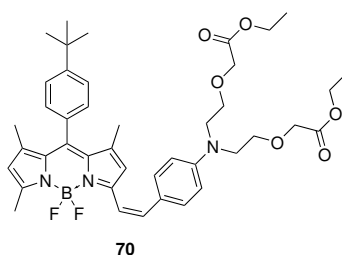
Figure 5.17: fluoroionophore **70**.

A Schlenk tube was heated out three times. 94 mg (0.3 mmol, 1 eq) of dye **69** and 47 mg (0.15 mmol, 0.5 eq) of compound **36** were dissolved in 10 toluene. 10 mml AcOH and 12 mml piperidine were added and 5 drops of molecular sieve were added. The solution was heated for

48 hours at 104°C in the oil bath. The solvent was evaporated and the product was separated via column chromatography. The final product was obtained as purple powder.

Yield: 24 mg (22 %)

^{1}H NMR (300 MHz, CD_2Cl_2) δ=7.99 (d, 2H), 7.52 (d, J = 5.5 Hz, 2H), 7.23 (d, J = 8.2 Hz, 2H), 6.75 (d, J = 8.8 Hz, 2H), 6.62 (s, 1H), 6.00 (s, 1H), 4.18 (q, J = 7.1 Hz, 4H), 4.07 (s, 4H), 3.80-3.63 (m, 8H), 2.53 (s, 2H), 2.04 (s, 6H)

6 References

[1] Richard E. Zeebe and Dieter A. Wolf-Gladrow. *CO2 in Seawater: Equilibrium, Kinetics, Isotopes.* Google-Books-ID: g3j3Zn4kEscC. Gulf Professional Publishing, 2001. 381 pp. ISBN: 978-0-444-50946-8.

[2] N.I.colas Leclercq, J.E.A.N.-Pierre Gattuso, and J.e.a.n. Jaubert. "CO2 partial pressure controls the calcification rate of a coral community". In: *Global Change Biology* 6.3 (Mar. 1, 2000), pp. 329–334. ISSN: 1365-2486. DOI: `10.1046/j.1365-2486.2000.00315.x`. URL: `http://onlinelibrary.wiley.com/doi/10.1046/j.1365-2486.2000.00315.x/abstract` (visited on 10/18/2016).

[3] Mark J. Mitchell, Oliver E. Jensen, K. Andrew Cliffe, and M. Mercedes Maroto-Valer. "A model of carbon dioxide dissolution and mineral carbonation kinetics". In: *Proceedings of the Royal Society of London A: Mathematical, Physical and Engineering Sciences* (Dec. 11, 2009), rspa20090349. ISSN: 1364-5021, 1471-2946. DOI: `10.1098/rspa.2009.0349`. URL: `http://rspa.royalsocietypublishing.org/content/early/2009/12/04/rspa.2009.0349` (visited on 10/18/2016).

[4] Huarui He, Kenneth Jenkins, and Chao Lin. "A fluorescent chemosensor for calcium with excellent storage stability in water". In: *Analytica Chimica Acta* 611.2 (Mar. 24, 2008), pp. 197–204. ISSN: 0003-2670. DOI: `10.1016/j.aca.2008.01.059`. URL: `http://www.sciencedirect.com/science/article/pii/S0003267008002389` (visited on 01/12/2016).

[5] Daying Liu, Jing Qi, Zhiqiang Yu, Xiaoyan Liu, Renwei Yang, Haitao Yang, Hexi Chang, Huarui He, and Guangming Yang. "A fluorescent sensor with high selectivity for Ca2+ against Mg2+ in seawater". In: *Analytical Methods* 6.11 (May 15, 2014), pp. 3555–3559. ISSN: 1759-9679. DOI: `10.1039/C4AY00312H`. URL: `http://pubs.rsc.org/en/content/articlelanding/2014/ay/c4ay00312h` (visited on 01/11/2016).

[6] *Valeur B - Molecular Fluorescence Princeples And Applications - (Wiley-Vch 2001_ 399 P).* URL: `http://physweb.bgu.ac.il/~bogomole/Books/Valeur%20B%20-%20Molecular%20Fluorescence%20Princeples%20And%20Applications%20-%20(Wiley-Vch%202001_%20399%20P).pdf` (visited on 11/14/2016).

[7] Bernhard J. Müller, Sergey M. Borisov, and Ingo Klimant. "Red- to NIR-Emitting, BODIPY-Based, K+-Selective Fluoroionophores and Sensing Materials". In: *Advanced Functional Materials* (Sept. 1, 2016), n/a–n/a. ISSN: 1616-3028. DOI: `10.1002/adfm.`

201603822. URL: http://onlinelibrary.wiley.com/doi/10.1002/adfm.201603822/abstract (visited on 10/24/2016).

[8] Eric Bakker and Ernö Pretsch. "Peer Reviewed: The New Wave of Ion-Selective Electrodes". In: *Analytical Chemistry* 74.15 (Aug. 1, 2002), 420 A–426 A. ISSN: 0003-2700. DOI: 10.1021/ac022086f. URL: http://dx.doi.org/10.1021/ac022086f (visited on 01/04/2017).

[9] Eric Bakker, Philippe Bühlmann, and Ernö Pretsch. "Carrier-Based Ion-Selective Electrodes and Bulk Optodes. 1. General Characteristics". In: *Chemical Reviews* 97.8 (Dec. 1, 1997), pp. 3083–3132. ISSN: 0009-2665. DOI: 10.1021/cr940394a. URL: http://dx.doi.org/10.1021/cr940394a (visited on 01/04/2017).

[10] Mark A. Arnold and Mark E. Meyerhoff. "Ion-selective electrodes". In: *Analytical Chemistry* 56.5 (Apr. 1, 1984), 20R–48R. ISSN: 0003-2700. DOI: 10.1021/ac00269a003. URL: http://dx.doi.org/10.1021/ac00269a003 (visited on 01/04/2017).

[11] Philippe Bühlmann, Ernö Pretsch, and Eric Bakker. "Carrier-Based Ion-Selective Electrodes and Bulk Optodes. 2. Ionophores for Potentiometric and Optical Sensors". In: *Chemical Reviews* 98.4 (June 1, 1998), pp. 1593–1688. ISSN: 0009-2665. DOI: 10.1021/cr970113+. URL: http://dx.doi.org/10.1021/cr970113+ (visited on 01/04/2017).

[12] Joydev Hatai and Subhajit Bandyopadhyay. "Altered selectivity of a dipicolylamine based metal ion receptor". In: 50.1 (Nov. 26, 2013), pp. 64–66. ISSN: 1364-548X. DOI: 10.1039/C3CC46285D. URL: http://pubs.rsc.org/en/content/articlelanding/2014/cc/c3cc46285d (visited on 12/01/2016).

[13] Ha Na Kim, Wen Xiu Ren, Jong Seung Kim, and Juyoung Yoon. "Fluorescent and colorimetric sensors for detection of lead, cadmium, and mercury ions". In: 41.8 (Mar. 23, 2012), pp. 3210–3244. ISSN: 1460-4744. DOI: 10.1039/C1CS15245A. URL: http://pubs.rsc.org/en/content/articlelanding/2012/cs/c1cs15245a (visited on 12/01/2016).

[14] Sergey V. Dorozhkin and Matthias Epple. "Biological and Medical Significance of Calcium Phosphates". In: *Angewandte Chemie International Edition* 41.17 (Sept. 2, 2002), pp. 3130–3146. ISSN: 1521-3773. DOI: 10.1002/1521-3773(20020902)41:17<3130::AID-ANIE3130>3.0.CO;2-1. URL: http://onlinelibrary.wiley.com.3966.ftubhan.tugraz.at/doi/10.1002/1521-3773(20020902)41:17%3C3130::AID-ANIE3130%3E3.0.CO;2-1/abstract (visited on 06/27/2016).

[15] *Ocean Acidification*. URL: http://www.pmel.noaa.gov/co2/story/Ocean+Acidification (visited on 12/01/2016).

[16] Roger Y. Tsien. "New calcium indicators and buffers with high selectivity against magnesium and protons: design, synthesis, and properties of prototype structures". In: *Biochemistry* 19.11 (May 1, 1980), pp. 2396–2404. ISSN: 0006-2960. DOI: 10.1021/bi00552a018. URL: http://dx.doi.org/10.1021/bi00552a018 (visited on 06/27/2016).

[17] G. Grynkiewicz, M. Poenie, and R. Y. Tsien. "A new generation of Ca2+ indicators with greatly improved fluorescence properties." In: *Journal of Biological Chemistry* 260.6 (Mar. 25, 1985), pp. 3440–3450. ISSN: 0021-9258, 1083-351X. URL: `http://www.jbc.org.43.ftubhan.tugraz.at/content/260/6/3440` (visited on 06/27/2016).

[18] S. R. Adams, Joseph P. Y. Kao, G. Grynkiewicz, A. Minta, and R. Y. Tsien. "Biologically useful chelators that release Ca2+ upon illumination". In: *Journal of the American Chemical Society* 110.10 (May 1, 1988), pp. 3212–3220. ISSN: 0002-7863. DOI: `10.1021/ja00218a034`. URL: `http://dx.doi.org/10.1021/ja00218a034` (visited on 06/27/2016).

[19] A. Minta, J. P. Kao, and R. Y. Tsien. "Fluorescent indicators for cytosolic calcium based on rhodamine and fluorescein chromophores." In: *Journal of Biological Chemistry* 264.14 (May 15, 1989), pp. 8171–8178. ISSN: 0021-9258, 1083-351X. URL: `http://www.jbc.org.43.ftubhan.tugraz.at/content/264/14/8171` (visited on 06/27/2016).

[20] Michael Shortreed, Raoul Kopelman, Michael Kuhn, and Brian Hoyland. "Fluorescent Fiber-Optic Calcium Sensor for Physiological Measurements". In: *Analytical Chemistry* 68.8 (Jan. 1, 1996), pp. 1414–1418. ISSN: 0003-2700. DOI: `10.1021/ac950944k`. URL: `http://dx.doi.org/10.1021/ac950944k` (visited on 06/27/2016).

[21] Gerry A. Smith, James C. Metcalfe, and Sonia D. Clarke. "The design and properties of a series of calcium indicators which shift from rhodamine-like to fluorescein-like fluorescence on binding calcium". In: 6 (Jan. 1, 1993), pp. 1195–1204. ISSN: 1364-5471. DOI: `10.1039/P29930001195`. URL: `http://pubs.rsc.org/en/content/articlelanding/1993/p2/p29930001195` (visited on 12/02/2016).

[22] Alfred Treibs and Franz-Heinrich Kreuzer. "Difluorboryl-Komplexe von Di- und Tripyrryl-methenen". In: *Justus Liebigs Annalen der Chemie* 718.1 (Dec. 13, 1968), pp. 208–223. ISSN: 1099-0690. DOI: `10.1002/jlac.19687180119`. URL: `http://onlinelibrary.wiley.com.2609.ftubhan.tugraz.at/doi/10.1002/jlac.19687180119/abstract` (visited on 11/30/2016).

[23] Aurore Loudet and Kevin Burgess. "BODIPY Dyes and Their Derivatives: Syntheses and Spectroscopic Properties". In: *Chemical Reviews* 107.11 (Nov. 1, 2007), pp. 4891–4932. ISSN: 0009-2665. DOI: `10.1021/cr078381n`. URL: `http://dx.doi.org/10.1021/cr078381n` (visited on 10/18/2016).

[24] Raphael Alford, Haley M. Simpson, Josh Duberman, G. Craig Hill, Mikako Ogawa, Celeste Regino, Hisataka Kobayashi, and Peter L. Choyke. "Toxicity of organic fluorophores used in molecular imaging: literature review". In: *Molecular Imaging* 8.6 (Dec. 2009), pp. 341–354. ISSN: 1536-0121.

[25] Joseph R. Lakowicz. *Principles of Fluorescence Spectroscopy*. Springer Science & Business Media, Dec. 5, 2007. 961 pp. ISBN: 978-0-387-46312-4.

[26]   Tabitha E. Wood and Alison Thompson. "Advances in the Chemistry of Dipyrrins and Their Complexes". In: *Chemical Reviews* 107.5 (May 1, 2007), pp. 1831–1861. ISSN: 0009-2665. DOI: `10.1021/cr050052c`. URL: `http://dx.doi.org/10.1021/cr050052c` (visited on 11/30/2016).

[27]   Mayur Shah, Kannappan Thangaraj, Mou-Ling Soong, Lionel T. Wolford, Joseph H. Boyer, Ieva R. Politzer, and Theodore G. Pavlopoulos. "Pyrromethene–BF2 complexes as laser dyes:1." In: *Heteroatom Chemistry* 1.5 (Oct. 1, 1990), pp. 389–399. ISSN: 1098-1071. DOI: `10.1002/hc.520010507`. URL: `http://onlinelibrary.wiley.com.1941.ftubhan.tugraz.at/doi/10.1002/hc.520010507/abstract` (visited on 11/30/2016).

[28]   Joseph H. Boyer, Anthony M. Haag, Govindarao Sathyamoorthi, Mou-Ling Soong, Kannappan Thangaraj, and Theodore G. Pavlopoulos. "Pyrromethene–BF2 complexes as laser dyes: 2". In: *Heteroatom Chemistry* 4.1 (Feb. 1, 1993), pp. 39–49. ISSN: 1098-1071. DOI: `10.1002/hc.520040107`. URL: `http://onlinelibrary.wiley.com.1941.ftubhan.tugraz.at/doi/10.1002/hc.520040107/abstract` (visited on 11/30/2016).

[29]   Zaiguo Li, Evan Mintzer, and Robert Bittman. "First Synthesis of Free Cholesterol-BODIPY Conjugates". In: *The Journal of Organic Chemistry* 71.4 (Feb. 1, 2006), pp. 1718–1721. ISSN: 0022-3263. DOI: `10.1021/jo052029x`. URL: `http://dx.doi.org/10.1021/jo052029x` (visited on 11/30/2016).

[30]   Eduardo Palao, Antonia R. Agarrabeitia, Jorge Bañuelos-Prieto, Teresa Arbeloa Lopez, Iñigo Lopez-Arbeloa, Diego Armesto, and Maria J. Ortiz. "8-Functionalization of Alkyl-Substituted-3,8-Dimethyl BODIPYs by Knoevenagel Condensation". In: *Organic Letters* 15.17 (Sept. 6, 2013), pp. 4454–4457. ISSN: 1523-7060. DOI: `10.1021/ol401993p`. URL: `http://dx.doi.org/10.1021/ol401993p` (visited on 11/30/2016).

[31]   Noël Boens, Volker Leen, and Wim Dehaen. "Fluorescent indicators based on BODIPY". In: 41.3 (Jan. 17, 2012), pp. 1130–1172. ISSN: 1460-4744. DOI: `10.1039/C1CS15132K`. URL: `http://pubs.rsc.org/en/content/articlelanding/2012/cs/c1cs15132k` (visited on 11/03/2016).

[32]   Mukulesh Baruah, Wenwu Qin, Nikola Basarić, Wim M. De Borggraeve, and Noël Boens. "BODIPY-Based Hydroxyaryl Derivatives as Fluorescent pH Probes". In: *The Journal of Organic Chemistry* 70.10 (May 1, 2005), pp. 4152–4157. ISSN: 0022-3263. DOI: `10.1021/jo0503714`. URL: `http://dx.doi.org/10.1021/jo0503714` (visited on 01/05/2017).

[33]   Martin Strobl, Tanja Rappitsch, Sergey M. Borisov, Torsten Mayr, and Ingo Klimant. "NIR-emitting aza-BODIPY dyes – new building blocks for broad-range optical pH sensors". In: *Analyst* 140.21 (2015), pp. 7150–7153. DOI: `10.1039/C5AN01389E`. URL: `http://pubs.rsc.org/en/Content/ArticleLanding/2015/AN/C5AN01389E` (visited on 01/05/2017).

[34] Yong Ni and Jishan Wu. "Far-red and near infrared BODIPY dyes: synthesis and applications for fluorescent pH probes and bio-imaging". In: *Organic & Biomolecular Chemistry* 12.23 (2014), pp. 3774–3791. DOI: 10.1039/C3OB42554A. URL: http://pubs.rsc.org/en/Content/ArticleLanding/2014/OB/C3OB42554A (visited on 01/05/2017).

[35] Taiping Zhang, Guangwei She, Xiaopeng Qi, and Lixuan Mu. "A BODIPY-based sensor for Hg2+ in living cells". In: *Tetrahedron* 69.34 (Aug. 26, 2013), pp. 7102–7106. ISSN: 0040-4020. DOI: 10.1016/j.tet.2013.06.025. URL: http://www.sciencedirect.com/science/article/pii/S0040402013009435 (visited on 07/12/2016).

[36] Charles D. Hurd and Carl N. Webb. "p-DIMETHYLAMINOBENZOPHENONE". In: *Organic Syntheses* 7 (1927), p. 24. ISSN: 00786209, 23333553. DOI: 10.15227/orgsyn.007.0024. URL: http://orgsyn.org/demo.aspx?prep=CV1P0217 (visited on 10/18/2016).

[37] Richard A. Bartsch, David A. Babb, and Brian E. Knudsen. "Synthesis and Alkali Metal Cation Complexation of N-Aryl [3.2.2] Cryptands". In: *Journal of Inclusion Phenomena* 5 (Oct. 7, 1986), pp. 515–519.

[38] Pinar Batat, Guillaume Vives, Robin Bofinger, Ren-Wei Chang, Brice Kauffmann, Reiko Oda, Gediminas Jonusauskas, and Nathan D. McClenaghan. "Dynamics of ion-regulated photoinduced electron transfer in BODIPY-BAPTA conjugates". In: *Photochemical & Photobiological Sciences* 11.11 (2012), pp. 1666–1674. DOI: 10.1039/C2PP25130B. URL: http://pubs.rsc.org/en/Content/ArticleLanding/2012/PP/C2PP25130B (visited on 11/04/2016).

[39] Jiangli Fan, Kexin Guo, Xiaojun Peng, Jianjun Du, Jingyun Wang, Shiguo Sun, and Honglin Li. "A Hg2+ fluorescent chemosensor without interference from anions and Hg2+-imaging in living cells". In: *Sensors and Actuators B: Chemical* 142.1 (Oct. 12, 2009), pp. 191–196. ISSN: 0925-4005. DOI: 10.1016/j.snb.2009.08.002. URL: http://www.sciencedirect.com/science/article/pii/S0925400509006194 (visited on 07/12/2016).

[40] Gary A Gill and William F Fitzgerald. "Picomolar mercury measurements in seawater and other materials using stannous chloride reduction and two-stage gold amalgamation with gas phase detection". In: *Marine Chemistry* 20.3 (Jan. 1, 1987), pp. 227–243. ISSN: 0304-4203. DOI: 10.1016/0304-4203(87)90074-0. URL: http://www.sciencedirect.com/science/article/pii/0304420387900740 (visited on 11/07/2016).

[41] Tomoya Hirata, Takuya Terai, Toru Komatsu, Kenjiro Hanaoka, and Tetsuo Nagano. "Development of a potassium ion-selective fluorescent sensor based on 3-styrylated BODIPY". In: *Bioorganic & Medicinal Chemistry Letters* 21.20 (Oct. 15, 2011), pp. 6090–6093. ISSN: 0960-894X. DOI: 10.1016/j.bmcl.2011.08.056. URL: http://www.sciencedirect.com/science/article/pii/S0960894X11011516 (visited on 07/13/2016).

[42] Serdar Atilgan, Tugba Ozdemir, and Engin U. Akkaya. "Selective Hg(II) Sensing with Improved Stokes Shift by Coupling the Internal Charge Transfer Process to Excitation Energy Transfer". In: *Organic Letters* 12.21 (Nov. 5, 2010), pp. 4792–4795. ISSN: 1523-7060. DOI: 10.1021/ol1019426. URL: http://dx.doi.org/10.1021/ol1019426 (visited on 11/07/2016).

[43] Yasuhiro Shiraishi, Hajime Maehara, Takahiro Sugii, Dongping Wang, and Takayuki Hirai. "A BODIPY–indole conjugate as a colorimetric and fluorometric probe for selective fluoride anion detection". In: *Tetrahedron Letters* 50.29 (July 22, 2009), pp. 4293–4296. ISSN: 0040-4039. DOI: 10.1016/j.tetlet.2009.05.018. URL: http://www.sciencedirect.com/science/article/pii/S0040403909010090 (visited on 11/07/2016).

[44] Dongping Wang, Yasuhiro Shiraishi, and Takayuki Hirai. "A BODIPY-based fluorescent chemodosimeter for Cu(II) driven by an oxidative dehydrogenation mechanism". In: 47.9 (Feb. 14, 2011), pp. 2673–2675. ISSN: 1364-548X. DOI: 10.1039/C0CC04069J. URL: http://pubs.rsc.org/en/content/articlelanding/2011/cc/c0cc04069j (visited on 11/07/2016).

[45] Yongjun Lv, Jian Xu, Yong Guo, and Shijun Shao. "A sandwich anion receptor by a BODIPY dye bearing two calix[4]pyrrole units". In: *Chemical Papers* 65.4 (Aug. 1, 2011), p. 553. ISSN: 0366-6352, 1336-9075. DOI: 10.2478/s11696-011-0033-2. URL: http://link.springer.com/article/10.2478/s11696-011-0033-2 (visited on 12/06/2016).

[46] Jun-Seok Lee, Hyeong Kyu Kim, Suihan Feng, Marc Vendrell, and Young-Tae Chang. "Accelerating fluorescent sensor discovery: unbiased screening of a diversity-oriented BODIPY library". In: *Chemical Communications (Cambridge, England)* 47.8 (Feb. 28, 2011), pp. 2339–2341. ISSN: 1364-548X. DOI: 10.1039/c0cc04495d.

[47] Ziya Kostereli, Tugba Ozdemir, Onur Buyukcakir, and Engin U. Akkaya. "Tetrastyryl-BODIPY-Based Dendritic Light Harvester and Estimation of Energy Transfer Efficiency". In: *Organic Letters* 14.14 (July 20, 2012), pp. 3636–3639. ISSN: 1523-7060. DOI: 10.1021/ol301462x. URL: http://dx.doi.org/10.1021/ol301462x (visited on 12/06/2016).

[48] Chunchang Zhao, Peng Feng, Jian Cao, Xuzhe Wang, Yang Yang, Yulin Zhang, Jinxing Zhang, and Yanfen Zhang. "Borondipyrromethene-derived Cu 2+ sensing chemodosimeter for fast and selective detection". In: *Organic & Biomolecular Chemistry* 10.15 (2012), pp. 3104–3109. DOI: 10.1039/C2OB06980F. URL: http://pubs.rsc.org/en/Content/ArticleLanding/2012/OB/C2OB06980F (visited on 12/06/2016).

[49] *HydroMed Products*. URL: http://www.advbiomaterials.com/products/hydrophilic/hydromed.html (visited on 11/03/2016).

[50] Enrica Caló and Vitaliy V. Khutoryanskiy. "Biomedical applications of hydrogels: A review of patents and commercial products". In: *European Polymer Journal.* 50 Years of European Polymer Journal 65 (Apr. 2015), pp. 252–267. ISSN: 0014-3057. DOI: 10.1016/j.eurpolymj.2014.11.024. URL: http://www.sciencedirect.com/science/article/pii/S0014305714004091 (visited on 11/03/2016).

[51] Enas M. Ahmed. "Hydrogel: Preparation, characterization, and applications: A review". In: *Journal of Advanced Research* 6.2 (Mar. 2015), pp. 105–121. ISSN: 2090-1232. DOI: 10.1016/j.jare.2013.07.006. URL: http://www.sciencedirect.com/science/article/pii/S2090123213000969 (visited on 11/03/2016).

7 List of Figures

8 List of Tables

9 Appendix

9.1 NMR Data

Figure 9.1: ^{1}H-NMR-spectrum of compound **38**.
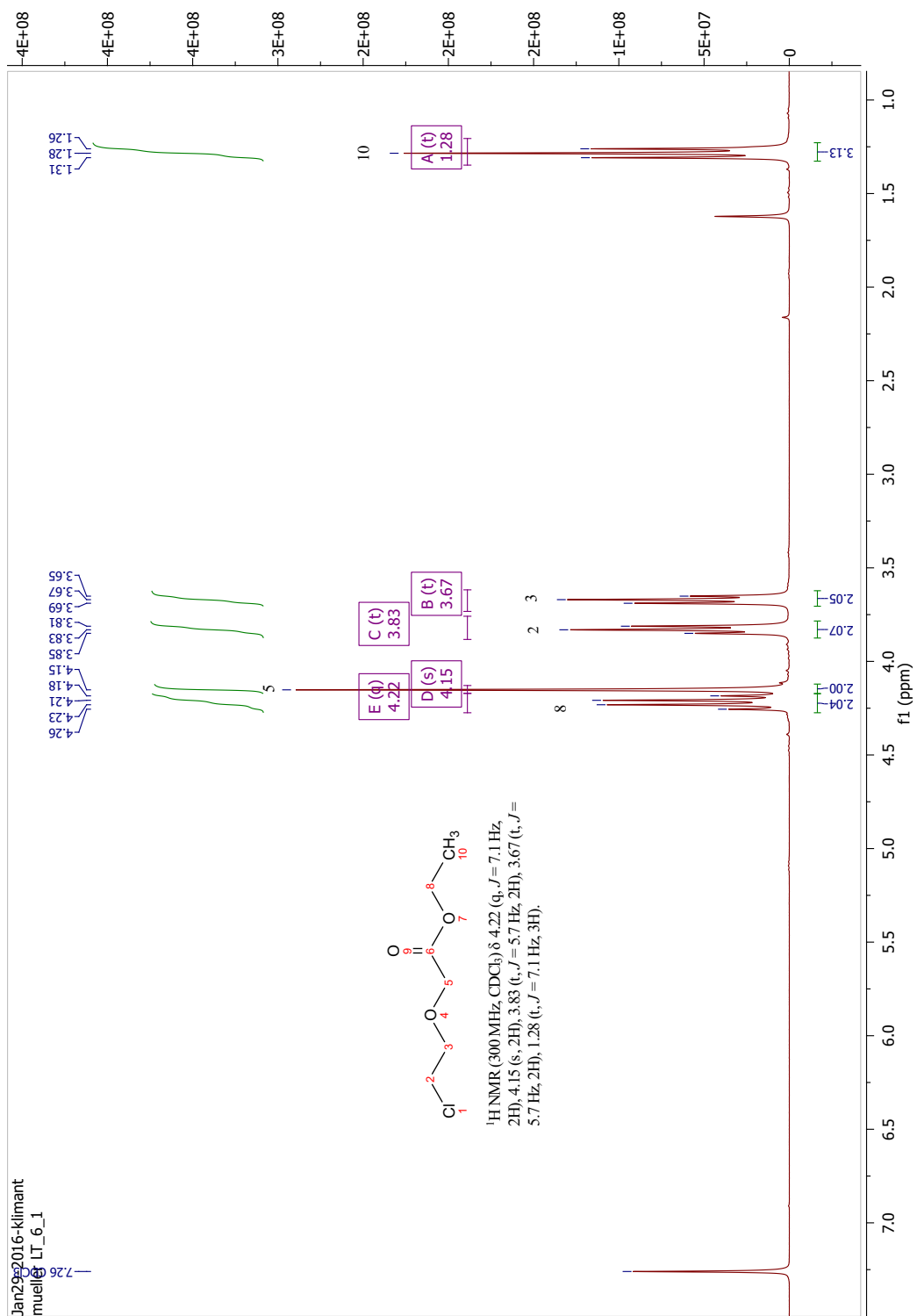
Figure 9.2: ^{1}H-NMR-spectrum of compound **39**.
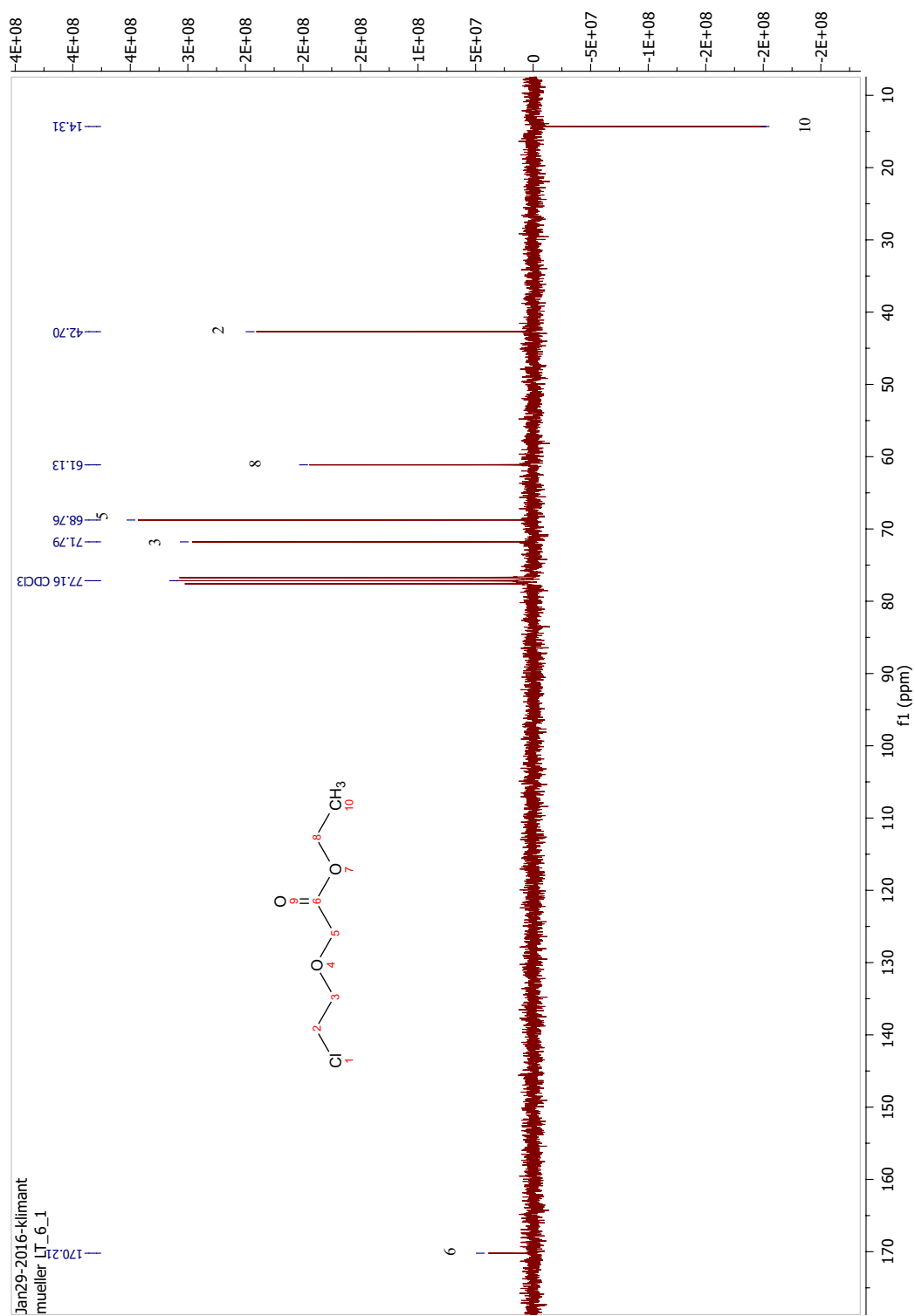
Figure 9.3: APT-NMR-spectrum of compound **39**.
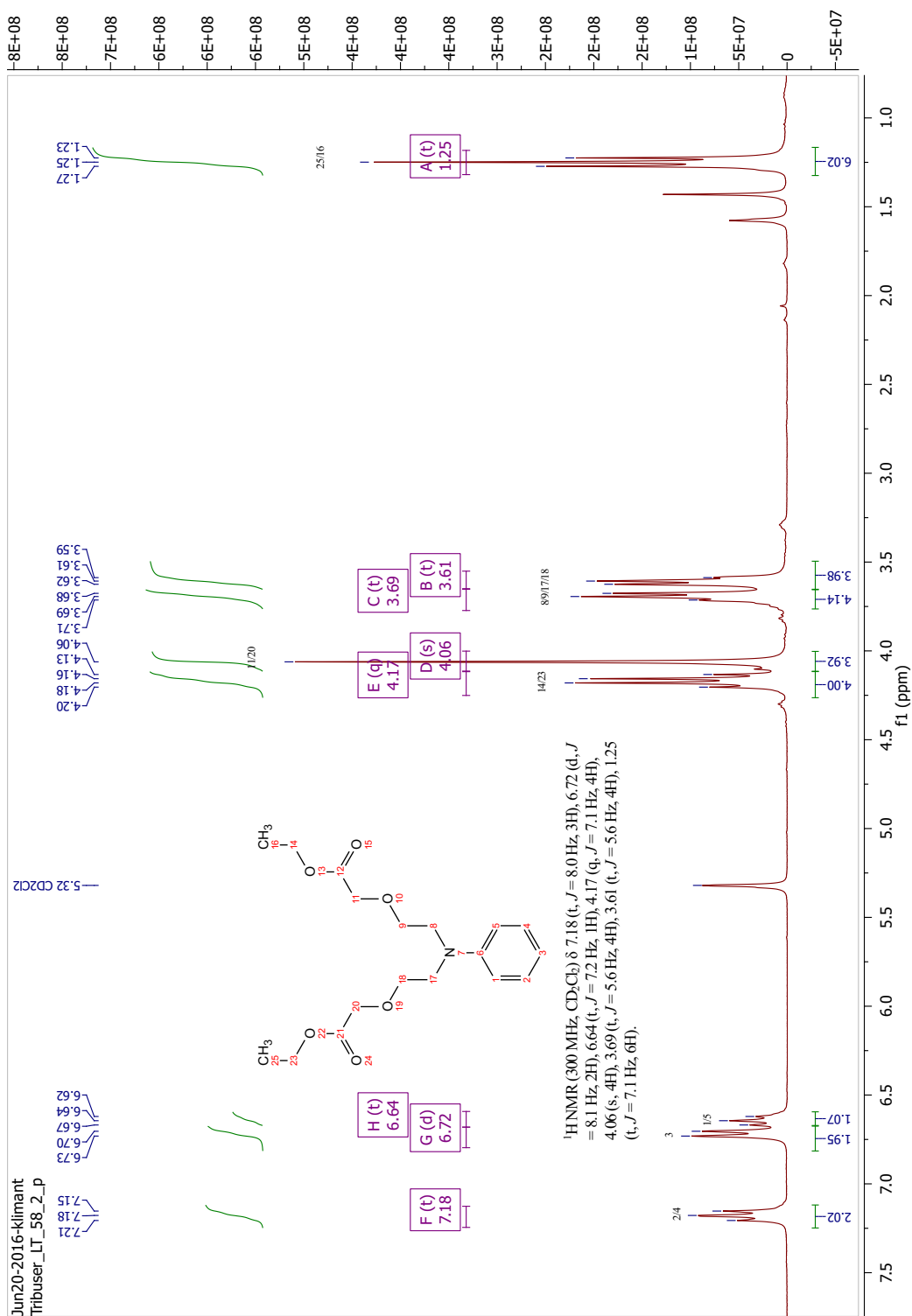
Figure 9.4: ^{1}H-NMR-spectrum of compound **41**.
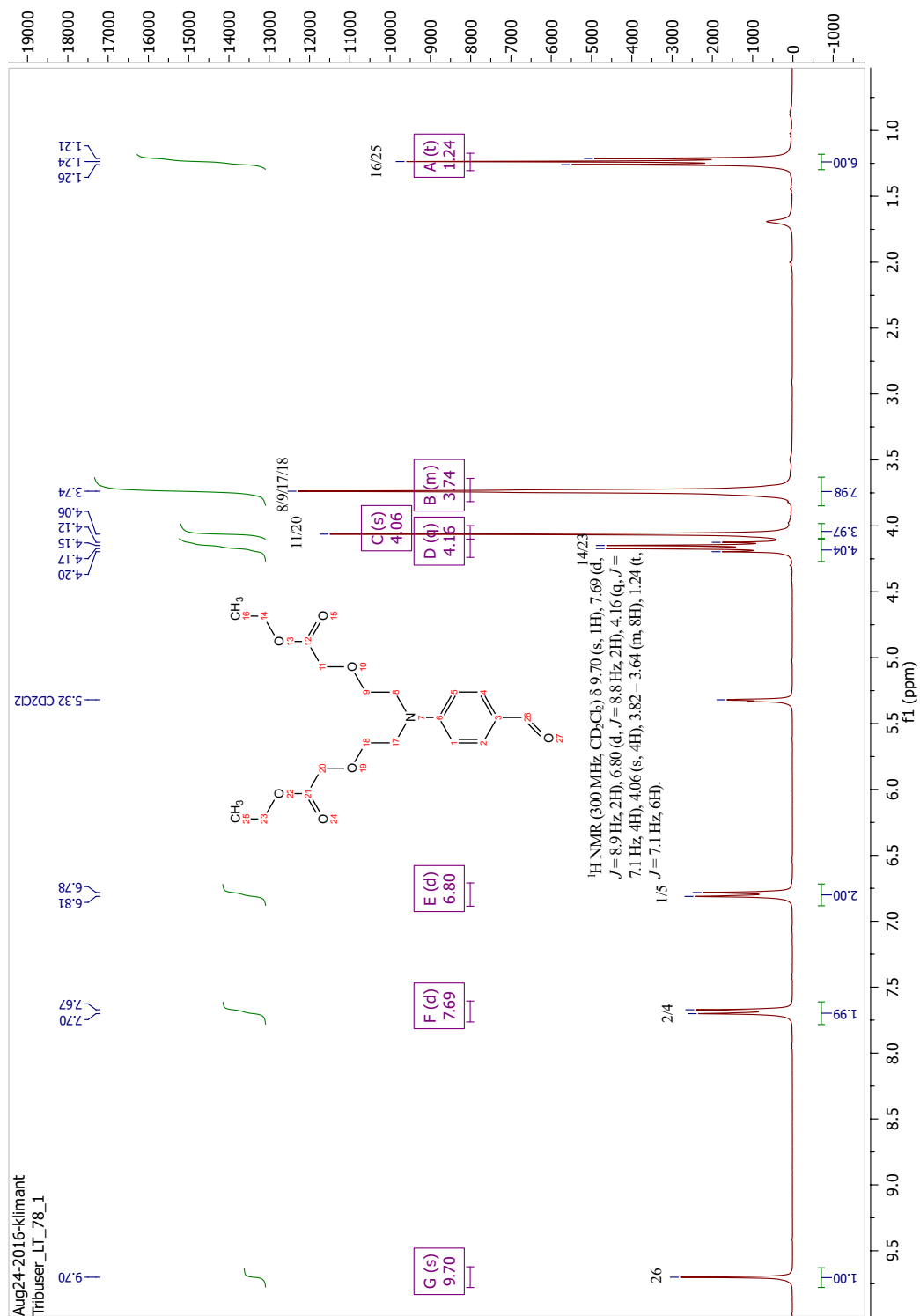
Figure 9.5: ^{1}H-NMR-spectrum of compound **36**.
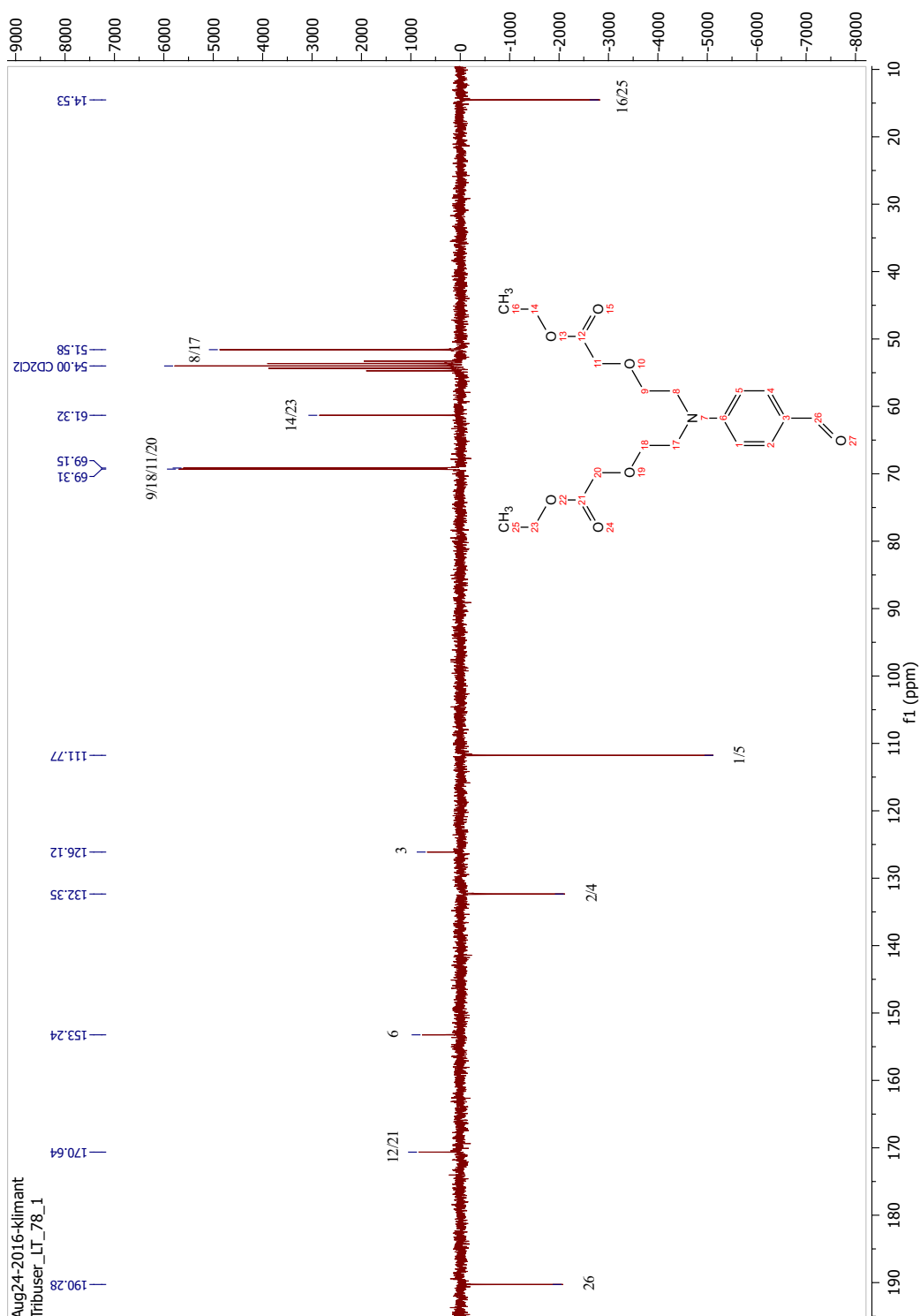
Figure 9.6: APT-NMR-spectrum of compound **36**.
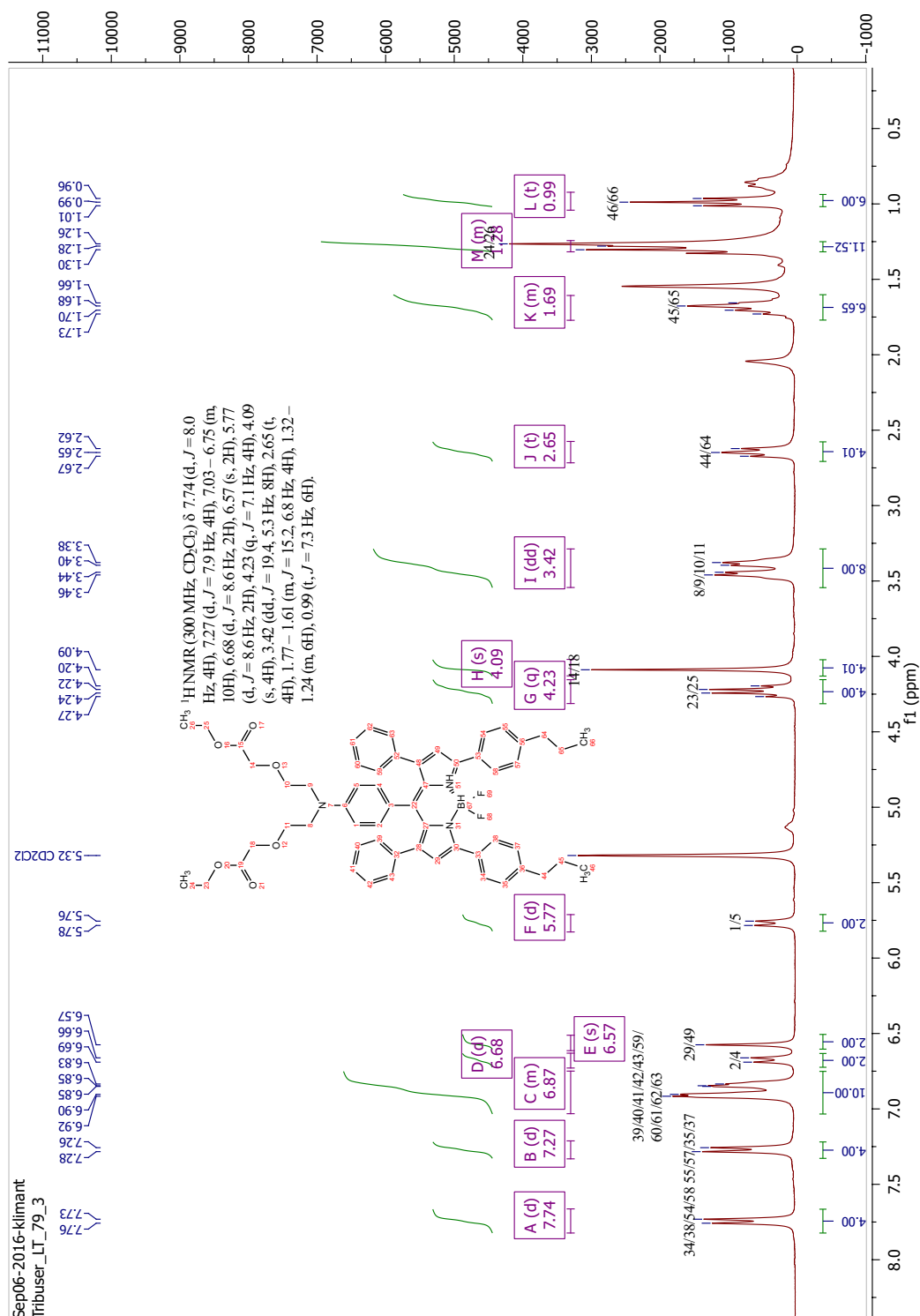
Figure 9.7: ^{1}H-NMR-spectrum of compound **FI1-ester**.
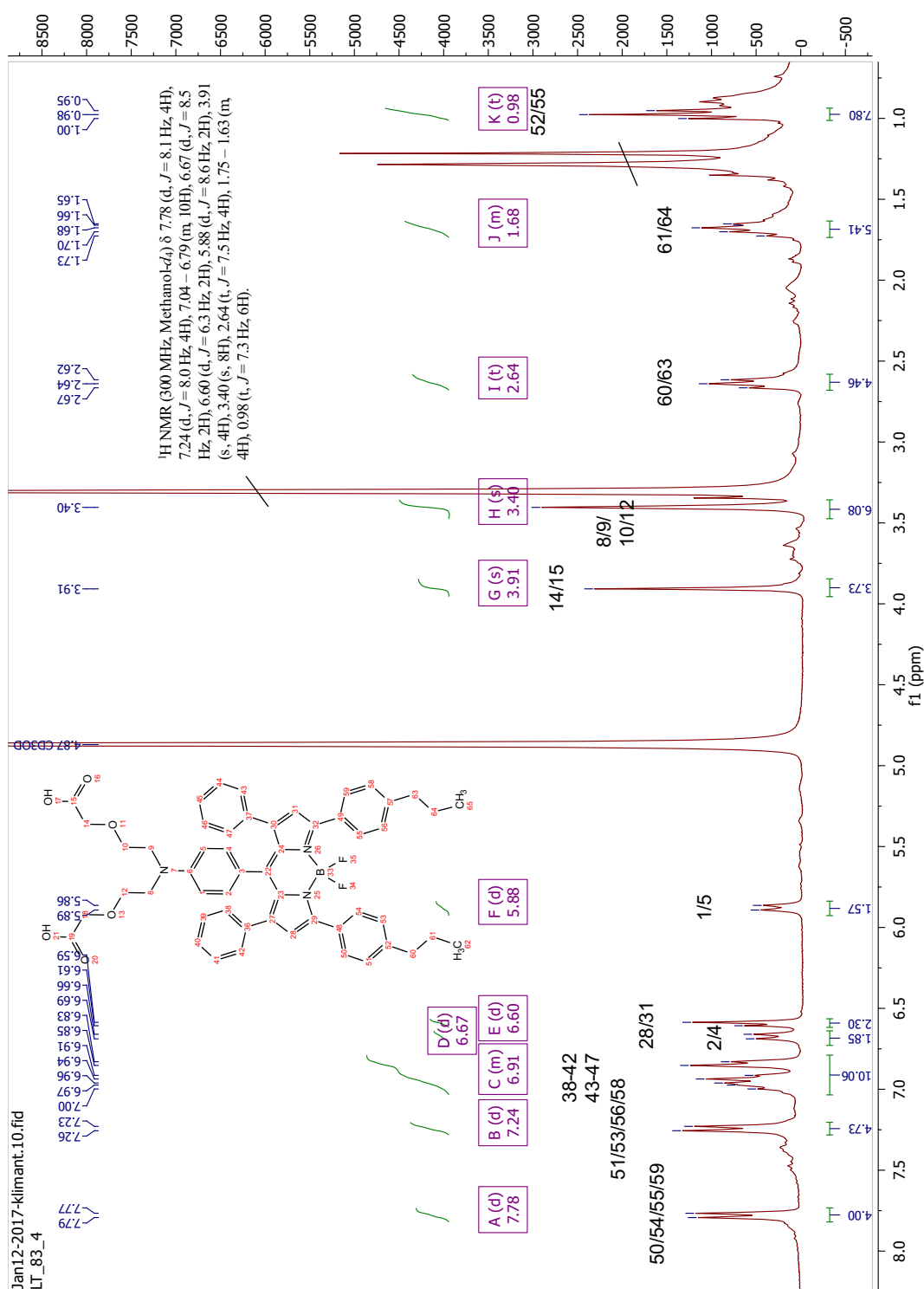
Figure 9.8: ^{1}H-NMR-spectrum of compound **FI1**.

Figure 9.9: ¹H-NMR-spectrum of compound **FI2-ester**.

Figure 9.10: ^{1}H-NMR-spectrum of compound **43**.
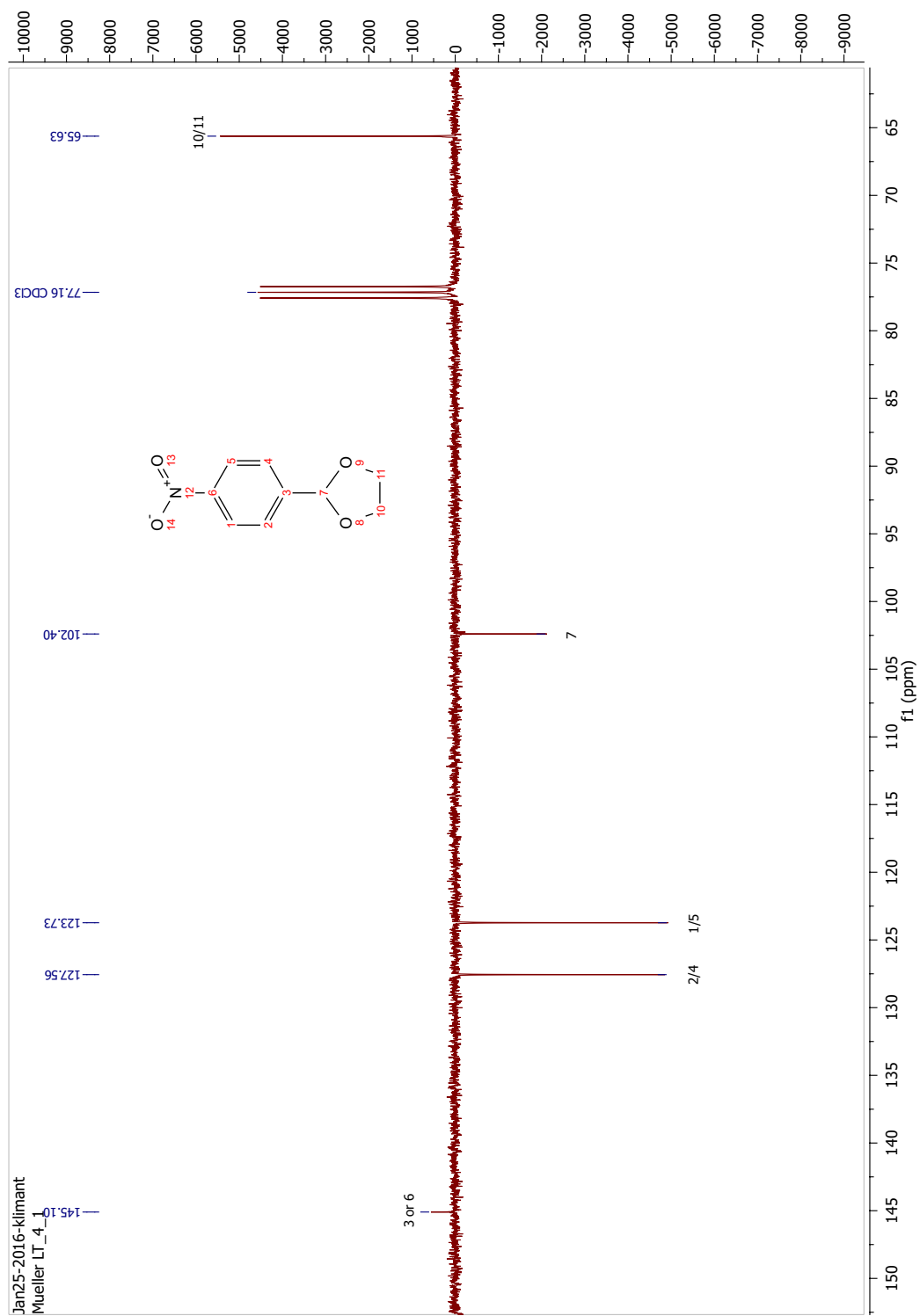
Figure 9.11: APT-NMR-spectrum of compound **43**.
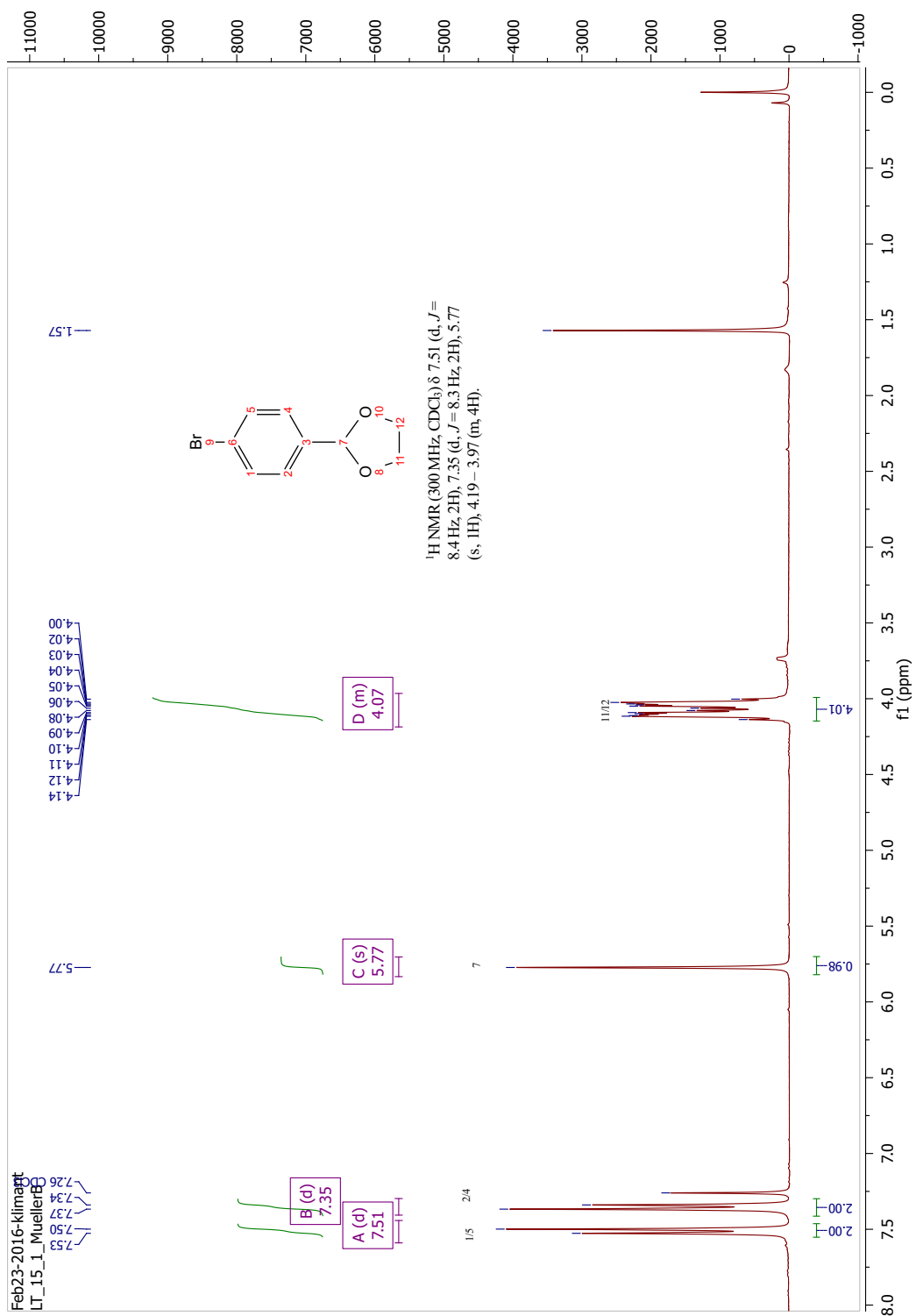
Figure 9.12: ^{1}H-NMR-spectrum of compound **47**.
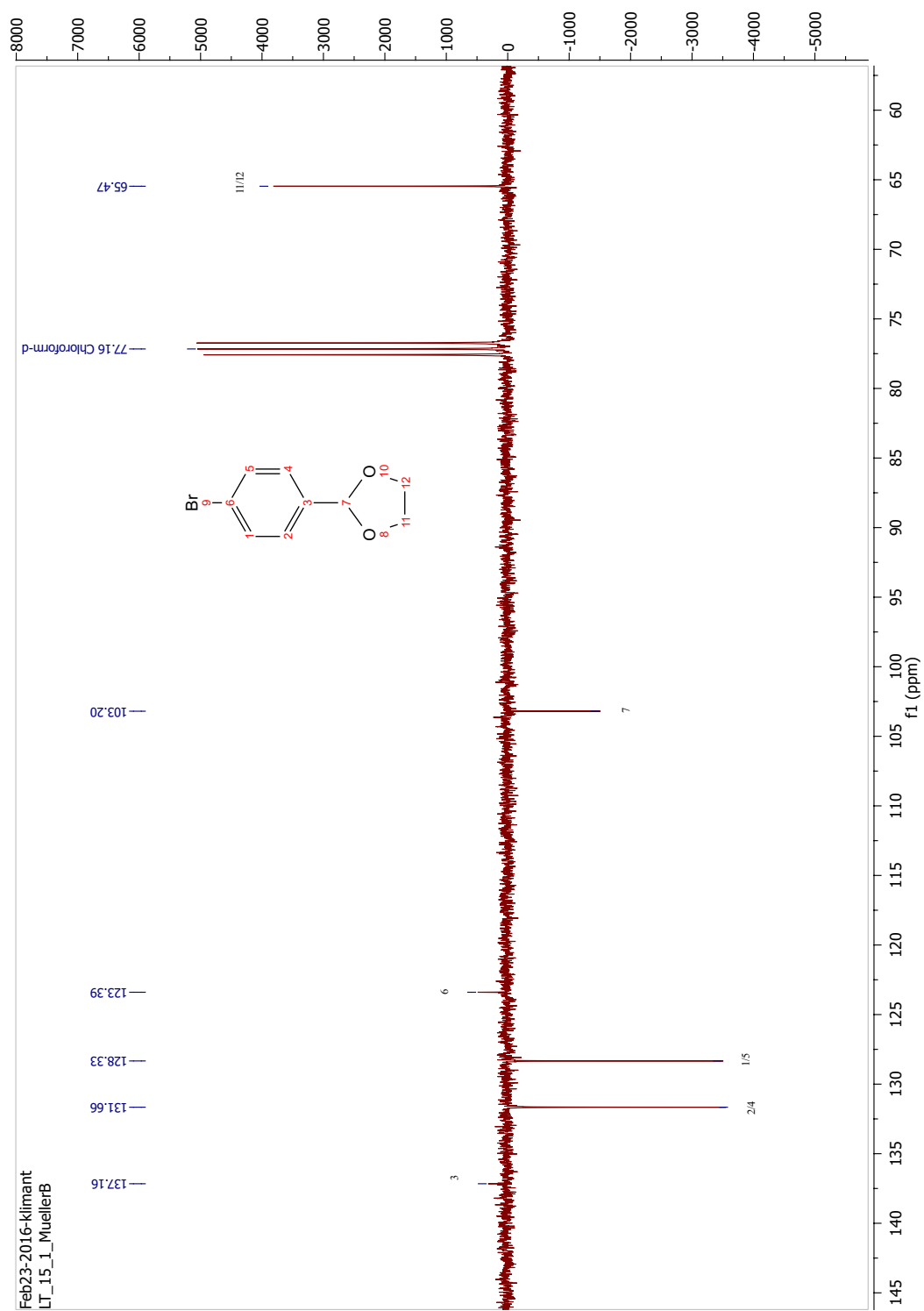
Figure 9.13: APT-NMR-spectrum of compound **47**.
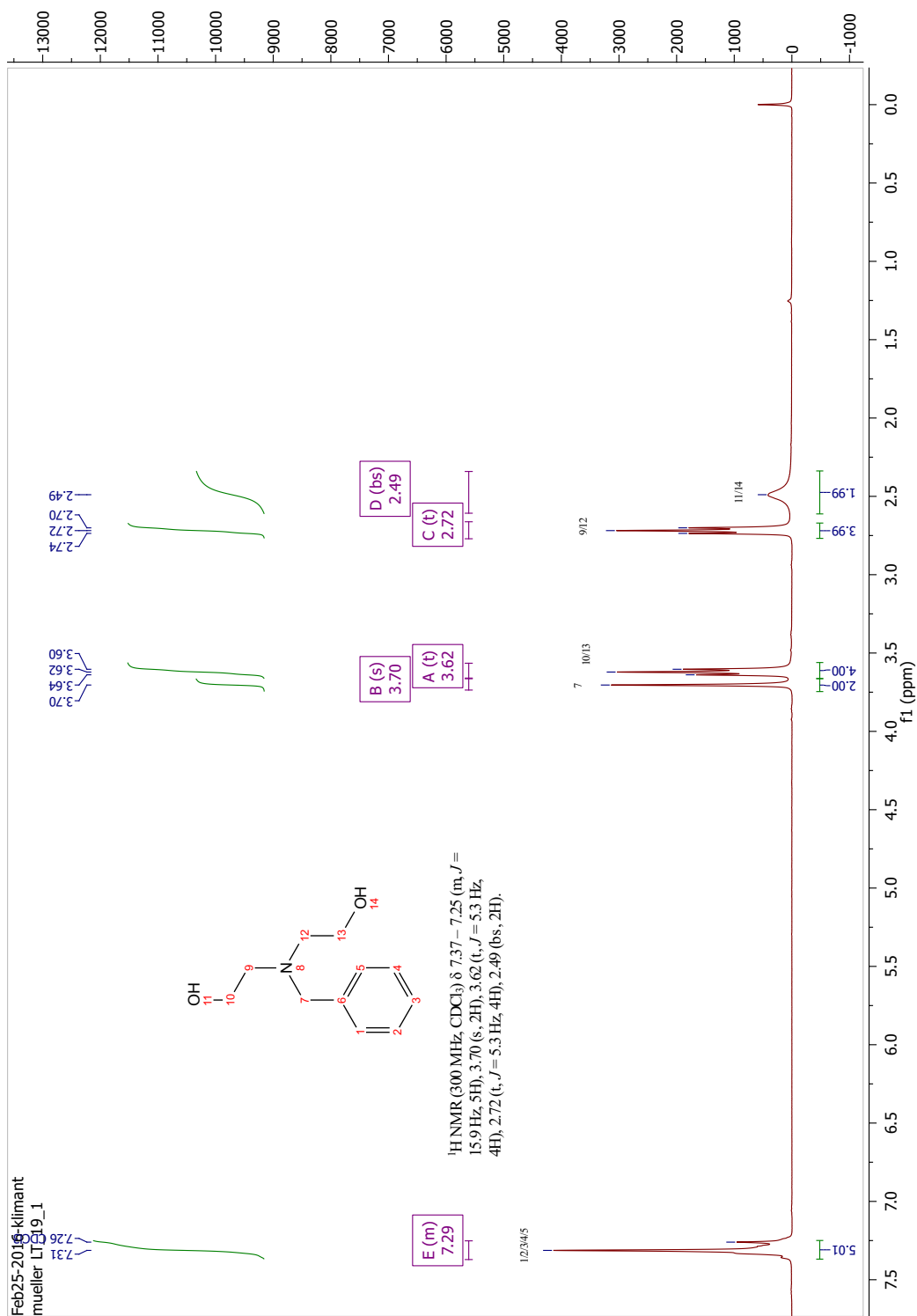
Figure 9.14: ^{1}H-NMR-spectrum of compound **53**.
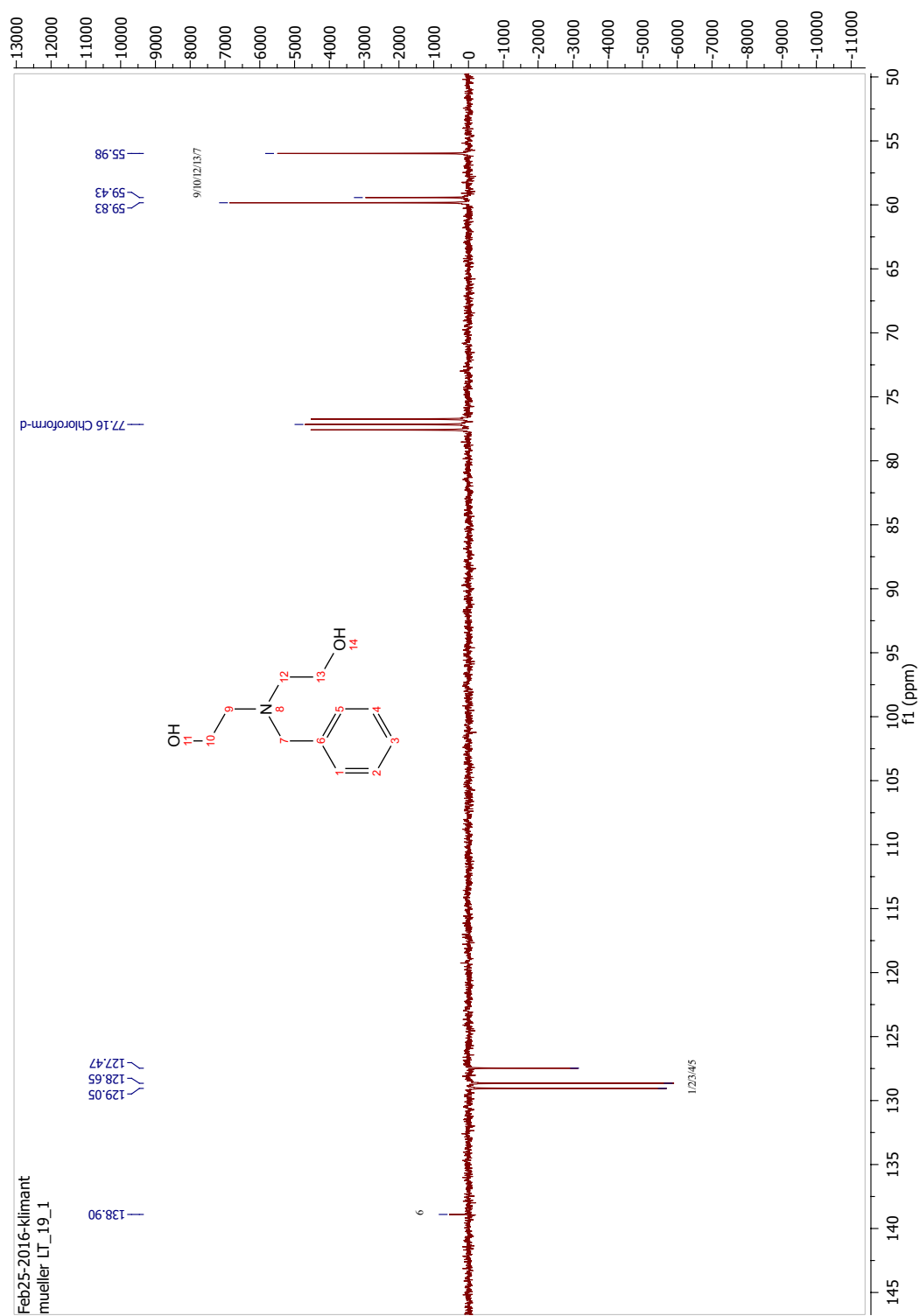
Figure 9.15: APT-NMR-spectrum of compound **53**.

Figure 9.16: ^{1}H-NMR-spectrum of compound **54**.
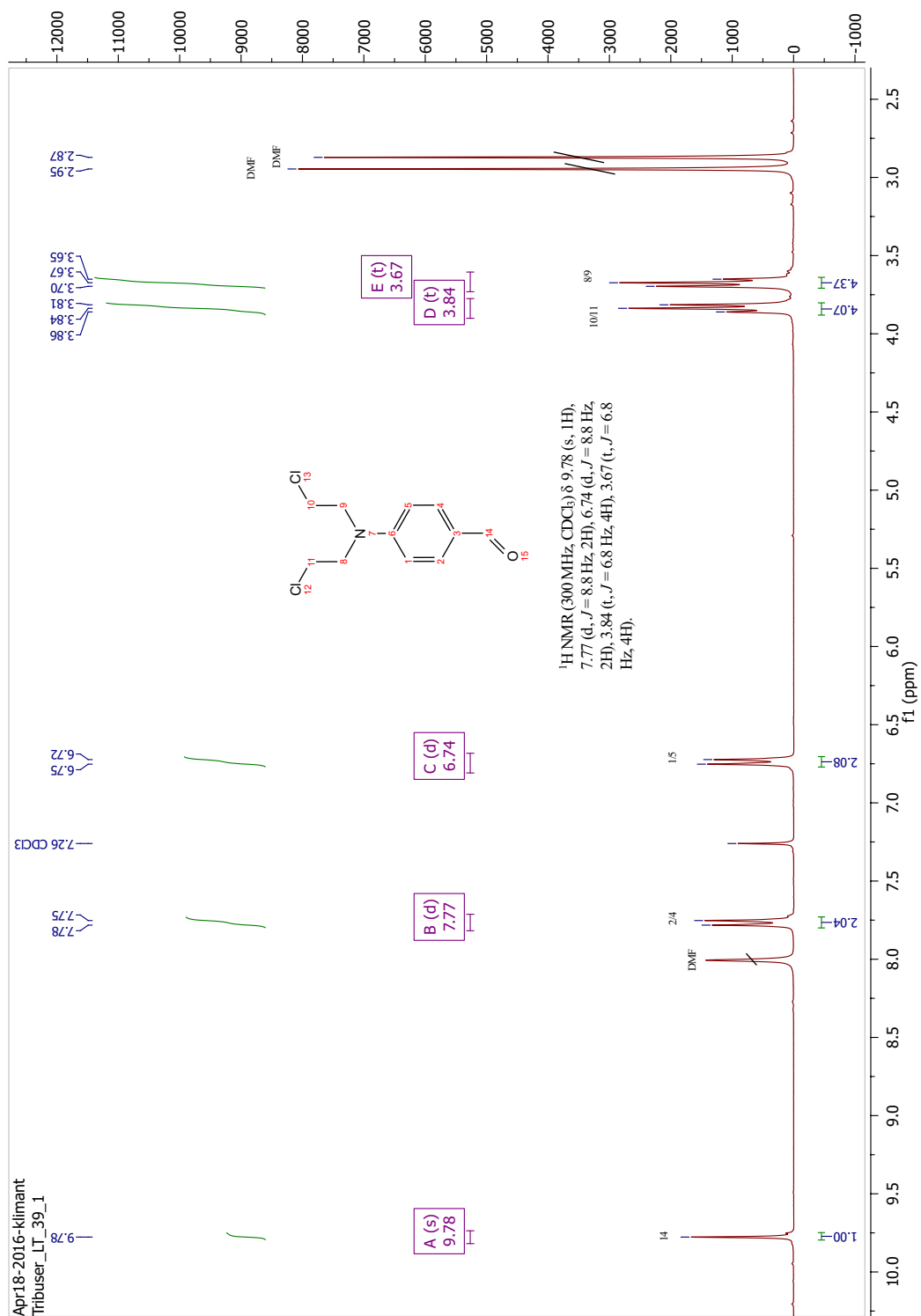
Figure 9.17: ^{1}H-NMR-spectrum of compound **57**.
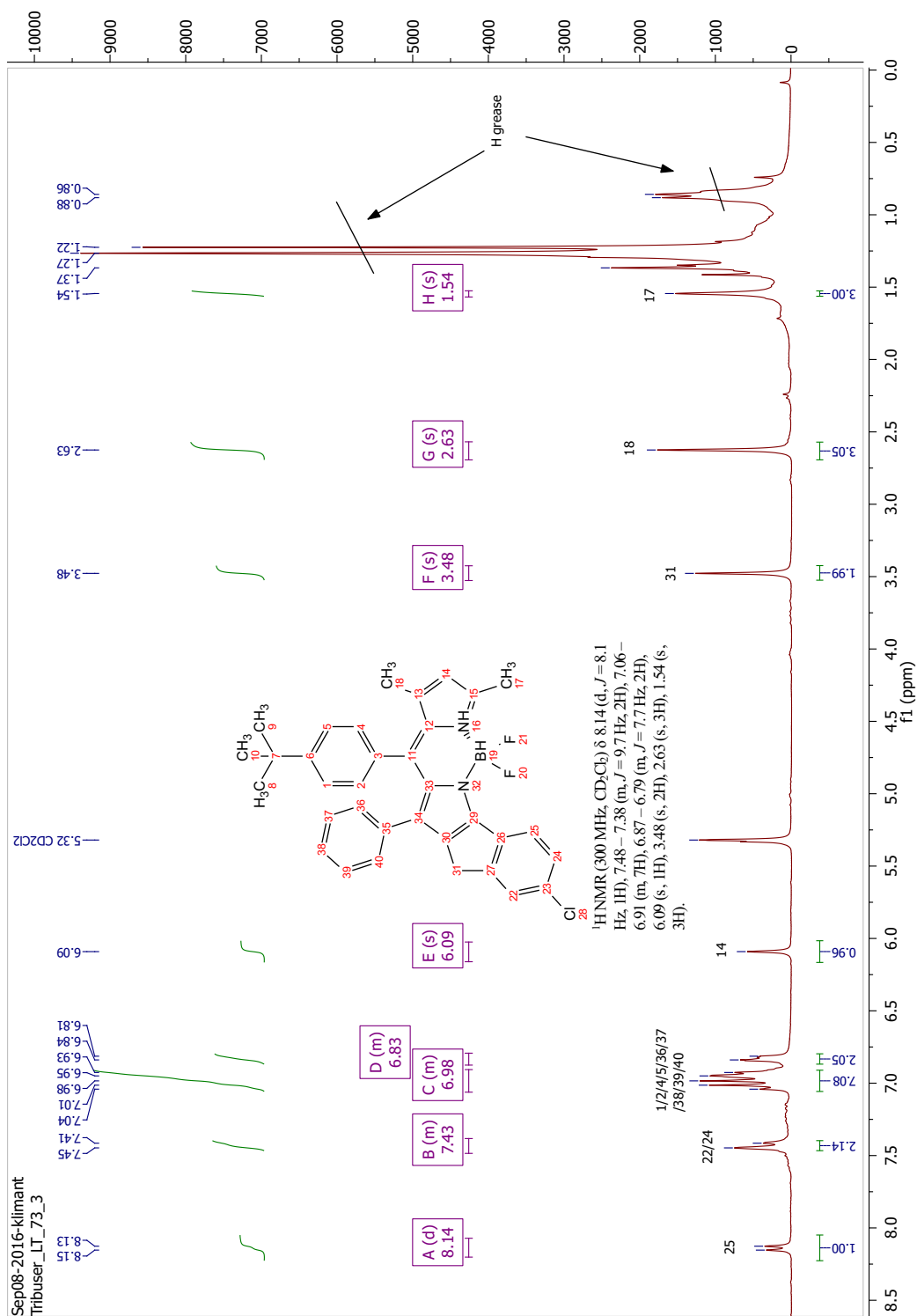
Figure 9.18: ^{1}H-NMR-spectrum of compound **72**.
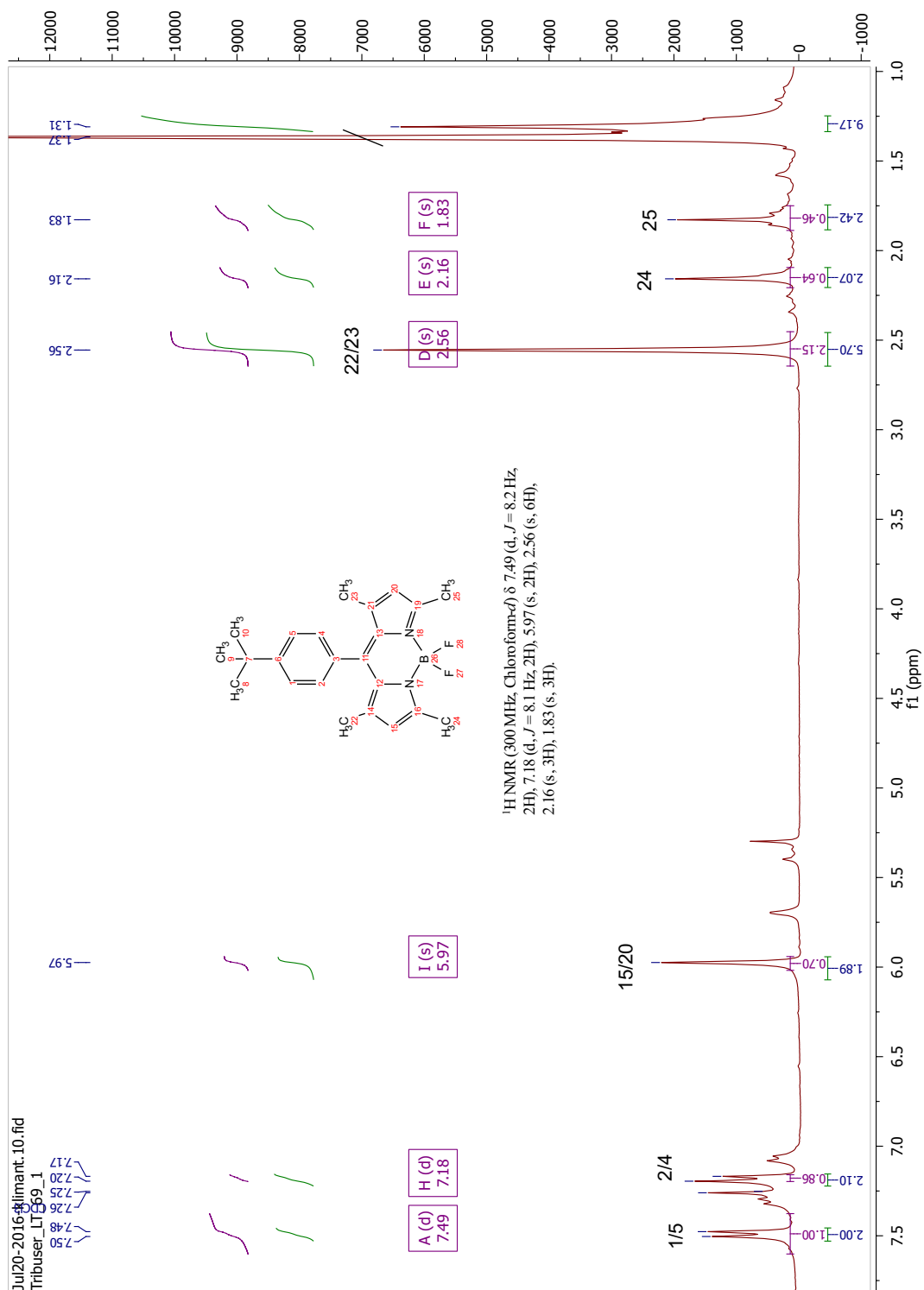
Figure 9.19: ^{1}H-NMR-spectrum of compound **69**.
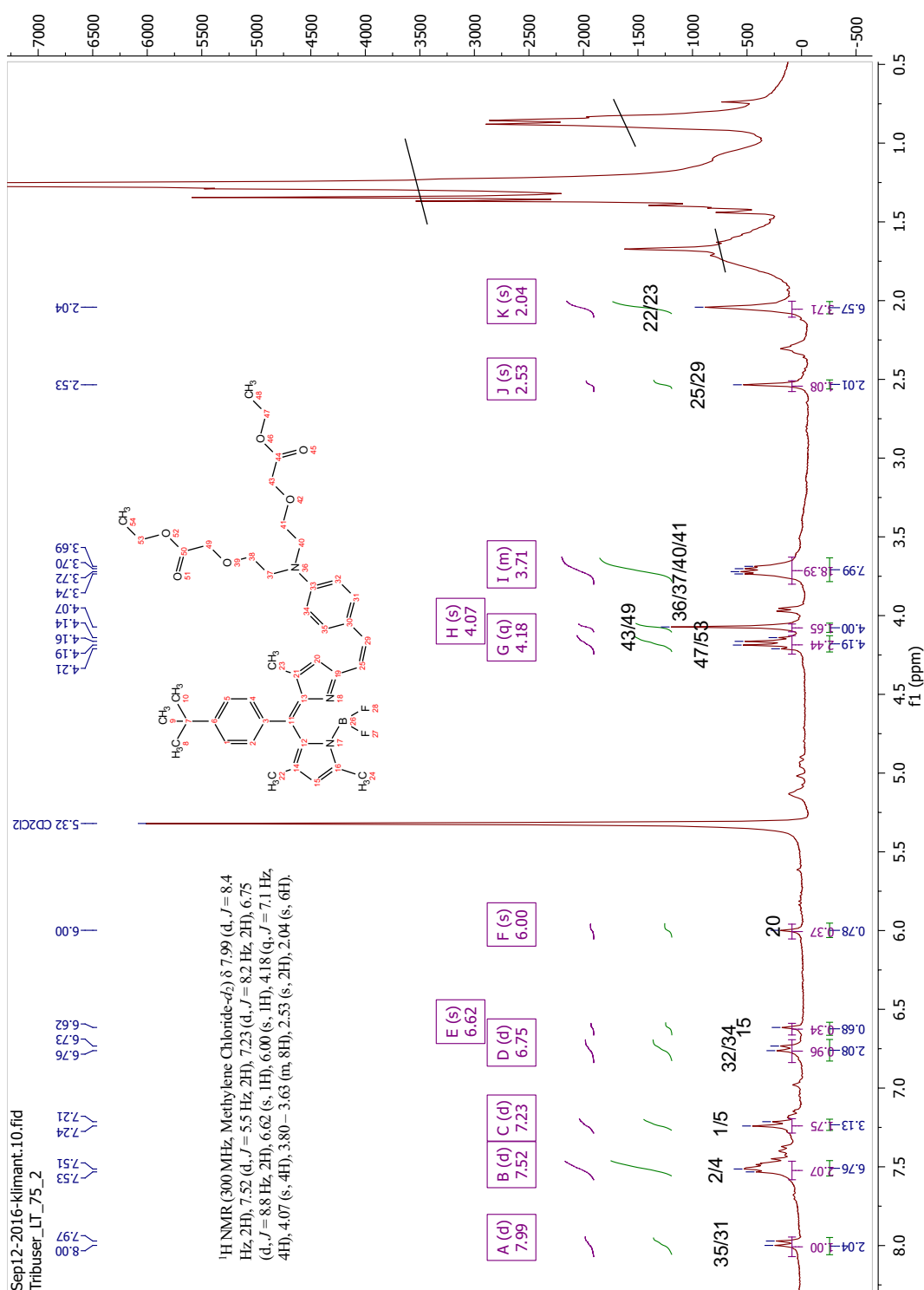
Figure 9.20: ^{1}H-NMR-spectrum of compound **70**.
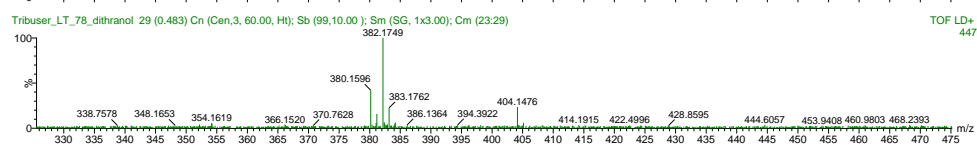
9.2 Maldi-TOF Data
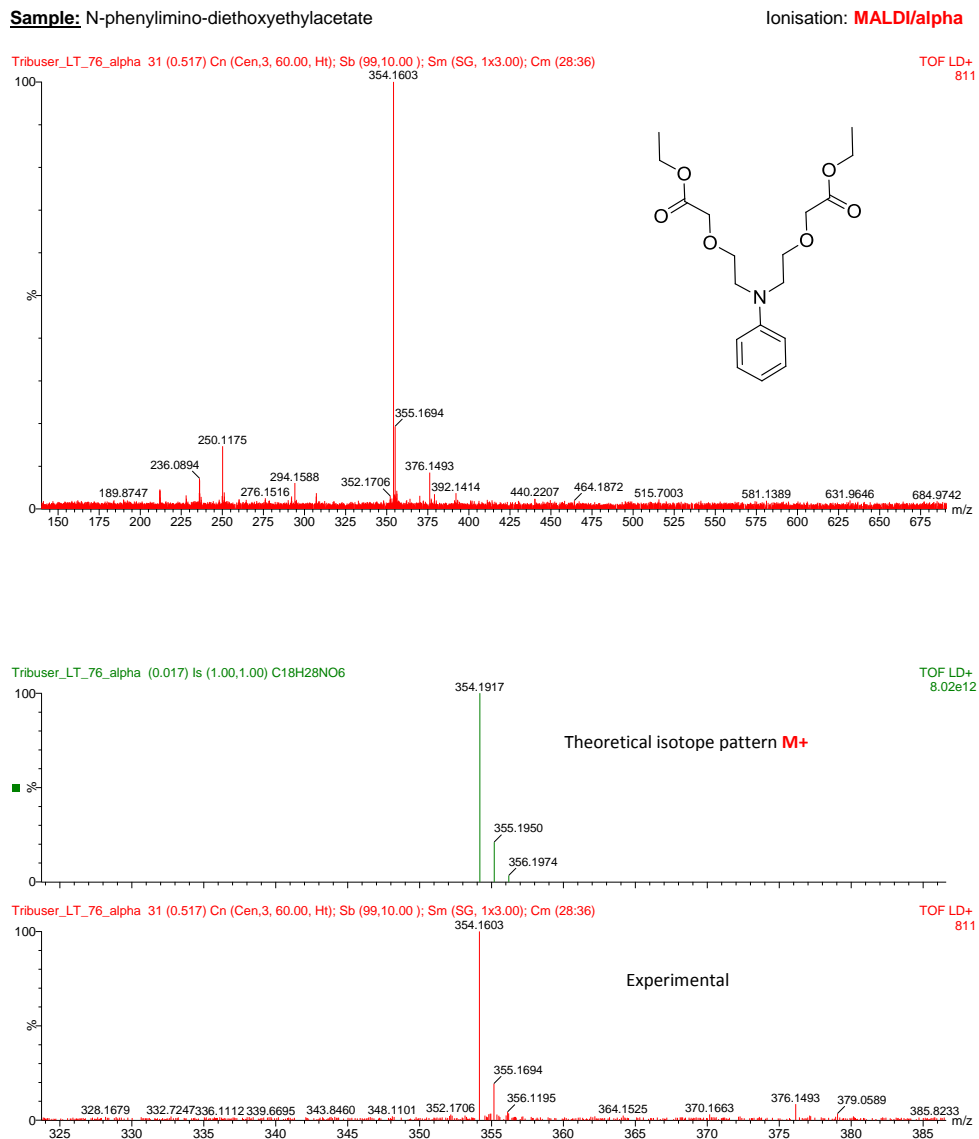
Figure 9.21:

Sample: N-(4-Formyl) phenylimino-diethoxyethylacetate   Ionisation: MALDI/Dith

Figure 9.22:
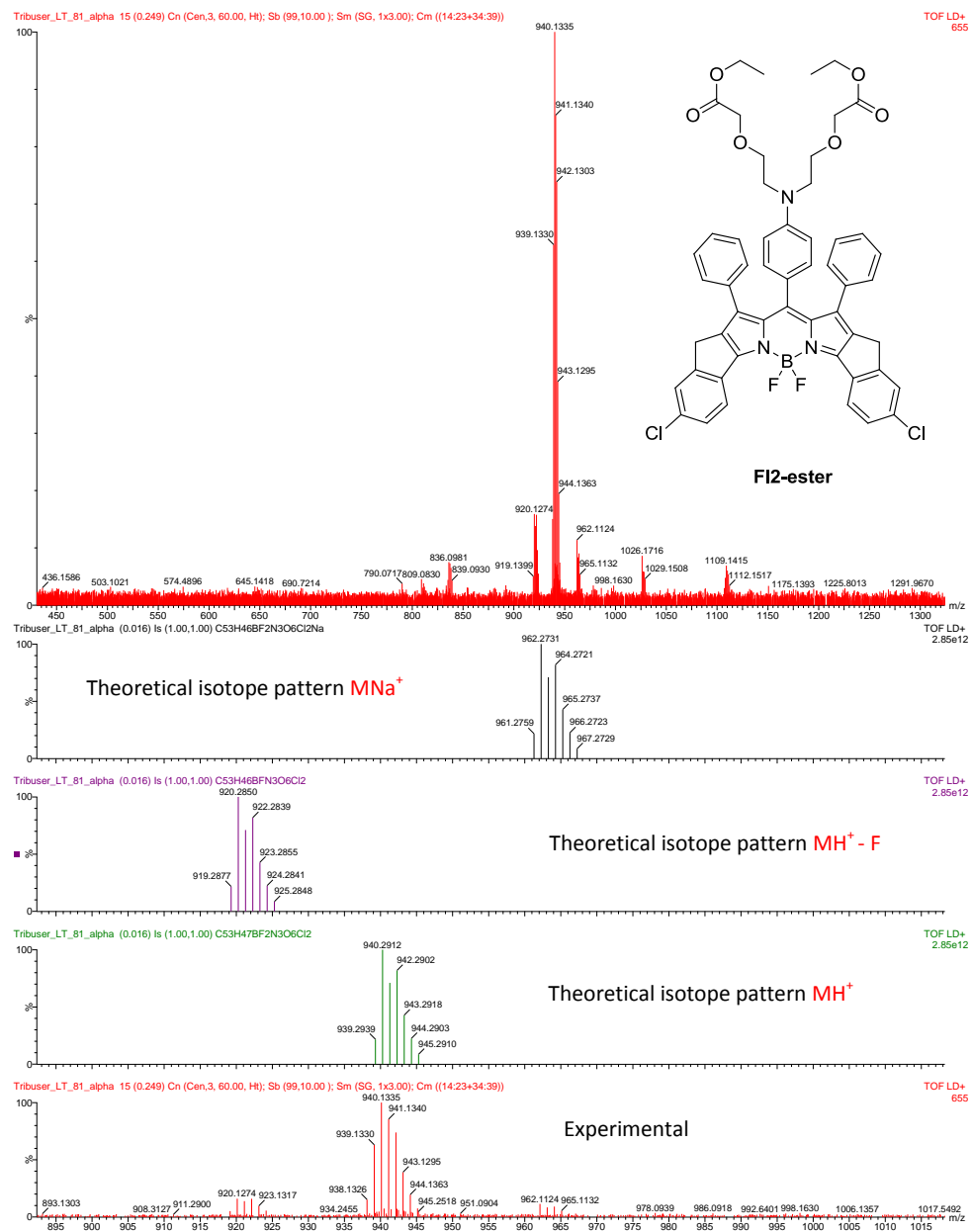
Figure 9.23:

Figure 9.24:

9.3 List of Chemicals

Chemical	Supplier	CAS-Number
1,4-Dioxan	Fluka	123-91-1
2-(2-Chloroethoxy)ethanol	TCI	628-89-7
2,3-Dichloro-5,6-dicyano-p-benzoquinone	Sigma-Aldrich	84-58-2
2-Chlorethanol	Sigma-Aldrich	107-07-3
2-Methylpropan-2-ol	Merck	75-65-0
4-Nitrobenzaldehyde	TCI	555-16-8
Acetone	Roth	67-64-1
Aniline	TCI	62-53-3
BAPTA	TCI	85233-19-8
BAPTA tetraethyl ester	ABCR	73630-07-6
Benzyl bromide	TCI	100-39-0
Boron trifluoride diethyl etherate	Sigma-Aldrich	109-63-7
Chloroacetic acid	Sigma-Aldrich	79-11-8
Chloroform	Roth	67-66-3
Cyclohexane	Roth	110-82-7
Dichlormethane	Roth	75-09-2
Dichlormethane anhydrous	Sigma-Aldrich	75-09-2
Diethanolamine	TCI	111-42-2
Diethylether	VWR	60-29-7
Diisopropylamine	Sigma-Aldrich	108-18-9
Ethanol	Brenntag	64-17-5
Ethyl thioglycolate	Sigma-Aldrich	623-51-8
Ethylacetate	VWR	141-78-6
Ethylene glycol	Roth	107-21-1
H2SO4	Merck	7664-93-9
HCl 37 %	VWR	7647-01-0
HNO3	Roth	7697-37-2
K2CO3	Roth	584-08-7
KI	VWR	7681-11-0
LiOH	Merck	1310-65-2
Lithium diisopropylamide	Sigma-Aldrich	4111-54-0
Methanol	Roth	67-56-1
N,N-Dimethylformamide	Sigma-Aldrich	68-12-2
Na2SO4 anhydrous	VWR	7757-82-6
NaH (60%)	Sigma-Aldrich	7646-69-7
NMP	TCI	872-50-4
Pd/C	Sigma-Aldrich	7440-05-3

Chemical	Supplier	CAS-Number
Peppsi	Sigma-Aldrich	905459-27-0
POCl3	Sigma-Aldrich	10025-87-3
Potassium tert-butoxide	Sigma-Aldrich	865-47-4
p-Toluenesulfonic acid monohydrate	Fluka	104-15-4
Silica Gel	Acros	112926-00-8
Sodium bicarbonate	Merck	144-55-8
Sodium chloride	Merck	7647-14-5
Tetrahydrofuran	Merck	109-99-9
Toluene	Roth	108-88-3
Triethylamine	Sigma-Aldrich	122-44-8
Trifluoroacetic acid	Fluka	76-05-1

9.4 Abbreviations

Ar	Argon
CH	Cyclohexane
DCM	Dichloromethane
DMF	N,N-Dimethylformamid
DDQ	2,3-Dichloro-5,6-dicyano-p-benzoquinone
EE	Ethylacetate
EtOH	Ethanol
MeOH	Methanol
MALDI-TOF	Matrix-assisted laser desorption/ionization-Time of flight
RT	Room Temperature
TEA	Triethylamine
THF	Tetrahydrofuran
UV-VIS	Ultraviolet-Visible
BAPTA	1,2-bis(o-aminophenoxy)ethane-N,N,N,N-tetraacetic acid
TFA	Trifluoroacetic acid
DIPEA	Diisopropylethylamine
NMP	N-Methyl-2-pyrrolidon
PEPPSI	[1,3-Bis(2,6-Diisopropylphenyl)imidazol-2-ylidene](3-chloropyridyl)palladium(II) dichloride
TLC	Thin-layer chromatography
LED	Light Emitting Diode
LDA	Lithium diisopropylamide